NTNU
Norwegian University of
Science and Technology

Integrated analysis of past, and potential future rock slope failures of various size from Rombakstøtta, Nordland

Odd André Morken

Geology
Submission date: May 2017
Supervisor: Reginald Hermanns, IGP

Norwegian University of Science and Technology
Department of Geoscience and Petroleum

Abstract

Catastrophic failure of large rock slopes has led to fatalities in Norwegian settlements several times per century. The Geological Survey of Norway (NGU) currently carry out systematic geological mapping of potentially unstable rock slopes in Norway, on assignment from the Norwegian Water Resources and Energy Directorate (NVE). In this context, a hazard analysis and preliminary consequence assessment of the unstable rock slope at Rombakstøtta in Narvik kommune, Nordland fylke has been carried out. In addition, an analysis of rock fall run-out lengths and frequencies since deglaciation has been carried out in the modelling software Rockyfor3D. A fragmentation cycle analysis, used to assess the fragmentation during a failure and to separate rock fall deposits from rock avalanche deposits, has been developed and tested.

The study area is located in a north facing slope along a fjord ca. seven kilometers east of the city Narvik. Based on delimiting lineaments observed in the field, aerial photos, photo panoramas and digital elevation models, eight failure scenarios (1.A-B, 2.A, 3.A and 4.A-D) are defined at Rombakstøtta. Application of NGU´s hazard analysis resulted in one scenario being assigned to the medium/low hazard class, six to the medium hazard class, and one to the high hazard class. Volume estimation and run-out analysis were carried out for all scenarios as a part of the preliminary consequence assessment. Resulting volumes for the scenarios range from 10 000 m^3 to 4 650 000 m^3, and four of the scenarios have modelled run-out reaching houses, Ofotbanen, the E6 highway, and the fjord. An additional two scenarios have run-out reaching Ofotbanen.

The rock fall analysis show that rock fall blocks larger than ~7.8 m^3 have reached coarse rock avalanche deposits with a possible frequency of 5-13 blocks per 1x1 m since deglaciation. This could affect cosmogenic nuclide dating of rock avalanche deposits, carried out within the CryoWALL project to which this thesis has affiliations. The calculation is based on rock fall modelling and an extrapolation of a dataset with ~100 years of rock fall registrations.

The fragmentation cycle analysis has been developed and applied inspired by Charrière et al. (2016). Results suggest that rock avalanche deposits at Rombakstøtta underwent 0-3 fragmentation cycles during failure. And that rock fall deposits below Rombakstøtta generally experienced more than 4 fragmentation cycles during failure. Results are discussed and compared to the results of Charrière et al. (2016) from the Frank Slide, Canada.

Samandrag

Store fjellskred har fleire gonger teke liv i norske busetjingar. Noregs geologiske undersøking (NGU) utfører systematisk kartlegging av potensielle ustabile fjellparti i Noreg, på oppdrag frå Noregs vassdrags- og energidirektorat. I denne samanhengen er det utført fareanalyse og ei innleiande konsekvensanalyse av det ustabile fjellpartiet Rombakstøtta i Narvik kommune, Nordland fylke. I tillegg, er det utført analyse av utløpslengde og frekvens av steinsprang sidan siste istid, i modelleringsprogrammet Rockyfor3D. Ei nedknusingsanalyse, brukt til å anslå fragmentering av blokker under et fjellskred og til å skilje steinsprangavsetjingar frå fjellskredavsetjingar, er utvikla og testa.

Studieområdet ligg i ei nordvendt skråning langs ein fjord ca. sju kilometer aust for Narvik. Åtte scenario (1.A-B, 2.A, 3.A og 4.A-D) er definert på Rombakstøtta, basert på avgrensande lineament observert i felt, på flybilete, panoramafoto, og digitale høgdemodellar. Ved å anvende NGU si fareanalyse er eitt scenario plassert i medium/låg fareklasse, seks scenario i medium fareklasse og eitt scenario i høg fareklasse. Volumanslag og utløpsanalyse er utført for alle scenario som ein del av den innleiande konsekvensanalysa. Det resulterte i volum frå 10 000 m^3 til 4 650 000 m^3 for dei ulike scenarioa. Fire av scenarioa har modellerte utløpslengder som rekk ned til hus, Ofotbanen, hovudvegen E6 og fjorden. Ytterlegare to scenario utløpslengder som når Ofotbanen.

Steinspranganalysa viser at blokker større en ~7.8 m^3 har nådd til dei grove fjellskredavsetjingane med ein mogleg frekvens på 5-13 blokkar per 1x1 m etter siste istid. Dette kan påverke kosmogene nuklid dateringar av fjellskredavsetningane, utført i CryoWALL prosjektet som denne masteroppgåva har tilknyting til. Berekningane er basert på steinsprangmodellering og ekstrapolering av eit datasett med ~100 års steinsprangregistreringar.

Nedknusingsanalysa er utvikla og anvendt inspirert av Charrière et al. (2016). Resultata tydar på at fjellskredavsetjingane under Rombakstøtta gjennomgjekk 0-3 fragmenteringssyklusar i skreda. Og at steinsprangavsetjingane under Rombakstøtta generelt gjennomgjekk meir enn 4 fragmenteringssyklusar under nedfall. Resultata er diskutert og samanlikna med resultata til Charrière et al. (2016) frå fjellskredet Frank Slide i Canada.

Acknowledgements

This thesis is the final work of my Master of Science (M.Sc.) degree in geology at the Department of Geoscience and Petroleum at the Norwegian University of Science and Technology (NTNU). It is written in collaboration with the Geological survey of Norway (NGU). Reginald Hermanns (head of the Geohazard and Earth Observation team at NGU and professor II at NTNU) have been my supervisor.

First, I would like to thank Reginald Hermanns for discussions, meetings, reviews, feedback and guidance through the process of writing a thesis. I am grateful for the possibility to have a summer job at NGU, it was a valuable experience and I learnt a lot. I appreciate that you have treated me as a colleague in the landslide team at NGU from the first day.

I would also like to express my gratitude to the rest of the landslide team at NGU, and in particular, Martina Böhme and Pierrick Nicolet for finding time to help me and answer my questions.

Former fellow student and field partner Kaja Krogh, thank you for being my field partner! I value your knowledge, humor and company.

I found a good discussion partner in my fellow student and friend Ole-Jakob Olsen, when writing the MATLAB script.

To the friends, I have made through my time studying, and especially the guys in “Kontoret”: it’s been five years of curves, ups, downs, and a lot of fun! I could not have done it without you!

Marie, you make my days brighter!

Trondheim, 15.05.17

Odd André Morken

Table of contents

Abbreviations

ALS	Airborne Laser Scanning
DBH	Diameter at Breast Height
DEM	Digital Elevation Model
dGNSS	Differential Global Navigation Satellite System
DSM	Digital Surface Model
DTM	Digital Terrain Model
FINT	Find Individual Trees
ICE	Image Composite Editor
InSAR	Interferometric Synthetic Aperture Radar
LiDAR	Light Detection and Ranging
NGU	Geological Survey of Norway
NGI	Norwegian Geotechnical Institute
NTNU	Norwegian University of Science and Technology
NVE	Norwegian Water Resources and Energy Directorate
NSM	Normalized Surface Model
SLBL	Sloping Local Base Level
TLS	Terrestrial Laser Scanning

1 Introduction

1.1 Introduction to unstable rock slopes in Norway

Norway is a country with extreme relief. Multiple glaciations have carved deep valleys and even deeper fjords into the roots of the old Caledonian mountain range. Along the western and northern shoreline, mountains with altitudes up to ~2000 m.a.s.l. give rock masses enormous potential energy that can be released in landslides. These landslides pose a threat themselves, but they can also cause hazardous secondary effects like damming of rivers and displacement waves (Hermanns and Longva, 2012; Harbitz et al., 2014). This is an unfavorable situation, when combined with the fact that a large part of the Norwegian population lives along the coast. Norway has historically experienced 2-6 large rock avalanches per century, some of which have produced displacement waves causing fatalities and extensive destruction of infrastructure (Hermanns et al., 2014). In the Norwegian landslide inventory database (Norwegian Water Resources and Energy Directorate, 2017) 4475 fatalities due to gravitational mass movements are documented. Rock fall, rock slide, and secondary effects have resulted in 932 fatalities (Hermanns et al., 2012a). Due to increased population, tourism, and settlement along the shore, it is expected that future events will be more disastrous than historic ones (Harbitz et al., 2014).

To mitigate the hazard of rockslides, it is a prerequisite to know which slopes that pose a threat. To attain this knowledge NGU started mapping unstable rock slopes in 2005, and continues to do so today, financed through the Norwegian Water Resources and Energy Directorate (NVE) (Devoli et al., 2011; Hermanns et al., 2014). Over 300 potential unstable rock slopes have been identified in the 17 counties, which are considered relevant for mapping (e.g. Blikra et al., 2006; Hermanns et al., 2012b). The mapping of Norway is divided into regions, where regions with a high concentration of unstable rock slopes are given priority and systematic mapping is carried out there first, i.e. Møre og Romsdal, Troms, Sogn og Fjordane, Rogaland and Hordaland. Rombakstøtta belongs to the region “rest of Norway”, which considers all the unstable rock slopes outside the five mentioned counties, and mapping here concerns mostly well-known instabilities.

After a potential unstable slope is discovered, it undergoes a preliminary consequence analysis. If the preliminary analysis prescribes so, this leads to an iterative process with an increasing degree of detail in field investigations and analysis, following directions given in Hermanns et al. (2012b). This is to ensure that resources are directed to sites with high risk. Hazard and risk level is determined based on a classification system developed at NGU (Hermanns et al., 2014).

The final stage for a high hazard and risk site is the establishment of a continuous monitoring system, to ensure evacuation of people in advance of a failure. Seven sites are being continuously monitored as of 2015, while there are conducted periodic displacement measurements on 90 sites (Oppikofer et al., 2015; Blikra et al., 2016).

CryoWALL is a research project aimed to gain more knowledge on permafrost in steep rock walls in Norway. Among the objectives of the project is linking Holocene development of selected rock walls to the present and future thermal regime, and evaluate potential risk to infrastructure from permafrost rock walls in Norway (Etzelmüller, 2015). Fieldwork for this thesis were carried out simultaneously as CryoWALL related fieldwork at Rombakstøtta. Some results from this master´s thesis might be interesting for a PhD in process within the CryoWALL project.

Rombakstøtta has been recognized as a possible instability for a long time (Bargel et al., 1995; Larsen and Domaas, 1997; Larsen, 1999). Locals have spotted signs of deformation, as this is a popular recreational area for the inhabitants of Narvik. During field work in the summer of 2015 and 2016, a distinct back scarp and other signs of instability have been mapped by geologists from NGU and the author of this thesis. These observations in addition to the deposits below the slope, which could originate from several post-glacial landslides, indicates that Rombakstøtta is an unstable mountain slope.

1.2 Aims of the study

This master´s thesis aims to investigate the unstable rock slope at Rombakstøtta, and in addition the deposits below. This will result in a hazard assessment of different failure scenarios in addition to a model for the size reduction of blocks during a rock slope failure.

The main work includes:

- Map the discontinuities (e.g. foliation and joints) and the geomorphological features (e.g. depression and scarps) in detail, through field work and analysis of high resolution digital elevation models (DEM)
- Map and define the unstable areas to determine the volume of separate failure scenarios.
- Perform a structural analysis to identify the spatial variation in the mapped structures, both for single stations and structural domains. Carry out kinematic analysis for each domain to address possible failure mechanisms.
- Define failure scenarios based on the observed deformation and limiting structures.

- Assess hazards for each failure scenario based on the NGU standardized hazard and risk classification.
- Perform volume calculations for the different scenarios using the Sloping Local Base Level (SLBL) method and run-out analysis for each scenario using the software Flow-R.
- Determine the probable block size at the onset of a failure, based on the degree of fracturing in the unstable area, and compare that to the block size of the deposits. This, to better understand whether the deposits originate from rock fall or from rock avalanches.
- Use the probable block size and deposited block size to perform a run out analysis in Rockyfor3D, and normalize the rock fall frequency since deglaciation.
- The two prementioned bullet points can also aid the interpretation and understanding of cosmogenic nuclide dating of the deposits, carried out by others within the CryoWALL project.
- C-14 dating of a piece of wood to possibly delimit the minimum age for some of the deposits.

1.3 Available data

Work and results presented in this thesis are heavily based on data collected during field mapping carried out by the author and Kaja Krogh, during 11 field days in August/September 2016. Data from NGUs field campaign in 2015 have been used as well. In addition, the DEM obtained by Light Detection and Ranging (LiDAR) and the aerial photos have aided the work greatly.

Data that were available during the work are listed in table 1.1.

Table 1.1 Available data

Available data	Source
LiDAR data (DEM)(1x1 m resolution)	NGU
Helicopter photos of the site	NGU
Aerial photos (years: 1967, 1975, 1990 and 2013)	The Norwegian Mapping Authority (Kartverket)

1.4 Location, background and geological setting

Rombakstøtta is a mountain located ca. seven kilometers east of the city of Narvik in Nordland fylke, Norway (Figure 1.1). Since the mountain is located in a region with Sami influence, it also holds the Sami name Áhkačohkka, while locals address the mountain Tøttatoppen. In this thesis, the official Norwegian name Rombakstøtta is used. The peak is 1230 m.a.s.l., while the instability is located ca. 1000 – 1100 m.a.s.l., The slope of interest is a north facing slope with the foot in the fjord Rombaken. Power lines, the railway Ofotbanen, and the E6 highway lie within scree originating from Rombakstøtta. The scree deposits go all the way into the fjord. Ofotbanen is the busiest railway in Norway, mainly used for the transportation of the ore deposits from Kiruna to the harbor in Narvik. Jernbaneverket is planning a double track to make the railway more efficient (Jernbaneverket, 2016).

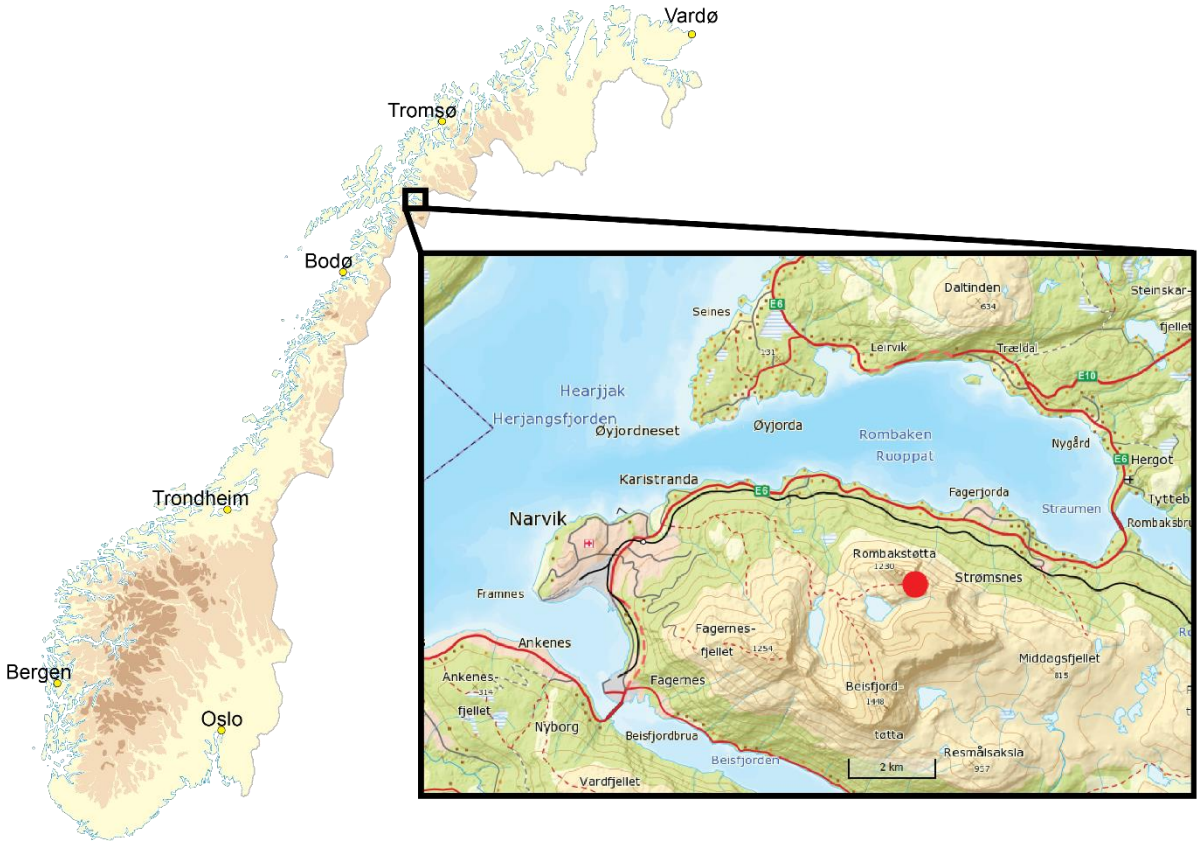

Figure 1.1: The location of Rombakstøtta (indicated by a red dot) in Norway, and the area around the mountain. A new bridge for the E6 highway is being built from Karistranda to Øyjordneset, but this is not indicated in this map yet. Edited from «Norge, Illustrasjonskart» by Kartverket and norgeskart.no.

1.4.1 Background for mapping Rombakstøtta

As mentioned in the previous section (1.4), there are major scree deposits below Rombakstøtta which are a witness of previous landslide activity in the area. A prominent crack or backscarp

is also identified close to the summit of the mountain and has been a reason for concern in previous years (Bargel et al., 1995).

1.4.2 Historical events

The landslide inventory database holds 19 events along the railway and the road below Rombakstøtta, however only four of these entries are regarding rock fall, while the other entries are mostly snow avalanches and debris flows.

1.4.2.1 The rock fall of 1996

In the fall of 1996 a block of 50-100 m^3 detached from the steep north face and caused damage to the railway. Due to this, experts from the Norwegian Geotechnical Institute (NGI) made a field survey to consider, if there could be a coherence between the rock fall and movement of the entire slope. The report concluded that a coherence was unlikely, and that the rockfall was triggered by frost weathering along an existing discontinuity (Larsen and Domaas, 1997). However, measuring bolts over the tension crack were installed during the summer of 1997, and in the subsequent report the possibility of a failure scenario of up to 100 000 m^3 was discussed. The likelihood was, however, considered low such for large rock avalanche events. The report also suggested that large rock fall events have a return period of 10-20 years on this slope. The landslide inventory database for Norway supports this (Larsen, 1999). Measurements of the bolts have been conducted approximately every second year since installation, except for during a 5-year period from 1999 to 2004. In this period one bolt couplet have moved 88 mm relative to each other, which is far more than the inaccuracy of the method (measuring-tape).

During NGU´s field campaign in the early autumn of 2016, new bolts were installed for measurement with extensometer, which is a more precise method for measuring slope movement than measuring tape. It is also quite precise (Hermanns, 2015)

Occurrence of landslides and rock falls is often linked to high precipitation which can alter the ground water conditions and increase the water pressure (e.g. Crosta and Agliardi, 2003; Sartori et al., 2003; Wyllie and Mah, 2004). The meteorological station with the longest time series close to Rombakstøtta is located in Bjørkåsen at 54 m.a.s.l. and approximately 33 km SW of Rombakstøtta. The annual average precipitation is 1458 mm, based on the period 1965 to 2015, while for the last normal period (1961-1990) it was 1290 mm. Thus, the annual precipitation has increased in later years. In the days prior to the 1996 rock fall, this station had received only 20.7 mm. The long-term precipitation is nothing exceptional either, with rainfall in September

1996 being below the monthly average. However, august this year was the fifth wettest recorded since 1965 with 165.9 mm (Norwegian Meteorological Institute, 2016).

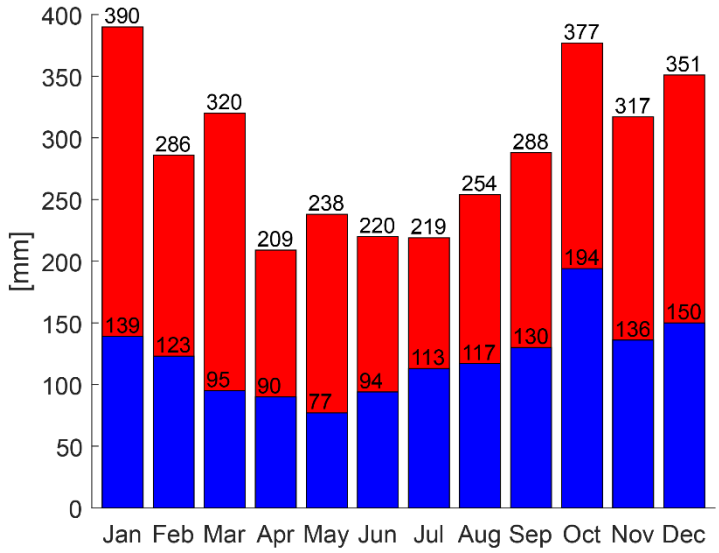

Figure 1.2 Monthly average precipitation for the period 1965-2015 for Bjørkåsen meteorological station in blue, and monthly extremes for the same time period in red. Based on data from the Norwegian Meteorological Institute (Norwegian Meteorological Institute, 2016).

1.4.3 Geological setting

On a regional scale, the bedrock consists of Cambro-Silurian thrust nappes. (1:50 000 scale bedrock map, Karlsen, 1991). At Rombakstøtta disthen-garnet-twin mica-gneiss is the most prominent rock in the westerly unstable area. A bit further east, around the most easterly instability, the rock is classified as a quartz-rich, garnet-twin mica schist with some layers of quartzite/quartz schist and partly epidote carrying. Down in the slope, quartzite or quartz schist with thin layers of mica schist, amphibolite, and calcite marble are mapped (Karlsen, 1991). The bedrock in the area is part of Narvik Nappe Complex, which is mainly composed of several amphibolite-facies thrust sheets (Augland et al., 2014). A bedrock map is presented in appendix A.

Around Narvik, like in the rest of western Norway, the general ice movement during the glacial cycles has been from east to west. However, the erosion has most likely been more extensive around Narvik than in other areas. This is due to the proximity to the, by estimation, thickest part of Fennoscandian Ice Sheet, and to the sea. Vast volumes of ice has been transported past Narvik and out Ofotfjorden and Vestfjorden during glaciations and deglaciations leading to heavy erosion (Bargel, 2003). According to Bargel et al. (1995), the fjord Rombaken was covered with remnants of the inland ice sheet 9500-10000 years ago, while the more elevated

areas were ice free or covered with local glaciers (Figure 1.3). Radiocarbon dating of shells from end moraines next to Rombaken has shown ages of 10872 ± 167 years BP (and 10913 ± 213 years BP) at the mouth of the fjord and 10604 ± 162 years BP in the middle, narrowest point of the fjord. At the northern shore of the fjord two ages of 10156 ± 188 years BP and 10360 ± 145 years BP are reported. The dated ages show a trend of a retreating glacier in Rombaken within this timespan, and possibly a faster retreat on the northern shore than on the southern shore where Rombakstøtta is located (Andersen et al., 1981; Hughes et al., 2015).

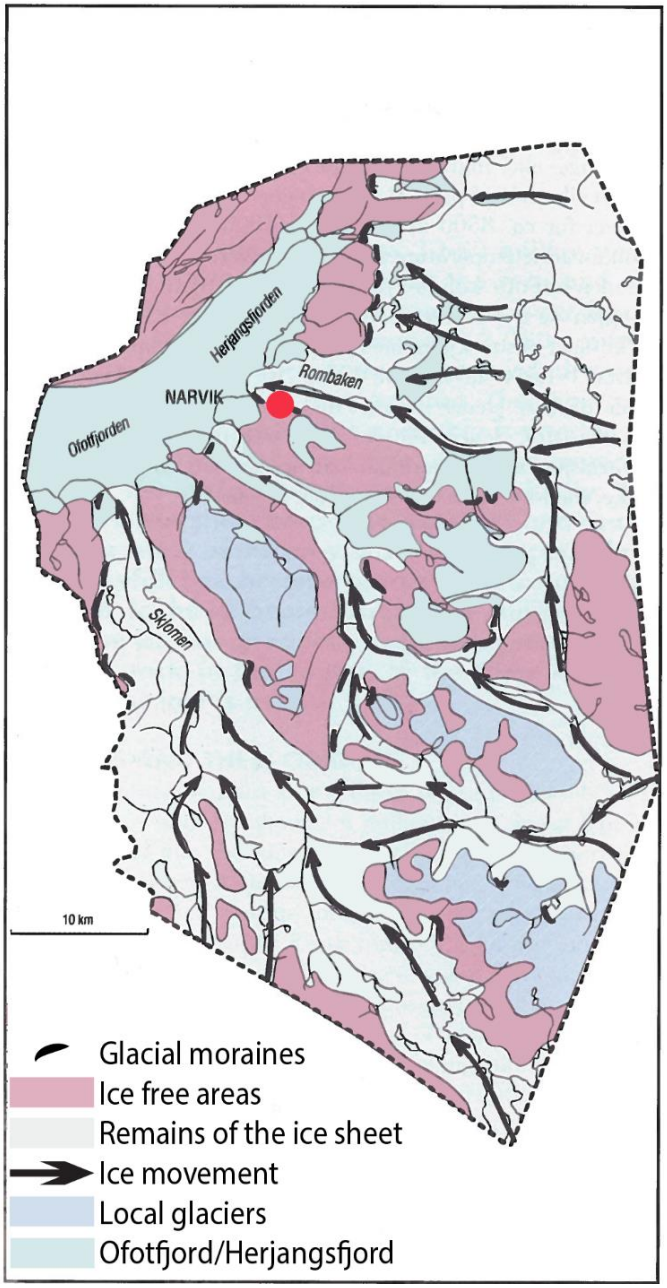

Figure 1.3 Map showing a possible reconstruction of the deglaciation 9500-10000 years ago, in the Narvik area. Edited from Bargel et al. (1995).

1.4.4 Permafrost

Thawing permafrost is thought to have a degrading effect on the stability of mountain slopes (Sosio et al., 2008; Huggel et al., 2010). Christiansen et al. (2010) found that the altitude for permafrost initiation in northern Norway descends from ca. 990 m.a.s.l. in the western part to ca. 550 m.a.s.l. in the interior of the country. With the instability located at a north facing slope, ca. 1000-1100 m.a.s.l., permafrost might be present. According to the permafrost map for Norway, Sweden, and Finland, the area holds sporadic permafrost (Gisnås et al., 2016). Formation of permafrost might be very local due to significant accumulation of freezing air in fractures during early winter, known as the Balch effect. Later in winter this cooling comes to a rest due to isolation by snow (Blikra and Christiansen, 2014). During the 2016 field campaign, temperature loggers were installed in some north- and west facing vertical slopes, however, results from these loggers will not be available for this thesis.

2 Theory

2.1 Landslide terminology

Landslides are a complex phenomenon, studied by several disciplines, this is reflected in the diversity of definitions and classification systems. Hermanns (2016) suggest the following general definition of a landslide:

> *A landslide is the gravitational downslope movement of solids on natural or artificial slopes. The solids are geotechnical materials that can contain water, ice, and air; however, the solids are volumetrically dominant over the transport medium (water, ice, and air).* (Hermanns, 2016, p. 1)

Varnes (1978) developed a classification system for landslides. The system was updated by Hungr et al. (2014). The classification is based on the type of movement (Figure 2.1) and the material in motion, and is widely used today, however with some modifications (e.g. Highland and Bobrowsky, 2008).

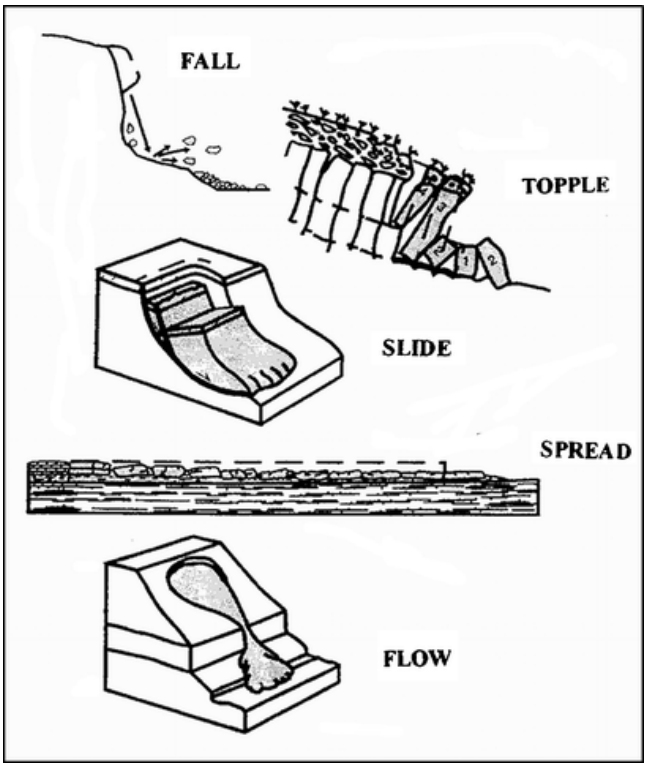

Figure 2.1 Types of movements from Cruden and Varnes (1996). These movement types can be associated with rock, debris or earth as materials.

Terminology describing the features of a landslide are also suggested in Varnes (1978) and modified in Highland and Bobrowsky (2008). This terminology is also adopted in this master´s thesis with some exceptions (Figure 2.2).

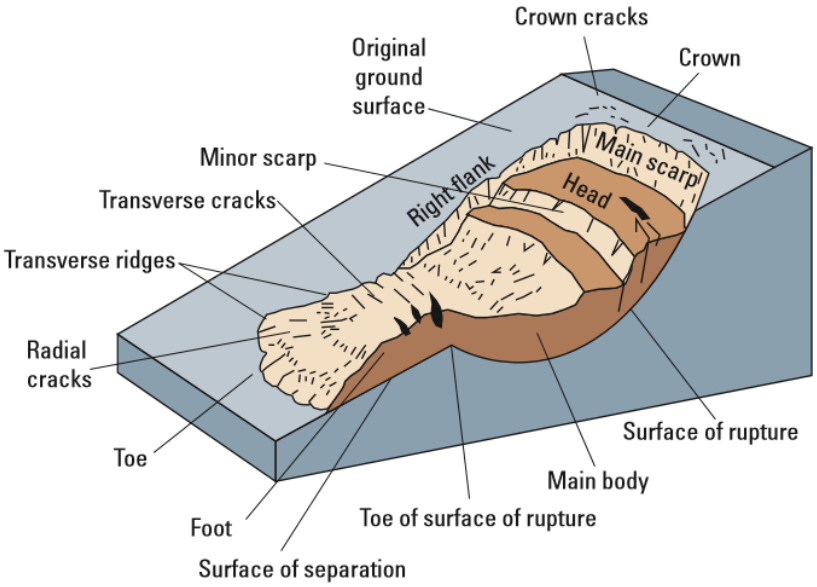

Figure 2.2 An illustration of a rotational slide that has evolved into an earthflow. The figure labels the separate features of a landslide (Highland and Bobrowsky, 2008).

In Norwegian terminology, the separation between rock fall (steinsprang), rockslide (steinskred), and rock avalanche (fjellskred) is done partly based on volume. Rock fall is defined as one or several blocks with a combined volume less than ca. 100 m^3. If the volume of the rock masses is between 100 and 10 000 m^3 it is defined as rockslide, while for moving masses over 10 000 m^3 the term rock avalanche is used (Høeg et al., 2014). However, at NVE and NGU the separation between rockslide and rock avalanche is set to ~100 000 m^3, which is more in line with international literature (Devoli et al., 2011).

2.2 Mapping approach chosen at NGU

The goal of mapping unstable mountain slopes at NGU is to detect potential future rock avalanches that might fail catastrophically, and to predict the area that these avalanches can affect. The work is financed and supervised by NVE (Hermanns et al., 2014). Catastrophic failure is defined as "rock slope failures that involve substantial fragmentation of the rock mass during run-out and that impact an area larger than that of a rock fall. Hence the definition also include rock slope failure that might cause a displacement wave or damming of valleys" (Hermanns et al., 2014, p. 130).

Mapping is done as an iterative process to ensure that resources are directed to the sites with the highest risk. In addition, clear rules of which geological parameters that should be mapped for each risk level are important to make sites comparable. The work is organized in several stages, as described below (Figure 2.3).

2.2.1 Detection of unstable rock slopes

Potential unstable rock slopes are detected through expert-based analysis of optical remote sensing imagery, and through satellite based radar interferometry (InSAR). Location of the slopes may in some cases be known from before through former surveys, or tips from locals or others (Hermanns et al., 2014).

2.2.2 Reconnaissance

Superficial processes, such as solifluction, are detected by InSAR and can be mistaken for rock slope deformation. Thus, all detected sites undergo an initial field reconnaissance. In this step, rock masses without signs of large deforming rock volumes are divided into three categories:

A) Unstable rock slopes that are too small to cause a catastrophic failure in in the sense mentioned above.
B) Rock slopes that have no structural or lithological conditions that could lead to a catastrophic failure in the future.
C) Rock slopes that have the structural or lithological conditions for failure in the future, but no sign of past or present displacement or deformation.

Category C sites need to be revised after years to decades, as their condition might change (Hermanns et al., 2014).

2.2.3 Preliminary consequence analyses

After the reconnaissance phase, a preliminary consequence analysis is carried out for the unstable rock slopes. Sites with no consequences, i.e. no buildings or life lines, in the potential run-out area, are categorized as low-risk sites and no further investigations are made. Nonetheless, the volume will be estimated and an automated run-out analysis will be calculated. Unstable slopes with evident consequences, are further investigated (Hermanns et al., 2014).

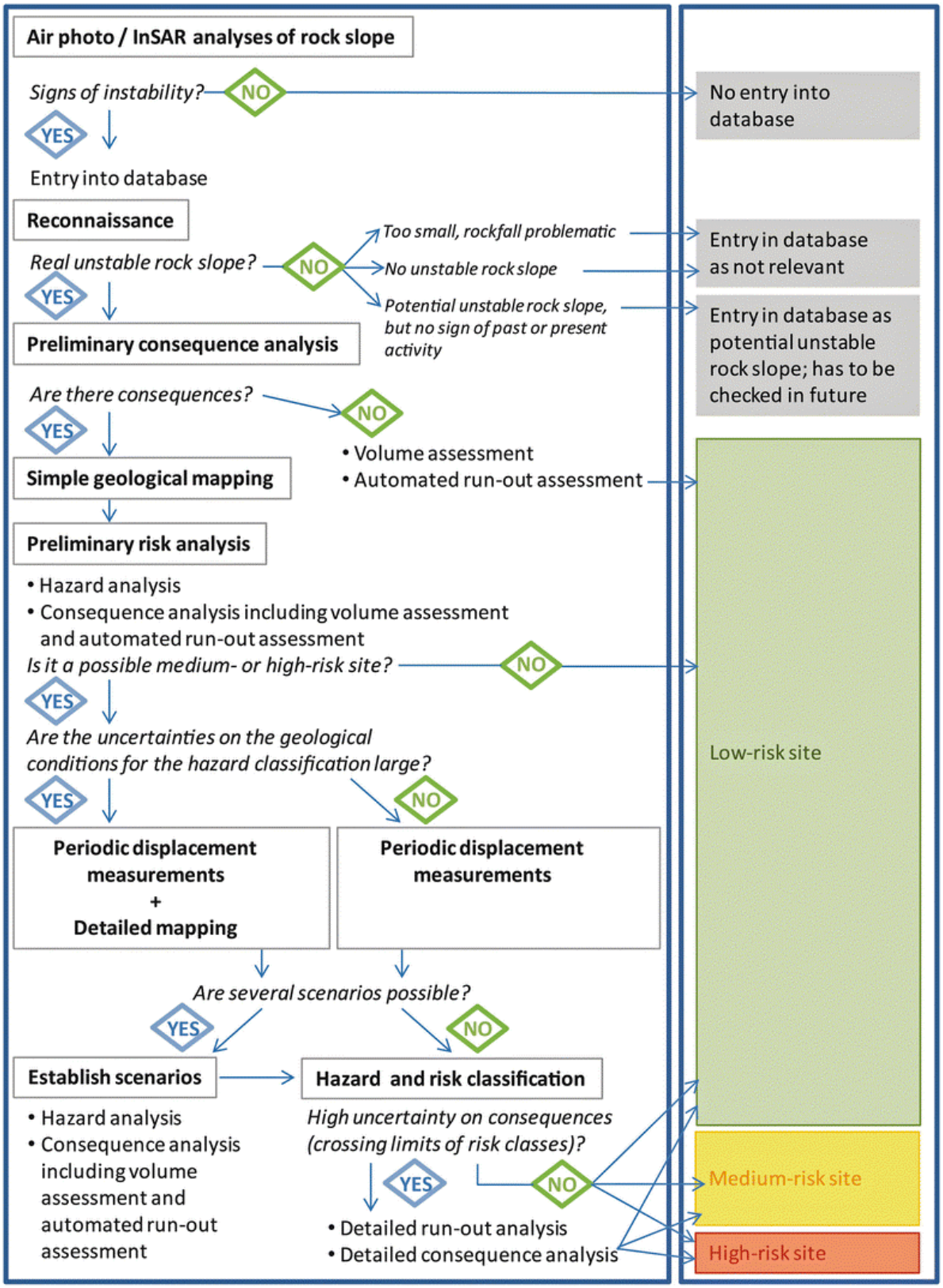

Figure 2.3 Workflow for the mapping approach for unstable rock slopes in Norway. Potential unstable rock slopes that do not display signs of past displacements and sites without possible consequences are discarded from further geological studies at an early stage. From Hermanns et al. (2014).

2.3 LiDAR technology

Light detection and ranging (LiDAR) is a remote sensing technique that utilizes laser technology to create a 3D-model of the ground. Due to the possibility to acquire 3D-models with high accuracy and spatial resolution, the LiDAR technology has caused a revolution in landslide mapping (Jaboyedoff et al., 2012).

A point cloud is collected by sending laser pulses toward the ground and record the timing of the reflected pulses together with the dip and azimuth. These three factors enable one to calculate the position of the point in relation to the scanner, which also has a known position. Resolution of the model depends on the density of the point cloud collected, which again depends on the position of the sensor, among other factors. Sensors can be terrestrial (TLS) or airborne (ALS), where terrestrial supplies the highest resolution (centimetric to millimetric). It is possible to use LiDAR in vegetated areas. In this case the first return pulse, which is often equivalent to the vegetation, is processed out (Shan and Toth, 2008). The ability to "see" through vegetation enables geologists to distinguish features through remote sensing, that would be very hard to identify otherwise.

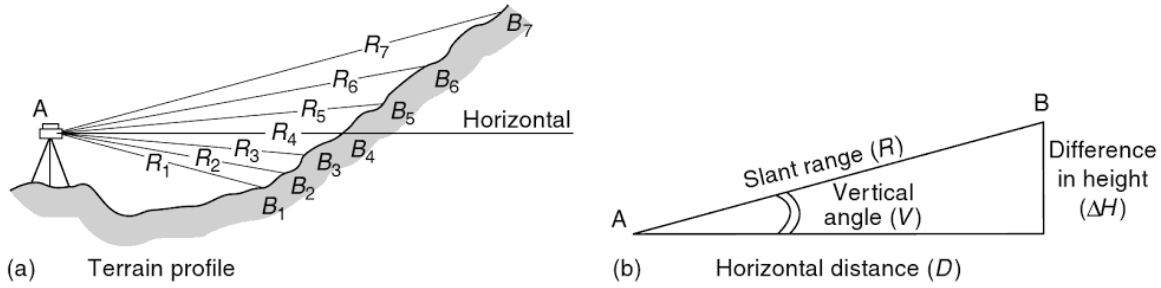

Figure 2.4 Working principle when creating a scan profile with LiDAR-technology. Using laser pulses, known position of the scanner and trigonometry to define the position of points. From Shan and Toth (2008).

Certain weather conditions are unfavorable when acquiring LiDAR-data. These are precipitation, fog, warm winds, very bright ambiences, and wet surfaces (Jaboyedoff et al., 2012).

2.4 Hazard assessment developed at NGU

Hazard assessment classification is based on nine criteria, where each criterion is assigned a probability. This is one of the strengths of the classification system, because it allows to express a high degree of uncertainty for some criteria. The hazard classification focuses solely on aseismic failures, due to today's incapability to predict earthquakes (Hermanns et al., 2012b).

2.4.1 Hazard classification

The nine criteria that defines the hazard classification are (see appendix B for examples):

1. Development of the back scarp.
2. Potential failure surfaces.
3. Development of lateral release surfaces.
4. Kinematic feasibility test.
5. Morphologic expression of the basal rupture surface.
6. Landslide displacement rates.
7. Change of displacement rates (accelerations).
8. Increase in rock fall activity on the unstable slope.
9. Presence of post-glacial events along the affected slope and its vicinity.

Each criterion offers several possible conditions that are assigned different scores. The sum of scores all criteria gives the total score. The total score, or hazard score (ρ), can range from 0-12 with an increment of 0.25. It is assumed that the likelihood of failure increases with ρ.

For effective communication and simplification, the hazard score is divided into five hazard classes with equal intervals. Probability for each hazard class is obtained by summing the probability of the hazard scores falling within the range of the hazard class (Table 2.1). In addition, the hazard class is correlated with the safety demands in the Norwegian regulations on technical requirements for structures (TEK 10). Annual probability for rock avalanche is 1/100 if the hazard score is above 9.6, 1/1000 if the hazard score is above 7.2 and 1/5000 if the hazard score is above 5.5 (Figure 2.5). The following considerations has been done when placing the probabilities in the risk matrix (Blikra et al., 2016):

1. The annual probability of 1/100 is placed based on the statistical probability of 2-3 fatal rock avalanches occurring in 100 years. Unstable rock slopes show signs of deformation several decades, and probably centuries before they collapse. Three scenarios in Norway are classified with this likelihood so far, which seems suitable to the statistical frequency.
2. Risk matrixes normally have a logarithmic scale both in probability and consequence. The probability of 1/5000 is placed in a logarithmic scale within medium hazard class.
3. Scenarios without movement should generally plot with lower probability than 1/5000, thus without consequences for urban planning.

Table 2.1 A fictive hazard assessment, showing the hazard classes, and the probability for each class both with the decision tree analysis and the normal distribution. For further information see Hermanns et al. (2012b).

Hazard class	Hazard scores ρ	Probability	
		Decision tree analysis	Normal distribution
Very low	[0.0; 2.4]	0.0 %	0.4 %
Low	[2.4; 4.8]	31.9 %	32.9 %
Moderate	[4.8; 7.2]	59.9 %	62.9 %
High	[7.2; 9.6]	8.2 %	3.8 %
Very high	[9.6; 12.0]	0.0 %	2.0%

2.4.2 Risk matrix

The hazard score and the potential life losses are combined into a risk matrix (Figure 2.5). The purpose of the risk matrix is to aid the decision of whether a rock slope should be periodically or continuously monitored. Most of the unstable rock slopes in Norway fall within the blue category. At such sites, further actions are not economically viable due to low consequences, or the geological conditions needs to change dramatically for the slope to fail (Hermanns et al., 2012b).

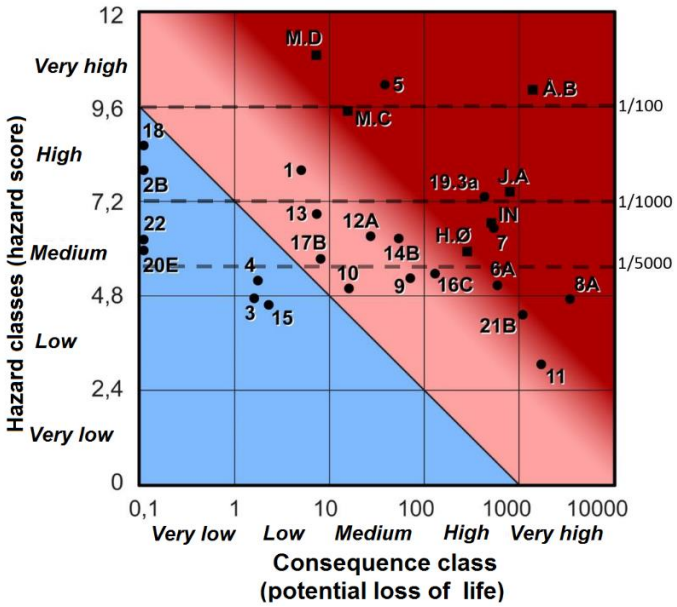

Figure 2.5 Risk matrix, with a few already classified unstable slopes. Blue = low risk; bright red = moderate risk; red = high risk. Note the transition zone between moderate and high risk, as well as the annual probabilities for failure on the right side, following TEK 10. Edited from Blikra et al. (2016).

2.4.3 Simple geological mapping

Simple geological mapping is conducted to gather information on all the criteria that are necessary for the final hazard classification. These criteria are: back scarp, potential sliding

structures, lateral release surfaces, morphological expression of the rupture surface, kinematic analysis, displacement rates, acceleration, increase in rock fall activity spatially, and past events (further explained in the hazard classification section). If an unstable slope is categorized within the light red or red risk classes (Figure 2.5), more thorough mapping must be carried out and/or periodic displacement rate measurements (Hermanns et al., 2014).

2.4.4 Periodic displacement measurements - detailed geological mapping

A straightforward way to reduce uncertainties in the hazard analysis is to assess the current displacement rates with monitoring equipment. Extensometers, differential Global Navigation Satellite System (dGNSS), satellite- and ground based InSAR with and without reflectors, terrestrial laser scanning (TLS) and photogrammetry are some of the techniques currently used at NGU (Hermanns et al., 2014).

Sites where simple kinematic models (as explained in section 2.4.3) cannot explain the observed deformation, more complex kinematic models need to be developed. It requires additional field mapping to develop such models (Hermanns et al., 2014).

2.4.5 Establish scenarios for the final hazard and risk classification

Scenarios are defined based on structural and morphological mapping, in combination with results of displacement measurements. If the structures do not vary over the entire unstable slope, and the slope deforms uniformly, a single failure scenario is likely. Several scenarios need to be defined for slopes that show different displacement rates, varying structural conditions (i.e. domains), and/or internal scarps, cracks and depressions that dissects the unstable slope (Hermanns et al., 2012b).

For each scenario, the hazard and automated run-out analyses, followed by consequence analyses must be performed, which leads to the risk classification (Hermanns et al., 2014).

2.4.6 Kinematic feasibility test

A kinematic analysis is conducted to check if the mapped discontinuities and the slope are oriented in such a manner that the slope is likely to fail, and what failure mechanism that is most likely. Possible failure modes are planar sliding, wedge failure and toppling. Criteria for the different failure modes are shown in stereographic plots in figure 2.2. Standard criteria from rock mechanics are used, as described by Hoek and Bray (1981) and Wyllie and Mah (2004). However, multiple slopes mapped in Norway show that failure does not follow these simple failure modes (i.e. Sollie, 2014; Böhme et al., 2016; Rem et al., 2016; Krogh, 2017).

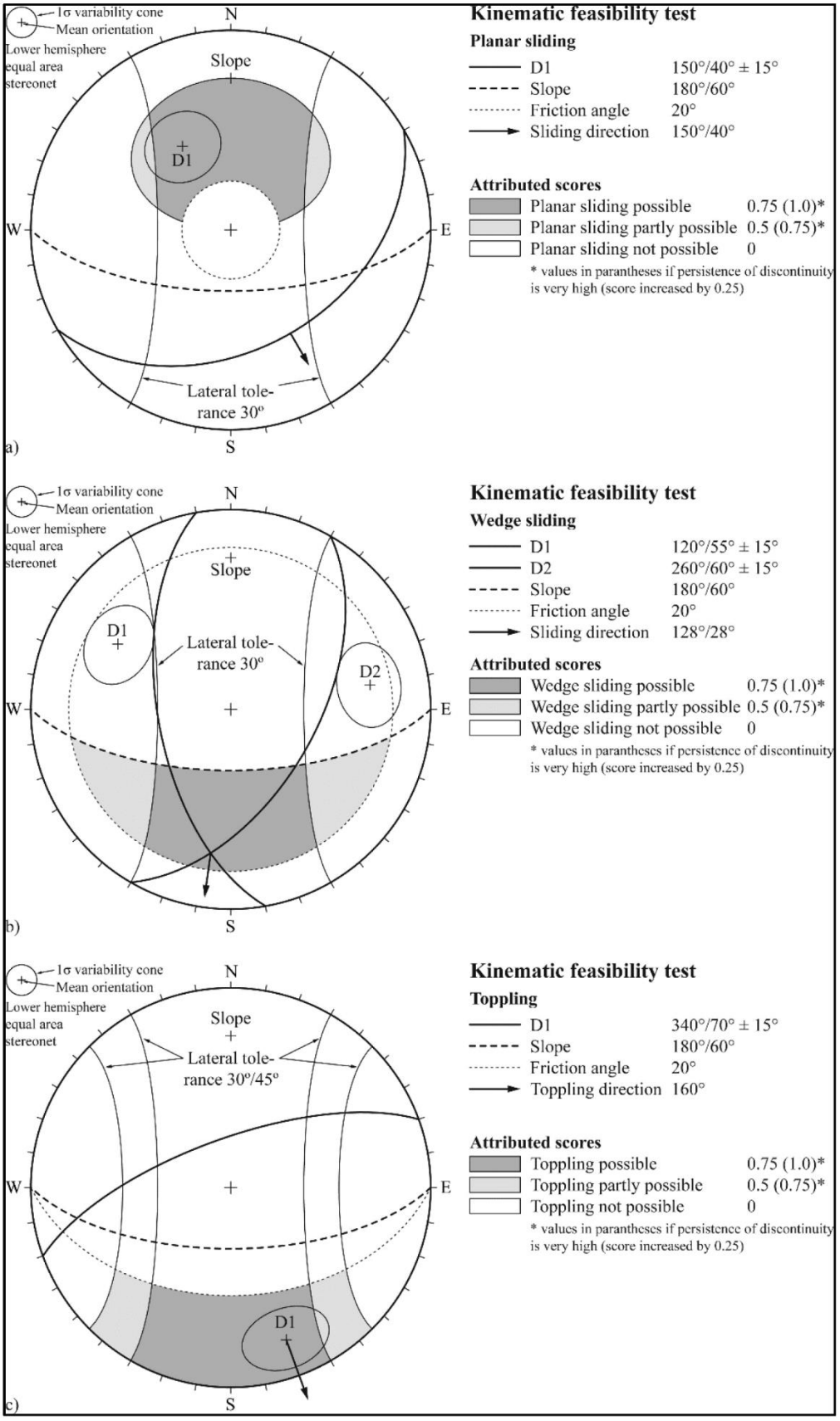

Figure 2.6 The criteria for the kinematic feasibility test of a fictive slope for a) planar sliding, b) wedge sliding, and c) toppling failure. If the difference between sliding direction and slope aspect is smaller than 30°, and if the persistence of discontinuities is very high (>20 m, according to Atkinson et al. (1978)) the score is increased by 0.25. From Hermanns et al. (2012b).

The friction angle is the dip angle which has to be overcome in order for a discontinuity to fail (Wyllie and Mah, 2004). Lateral tolerance is the difference between the aspect and the sliding direction. Hermanns et al. (2012b) recommends a friction angle of 20° and a lateral tolerance of 30°. However, the feasibility test assigns planar failure and wedge failure *partly possible* (score 0.5) if the difference between aspect and sliding direction is greater than 30°. For toppling failure, *possible* (score 0.75) is assigned if the difference between the dip direction of the discontinuities and slope aspect is less than 30°, and *partly possible* (score 0.5) if the difference is less than 45°. A 20° friction angle is a very conservative value, but is used due to the complexity of the discontinuities and the variable slope aspect (Hermanns et al., 2012b).

Persistence of the discontinuities is also considered; this is of specific importance for the planar and wedge failure. The score of the kinematic feasibility test is increased by 0.25 if the persistence is very high relative to the unstable mass (Hermanns et al., 2012b).

2.4.7 Theory behind the tools for volume and run-out analysis used for consequence assessment

The consequence assessment consists of five main steps, of which steps one, two, and five are necessary for all unstable rock slopes. Steps three and four is only applied in instances with the possibility of a landslide hitting a body of water or damming a river. As with the hazard assessment this workflow is also iterative with increasing detail and workload with increasing risk (Oppikofer et al., 2016). Only step one and two have been carried out in this thesis, step five is the quantification of the loss of life. This step deals mostly with statistics and was left out to spend more time on geological matters (Oppikofer et al., 2016).

2.4.8 Step 1: Volume estimation

Estimating the volume of the defined scenarios is the first step of the consequence analysis and influences the rest of the consequence assessment. However, the estimations are challenging and involve large uncertainties because the delimitation in depth are often based on assumptions or models. This is also the case for the workflow developed at NGU, where the volume is calculated through the sloping local base level (SLBL), originally developed at the University of Lausanne (Jaboyedoff et al., 2004; Jaboyedoff et al., 2009; Jaboyedoff et al., 2015). The SLBL-method calculates a possible elliptic rupture surface Based on a DEM, delimitation, length, and height of the instability and the geological conditions like orientations of structures. The height difference between the estimated SLBL-surface and the surface of the DEM is used to calculate the volume of the scenario (Böhme et al., 2016). SLBL volume estimates are best suited for larger scenarios and scenarios not controlled by persistent structures.

2.4.9 Step 2a: Run-out analysis: empirical relationship

An empirical relationship between the angle of reach α and the volume, is the first step of the run-out analysis. By examining numerous landslides, several studies have tried to obtain the reach of a landslide as an empirical function of its volume and the potential fall height (Heim, 1932; Scheidegger, 1973; Hsü, 1975; Corominas, 1996; Blikra et al., 2001). Blikra et al. (2001) examined 25 Norwegian landslides, over 90% of the 25 events have a shorter reach than the best-fit curve from Scheidegger (1973), thus "Scheiddeggers curve" are contemplated as conservative in the Norwegian context (Figure 2.7).

An Excel-tool calculates the angle of reach α for the landslide based on the equation from Scheidegger (1973) (equation 1). The inputs are the estimated volume and height difference from the top of the instability to the valley bottom/fjord. Based on findings in Corominas (1996), the Scheidegger-equation does not fit landslides smaller than 250 000 m^3, therefore 31° as a constant angle of reach are used for smaller landslides.

$$\tan\alpha = \frac{H}{L} = 10^{0.62419} \times V^{-0.15666} \quad (1)$$

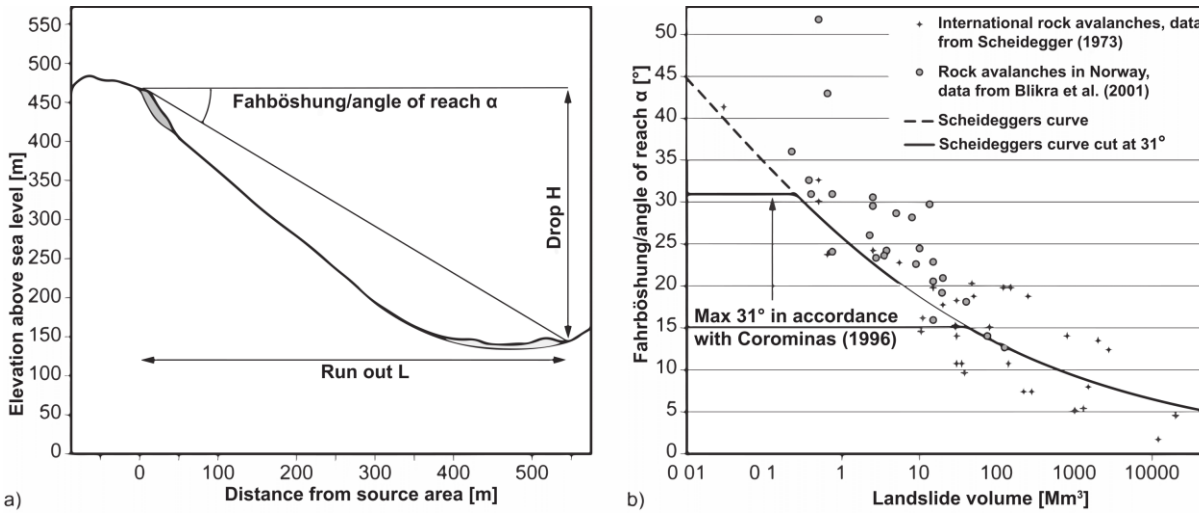

Figure 2.7 Empirical assessment of a landslides reach: a) schematic profile of a landslide; b) empirical relation between fahrböshung/angle of reach and volume, based on Scheidegger (1973). Norwegian rock avalanches (Blikra et al., 2001) in general have a higher angle of reach (i.e. a shorter run out) than Scheideggers best fit curve. Figure edited from Oppikofer et al. (2016).

2.4.10 Step 2a: Run-out analysis: Flow-R

A 2D run-out analysis is conducted with the software Flow-R (Horton et al., 2013). Flow-R was originally developed for modelling debris flows on a regional scale but has been adapted by Oppikofer et al. (2016) for modelling rock avalanches.

A DEM and a raster file with the source area is the only data inputs required to run a Flow-R simulation. Run out is calculated for every cell in the raster of the source area. Lateral propagation is calculated using multiple flow direction algorithms (Holmgren, 1994), modified to consider the thickness of the flow (landslide). The algorithm also consider that landslides tend to not change flow direction, addressed as the memory effect. It makes the landslide less affected by minor changes in the terrain. However, a certain opening angle is included to allow the landslide to change from cell to cell. The modified flow model of Holmgren (1994) is combined with the memory effect to calculate the probability of a flow spreading from one cell to the next. If the likelihood for spreading is less than a user defined value, the flow will stop (Oppikofer et al., 2016).

After the calculation of the spreading, the potential and the kinetic energy of the flow are considered based on a simple frictional model. In a landslide, the potential energy is transformed into kinetic energy and the landslide loses some energy, e.g. because of basal and internal friction. The energy loss can be represented by an energy line from the top of the instability and downwards with a certain angle φ. When this line cross the topography, all the energy is lost and the landslide comes to rest. This angle φ correspond to the fahrböshung or angle of reach α, calculated using Scheideggers relation (Oppikofer et al., 2016).

2.4.11 Step 2a: Run-out analysis: DAN3D

For 3D run-out analysis, DAN3D are used. If the Flow-R analysis show that a body of water or a river is within the run-out zone, DAN3D simulations are needed. The reason is that DAN3D calculates erosion and entrainment along the landslide track, which allows for a volume estimation of the mass that causes damming or displacement waves. The disadvantage is that DAN3D requires detailed input parameters that depend on local conditions. Such input parameters are best acquired through a back calculation of nearby landslides (Oppikofer et al., 2016).

2.5 Rockyfor3D

Rockyfor3D (Dorren, 2015) are used to simulate the run-out of rock fall. In this thesis, it was used to find the likelihood and reach for rock fall in the deposits below Rombakstøtta.

Rockyfor3D calculates the trajectories of single, individually falling rocks in three dimensions with the possibility to put forest into consideration. It is a probabilistic process-based rockfall trajectory model, due to the combination of physically-based deterministic algorithms with stochastic approaches (Dorren, 2015). Development of the model is based on earlier published research work, but also field observations, experiments, and tests with other published model algorithms. Rockfall trajectory is calculated as 3D vectors by calculating sequences of classical parabolic free fall and rebounds on the slope surface, including tree impacts if required. Rolling is represented by a sequence of short-distance rebounds, while sliding is not modelled.

As input data, Rockyfor3D requires a set of rasters. The main input is a digital terrain model (DTM) overlain by self-defined ASCII-rasters that add roughness-, surface-, and source area parameters to different polygons on the slope. Input also include block shape and size, which can be subject to a given variation. These ASCII-rasters were created in ArcMap, facilitating the toolbox PimpMyRockyfor which need two inputs; a shapefile containing the parameters needed, and a DTM. The toolbox was created by members of the Risk Analysis Group of the University of Lausanne (Nicolet, 2014).

Inputs representing the actual forest in the run-out area, can be added to the model by using the software Find Individual Trees (FINT) (Dorren, 2014). Where the user defines the minimum tree height to consider. The tree height is calculated with a normalized surface model (NSM). A NSM is the difference between a DSM and DTM, that is: the heights of the objects on the terrain (houses, vegetation, power lines etc.). These heights are obtained by processing the LiDAR-data in such a way that it contains only values for the first pulses, sorting out the points categorized as houses etc.

2.6 Basic principles of ^{14}C-dating

A piece of wood was dated to get an idea of a possible minimum age for a rock avalanche. Production of the radioactive carbon isotope ^{14}C is a natural secondary effect of cosmic rays bombarding the upper atmosphere. After production, it is oxidized within several days, and forms $^{14}CO_2$ which is distributed throughout the atmosphere. More than 95% of the $^{14}CO_2$ is absorbed in the oceans, only about 1% of the $^{14}CO_2$ are picked up by photosynthetic processes or in other ways incorporated in the carbon cycle. In living organisms, the metabolic processes maintain the ^{14}C levels in equilibrium with the atmosphere. When an organism dies, the amount of ^{14}C start to decrease by radioactive decay. For ^{14}C the radioactive half-life is 5730 ± 40 years. Eight half-lives are the limit for measurements. This means that it is possible to determine the

age of samples as old as 40000-60000 years depending on the method and amount of carbon available (Walker, 2005). Recent variability in ^{14}C production related to anthropogenic influence complicates determination of ages younger than 300 years. By using dendrochronology in combination with other dating methods, the atmospheric ^{14}C-levels before present have been reconstructed. This reconstruction is used to correlate a radiocarbon age to a calibrated age. 1950 is set to year 0 for radiocarbon ages, since this is close to the onset of nuclear bomb testing which altered the ^{14}C-levels significantly (Taylor, 1997; Reimer et al., 2009).

2.7 Schmidt hammer

The Schmidt hammer is a light (~1 kg), robust, and portable instrument that record the distance of rebound for a spring-loaded mass impacting a surface. The rebound distance (R) is related to the elasticity of the surface and thus its compressive strength (Nesje et al., 1994). In several studies, it has been used to measure the degree of weathering and as an indicator of surface age (Matthews and Shakesby, 1984; McCarroll, 1989; Cook-Talbot, 1991; Aa et al., 2007; Viles et al., 2011). The assumption is that more weathered rocks have lower rebound values than fresh surfaces. Most articles assume linear weathering rates. In this thesis, the rebound distances (R), were used for relative dating of separate lobes in the deposits below Rombakstøtta.

3 Methods

A total of 658 structural measurements were recorded as dip direction/dip angle on the most repeating and prominent surfaces in the unstable area. 947 measurements were recorded with Coltop3D (Metzger et al., 2009) for six different planes. However, these readings were narrowed down by removing outliers. If all Coltop3D-readings were put into the stereographic projection with the manual readings, the Coltop3D-readings would overshadow the manual readings. All coordinates are given in UTM WGS84 33N.

3.1 Geological mapping

3.1.1 Field work in the unstable area

A Freiberg geological compass was used for taking structural measurements in the field. It would have been favorable with more measurements from the field, but the time and the weather limited the fieldwork.

A Panasonic Toughbook field computer was used to ease the navigation and to recognize patterns from the shaded relief of the DEM, in the field. It was intended to use it more actively in the mapping of scarps, cracks, and morphological features in the deposits, but unfortunately the screen was malfunctioning in heavy rain. For positioning the measurements, a handheld Garmin eTrex 20 GPS-device was used. These devices typically have an error of 3-6 m in open terrain (McCaffrey et al., 2005).

Seven scanlines were recorded perpendicular to the backscarp of the instability; they were divided into two categories: *precise* and *less precise*. For the *precise* scanlines, orientation, horizontal opening, roughness, Schmidt-hammer R-values, and deepness of all open joints were recorded. For the closed joints, all the former was recorded if possible. In the case of the *less precise* scanlines, only orientation and opening were noted. In addition, the start and stop position and the total length of the scanline were recorded as well as the amount of intact rock. All the measurements were done along a measuring tape lying on the ground perpendicular to the back scarp. The sampling was a simplified version inspired by Priest (2012). The dip of the measuring tape was recorded as well.

3.1.2 Deposits

The longest axis and shortest axis were measured, and the roundness and sphericity were estimated for 600 blocks within the depositional area. These blocks were divided on six stations (100 blocks in each station) and within each station, the blocks were touching each other.

In total 300 Schmidt readings were recorded, divided on 50 Schmidt readings at 6 individual blocks, three blocks in each of two separate lobes. The lithology and size of each block were noted. Notes and pictures of morphological features were taken as the deposits were surveyed.

3.1.3 Sources of error for the work conducted in field

In the case of the scanlines, error can occur because of slack in the measuring tape and heavy winds over wide joints during the measuring process. Results will also suffer from linear sampling bias (Priest and Hudson, 1981). The results would benefit from more data on the structural variations within the unstable area.

The Schmidt-hammer is intended for use on concrete, but has qualified to be useful on rock surfaces as well. However, issues such as surface smoothness, weathering, lichen cover, and moisture content influence the results. Measuring R-values perpendicular to the foliation may give errors in the result because of small joints along the foliation that take up all the force (Aydin and Basu, 2005).

When measuring the weathering rate of the deposits we found it necessary to scrub off moss and dirt with a steel brush because of the extensive moss cover.

The deposits were covered in a thick layer of moss with some soil beneath it. In some places this affected the ability to see the blocks, and therefore it became harder to measure and describe them.

3.2 Photogrammetric models and photo panoramas

As mentioned in the introduction (Table 1.1), a 1-m resolution DEM obtained through LiDAR-scanning was available of the study area at Rombakstøtta. However, models with even greater detail allow for more precise determination of limits etc. To achieve such a model, numerous photos of the study area were captured from helicopter, in a systematic manner.

Due to the size and complexity of the slope, the density of the photos was not high enough to generate a complete 3-D photogrammetric model without holes. Thus, various photo panoramas for selected slope sections were constructed. The panoramas were made in the free software Image Composite Editor (ICE) 2.0 created by Microsoft (Microsoft, 2015). Photo panoramas that were stitched together wrong in ICE were treated in Hugin (d'Angelo, 2016). A free software that does the same as ICE, but allows the user to interact more in the process.

The photo panoramas contained a lot of information regarding the morphology, but they were not georeferenced. However, it was possible to recognize details in the panoramas and compare

them to the georeferenced aerial photos. Thus, details in the panoramas could indirectly be georeferenced.

When producing panoramas, it is necessary to pay close attention to the result, and compare it with actual overview photos of the area, as ICE sometimes can composite photos wrong but still make it look “natural”.

3.2.1 Sources for error in the GIS-analysis

A perfect orthorectification of the aerial photos in ArcMap 10.4 was hard to create, due to the limited amount of easily recognizable fixed points in the area. This may have affected the measurement of area and distances in some areas, and could also affect the volume calculation. However, for the placing of discontinuities along the scanlines the correlation between the measured distance in the field and the measured distance in ArcMap 10.4 were good for most of the scanlines.

3.3 Structural analysis

The structural analysis was done utilizing the software Dips 7.0 from Rocscience (2016a). All orientation data were plotted in stereographic projection (dip direction/dip, lower hemisphere, equal angle, and Fisher distribution). Joint sets were determined from cluster analysis with density concentrations as recommended by Rocscience (2016b): density concentrations greater than 6% are considered very significant, 4-6% are considered marginally significant, and less than 4% are considered not significant, assuming the overall quantity of data is high. The cluster size cone was limited to a maximum of 30°. Mean poles are shown with a variability cone with a standard deviation of 1σ.

To visualize spatial variations in the mapped discontinuities, the measurements were divided into stations based on where they were taken. Then a stereographic plot was made for each station, a total of nine stations was created. A map with the plots is shown in appendix C

Readings on spacing and persistence of the joints were noted in the field, and estimations refined by analyzing georeferenced orthophotos in ArcMap 10.4.

To add more structural readings to the analysis and to catch the orientation of persistent planes, the software Coltop3D (Jaboyedoff et al., 2007) was used. This tool allows to pick dip direction/dip readings from areas in a point cloud. Compared to manual readings, this method provides a lot of readings since each point in LiDAR DEMs have information on the dip direction and dip at that point (Metzger et al., 2009). Because of the large amount of readings,

it can be hard to present this data in the same stereo projection as the manual data. This was considered by picking the values closest to the mean of the Coltop3D-values from a plane, and then adding those values to the stereographic plots. Only persistent planes were used for picking readings from the DEM.

3.3.1 Structural domains

Based on the change in the orientation of the backscarp, the unstable area was divided into two structural domains as shown in Appendix D. One eastern (pink) and one western (green) domain were defined. The measurements of the stations that fell under the two structural domains were replotted into two new stereographic plots. One station (stereographic plot in appendix C) was measured on a tilted block in the flat area between the instabilities, this block has tilted due to movement of the area, because of this it was left out from the structural domain plot (Appendix D).

3.3.2 Definition of failure scenarios

Analysis of the DEM, aerial phots, and the photo panoramas, and identification of possible delimiting structures such as back-scarps, lateral limits, and toe lines allowed to point out compartments of the slope that might fail in a single event. And therefore, define them as scenarios. In total eight scenarios were defined at Rombakstøtta. The structures delimiting each scenario are given in the results section.

3.4 Application of the hazard assessment from NGU

The hazard assessment was applied to Rombakstøtta based on the methodology described by Hermanns et al. (2012b) and Hermanns et al. (2013). An elevated level of uncertainty is assigned to the criteria where sparse data are available. Uncertainties are especially connected to the morphologic expression of the rupture surface and the displacement measurements. All nine of the criteria were assessed for the each of the eight scenarios.

3.4.1 Kinematic feasibility test

In this thesis, the kinematic analysis was executed in the software Dips 7.0 from Rocscience (2016a), according to recommendations given by Hermanns et al. (2012b).

Input values delimiting the failure envelope is of severe importance for the outcome of the kinematic analysis. Such values are slope aspect and dip, friction angle, and lateral limits. To not underestimate the possibility of failure, the slope dip values were taken separately from the steep main scarp and the shallower main body (Sollie, 2014). This enables to capture more critical conditions at the steep main scarp. The mean slope aspect was obtained by measuring

the back scarp in ArcMap 10.4 (ESRI, 2016) for both structural domains. Zonal statistics as table tool in ArcMap was used to generate mean and max dip for the main body and the back scarp separately (Böhme, 2016).

The inputs in the kinematic analysis are assembled in Table 3.1.

Table 3.1 Input values to the kinematic analysis assembled in one table.

Domain	Subdomain	Dip direction	Dip	
			Mean	Maximum
West, green	Main scarp	040	41	86
	Main body		54	
East, pink	Main scarp	355	73	86
	Main body		52	

3.5 Application of the consequence assessment

Parts of the consequence assessment developed at NGU are carried out in this thesis, i.e. the volume estimation and the run-out analysis. A toolbox developed at NGU lowers the work load and speeds up this process by creating a standardized procedure.

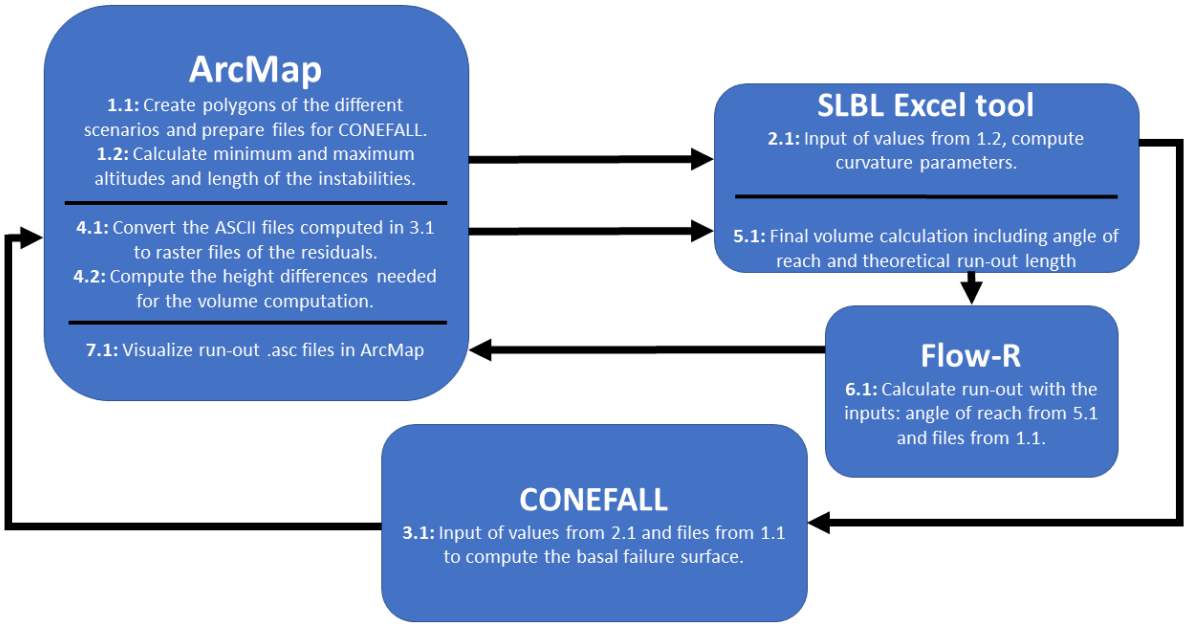

Figure 3.1 Conceptual workflow for the calculation of SLBL surfaces, volume and run-out analysis based on the procedure developed by NGU (Oppikofer et al., 2016). The procedure start in ArcMap.

3.5.1 Volume estimations facilitating the SLBL-method

The 1-meter resolution DEM was downscaled to 5-meter resolution for the steps shown in Figure 3.1. This reduces the calculation time, while it has minor effects on the final output (i.e. volumes and run-out) (Oppikofer et al., 2016). The initial input files in this process includes a DEM and polygons enveloping the different failure scenarios (Figure 3.1) (Oppikofer et al., 2016). An Excel-based tool, developed at NGU, was used to calculate the curvature parameters inputted to CONEFALL (Jaboyedoff and Labiouse, 2003). CONEFALL calculated the SLBL-surface, which were fed to the Excel-tool for the final volume calculation. Three SLBL-surfaces giving three different volumes are calculated ($V_{minimum}$, $V_{intermediate}$, $V_{maximum}$). Potential fall height and minimum altitude of the valley bottom, lake, or fjord are fed into the SLBL Excel tool, which estimates the reach based on the calculated volume (applying the theory mentioned in section 2.4.8).

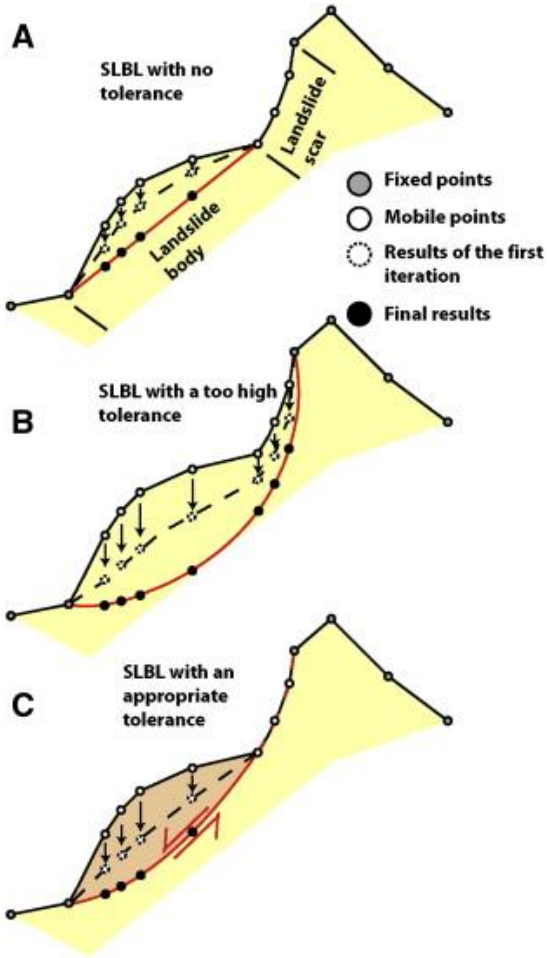

Figure 3.2 Illustration of the 3 different estimations for the SLBL; minimum, intermediate and maximum volumes. A) minimum volume, the SLBL is a straight line from back scarp to toe. B) maximum volume, the SLBL is vertical at the back scarp and horizontal at the toe. C) intermediate volume, the curvature tolerance fitted to the geometry input from the user, this is the most likely volume which should be used for the run-out analysis. Figure from Travelletti et al. (2010).

3.5.2 Flow-R and its inputs

One of the advantages of Flow-R is the low input requirement, as this model is made to be conservative. Angle of reach, delineation of the source area, and a DEM are the only input parameters required for the calculation.

Oppikofer et al. (2016) recommends a set of parameters that have been tested and proved to give trustworthy results in the Norwegian context:

- Exponent for the Holmgren (1994) multiple flow direction algorithm, x = 1
- Height modification of the Holmgren (1994) multiple flow direction algorithm, dh = 10 meter
- Memory effect, n = 25 cells
- Opening angle, θ = 120°

These parameters were used for the Flow-R simulations in this thesis, together with the volume created by the intermediate SLBL-surface.

3.6 Rockyfor3D

Rockyfor3D (Dorren, 2015) was used to separate rockfall deposits from landslide deposits. The model was calibrated with inputs similar to the 1996-rockfall, since this has a known source area, block size, and reach. The calibration also considered the reach of a few recent rock fall blocks that were observed in the field.

3.6.1 Inputs

Rock density was set to 2750 kg/m^3 based on values for the Quartzite-bearing gneiss and granite gneiss, and also mica schist in Dorren and Seijmonsbergen (2003).

Based on Breien and Høydal (2013) and references therein, the minimum tree height was set to 5 m, which with the standard formula (equation 2) for diameter at breast height (DBH) results in a mean stem diameter of 7.5cm.

$$DBH = H^{1.25} \quad (2)$$

where H is the tree height. Tree height values were randomized by ±20%. This diameter is conservative, as so small trees only has a neglectable effect in stopping 3-10 m^2 blocks. However, during tuning of the parameters, simulation with trees showed an effect on the run out length. Breien and Høydal (2013) found that even trees with low DBH can have an effect in breaking blocks, if the number of stems per area unit is high. Since the number of trees affected the workload and the calculation time to little degree, a decision to include more trees

was made. Trees with a height above 25 m were deleted, based on observations in the field. It is highly unlikely to find trees this tall in the field area, so these were thought to be artifacts or errors in the calculation of the NSM.

Polygons containing the ground parameters were drawn based on the aerial photos, observations, and photos from the field, while the parameters themselves were chosen based on the values proposed in Dorren (2015), and then altered in an empirical process to adjust the run-out lengths to those observed of blocks in the field. This empirical process was very time consuming, because new rasters with all the parameters were produced after every alteration of the inputs. Finally, the results were visualized in ArcMap 10.4.

3.7 Coherence between the source areas degree of fracturing and the deposits

To assess the fracture processes during the landslide events, the degree of fracturing in the source area was compared with the block sizes in the deposits. Data collected in the field included readings of the longest and shortest axis for 600 blocks from six separate stations in the deposits, as well as seven scanlines at the top of the instability.

Simplifications for calculating the block volumes both at the instability and the deposits were made. Volumes for the blocks in the deposits were estimated by the formula for a sphere (equation 3), where D is the mean of the longest and the shortest axis for each block (Charrière et al., 2016). Volumes in the source area were calculated based on the three scanlines (Figure 3.3) collected at the westernmost instability. Readings of the length from the edge of the slope, to the joints were overlain and compared to the most recent orthophoto of the area. The resolution of the orthophoto made it possible to recognize most of the joints recorded on the scanline in the field. A polygon of the block delimited by the joints were then drawn, and the area of the polygon was deduced from ArcMap. Then the volume was estimated by assuming the shortest axis of the blocks area equaled the thickness of the block, which is a strong simplification. Three profiles and volumes of 22 blocks were estimated this way.

$$\frac{4}{3}\,\pi\,\left(\frac{D}{2}\right)^{3} \tag{3}$$

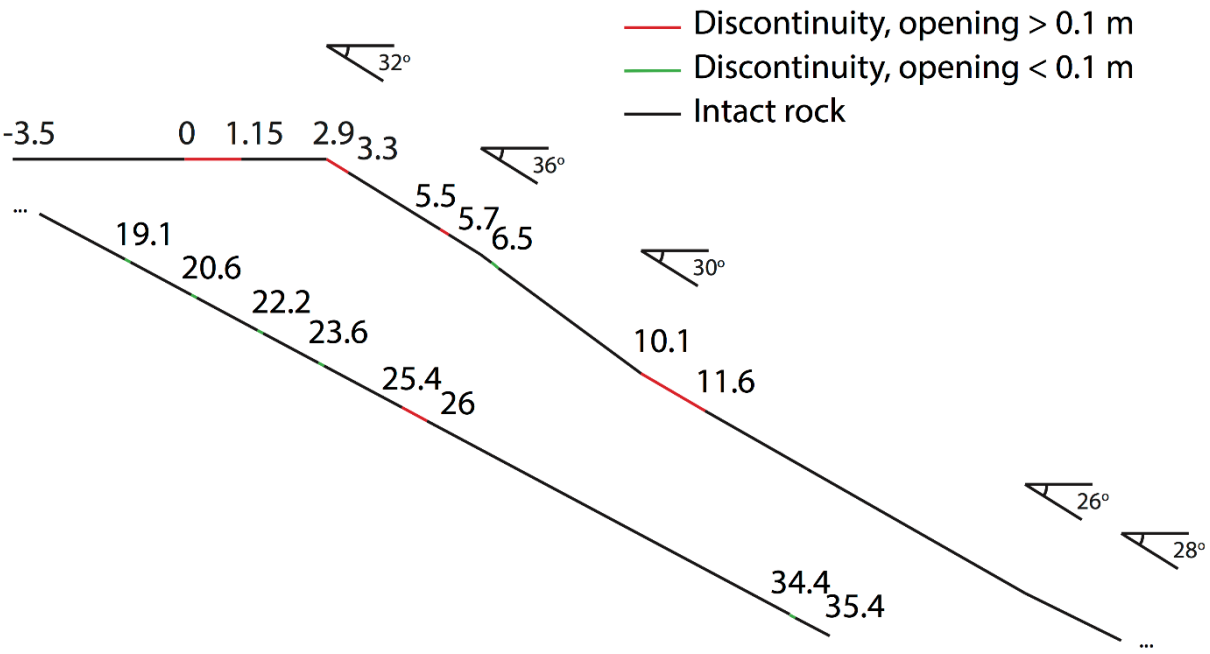

Figure 3.3 Example of a digitized scanline in profile. The numbers represent the distance from 0 in meters, and are measured to both sides of the joints. Dip of the slope was recorded as well, but have not been used in the calculation of block volumes. -3.5 m is at the edge of the slope, but 0 m in the scanline is at the edge of the first joint because the outermost block was completely detached from the rock mass, thus walking here was avoided because of safety reasons.

To model fragmentation of the blocks, a script was written in MATLAB (The MathWorks Inc., 2016). The script takes a vector with block volumes as input and creates a matrix where each row represents block volumes from a new breakage cycle as output (appendix E). Blocks are assumed to be broken into two random partitions of the original block in each cycle, although this is a strong simplification. The total original volume is kept through each cycle. Another script was written to plot the results as a semi-logarithmic block size distribution graph (appendix F). It is possible to assume the number of breakage cycles for the deposited blocks, by comparing graphs of the breakage cycles with the block size distribution graphs from the deposits.

3.8 Schmidt-measurements of deposits

A Proceq Schmidt L-type hammer was used to take R-value readings of the deposits. The intension was to do a relative dating of the deposits. Only sufficiently large blocks were chosen and a metal brush was used gently to remove moss and lichens on the surfaces. Information on the petrography and whether the surface was wet, moist or dry were noted. Impact points had a spacing of at least a plunger diameter, and 50 readings were taken on each block. The direction of the Schmidt-hammer during recording was noted in the field and the readings were corrected according to diagrams in Aydin (2008). As recommended by Aydin (2008) no measurements

were discarded, and mean, median, mode and the range of the readings are presented in the results (section 4.8).

3.9 Retrieval of the sample and ^{14}C-dating

A piece of wood was found squeezed between two large moss-covered blocks. The block on top provided shelter from the elements, so the wood was well conserved (Figure 3.4). From the bark, it was possible to tell that it was a pine tree. A hypothesis of the rock falling onto the tree, squeezing it and killing it, seemed feasible from the surroundings. So, a sample for C-14 dating was collected in plastic bags, and later wrapped in aluminum foil. The sample was brought to Trondheim for dating. The exact laboratory method for dating is not known.

Figure 3.4 The piece of wood from which the C-14 sample was retrieved, in its initial position.

4 Results

4.1 Geological structures

Orientation data in this thesis is given as dip direction/dip angle (###/##) measured in degrees. Magnetic declination is not considered. Variability is given as the radius of the variability cone in degrees, thus the variation applies to both dip direction and dip angle. The variability cone is calculated for one standard deviation (1σ).

4.1.1 Field investigations

As mentioned in section 1.4.3, two types of rock are found in the easily accessible part of the unstable area: a disthene-garnet-twin mica gneiss and a garnet-twin mica schist (Figure 4.1). These two rocks types are drawn as alternating in layers on top of each other in the bedrock map. The map indicates that there should be five contacts between these rocks within the investigated area. However, no contacts were found in field.

From the field investigations, most of the rocks in the unstable area can be categorized as gneiss, and in certain parts it contains large garnets. In some parts the mica content is high, and the mica form large sheets that are clearly visible to the naked eye.

The surface of the rocks is weathered and overgrown with lichens. This makes it difficult to recognize the mineral composition in the field and to see spatial variation in the rock mass. However, some beds were protruding from the rock along the foliation as a witness of beds of more resistant minerals.

There is a gentle folding in the rock. The folding undulates slightly and was discovered by studying the variation in the foliation (Figure 4.2).

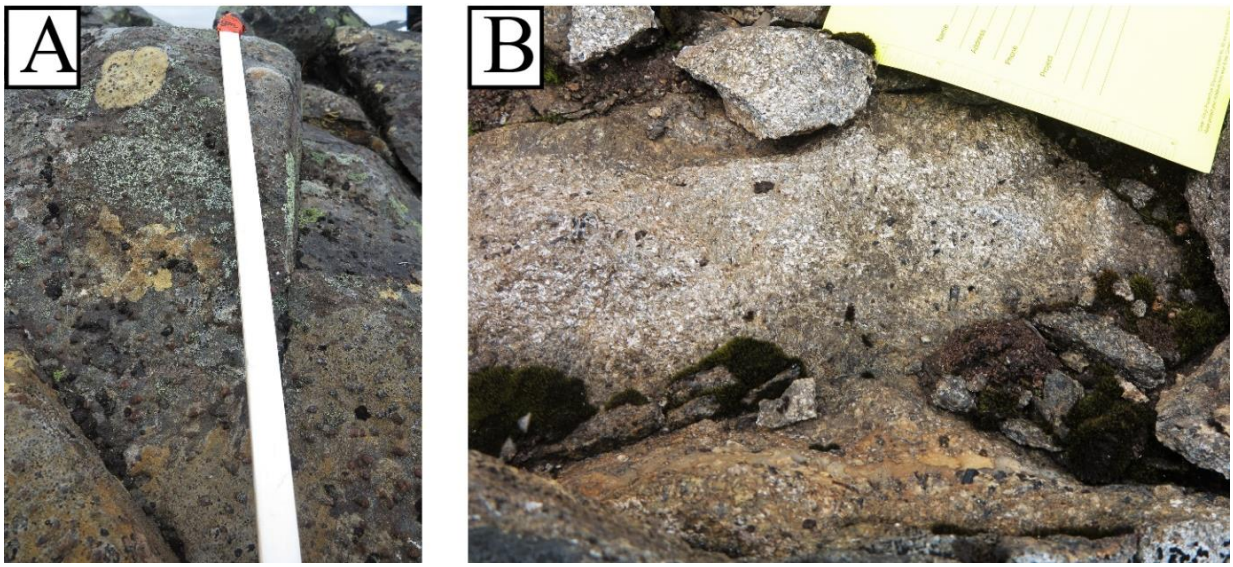

Figure 4.1 Close-up photo of the bedrock in central parts of the instability at Rombakstøtta. A) Disthene-garnet-twin mica gneiss. The scale is ca 2 cm wide. B) Note the large garnets, the presence of mica is also visible to the naked eye. The large dark prism-shaped mineral is most likely hornblende in the garnet-twin mica schist.

Figure 4.2 Lines drawn along the foliation, which is slightly folded. The folding varies within the study area.

4.1.2 Foliation (SF)

At first glance the foliation in the area is pronounced, however the degree of foliation varies within the instable area. Orientation of the foliation (denoted SF) varies in the two domains, as seen in the stereographic plots in appendix D and Table 4.1. However, the variation of one domain is within the variability cone of the other domain.

Table 4.1 The mean foliation in the two domains, and the number of poles from which it is calculated

Domain	Dip direction/dip ± 1σ	Number of poles in domain
West, green	281/19 ± 16	453
East, pink	278/27 ± 16	149

Sheet minerals, like mica, make the rock more foliated as the lamellar minerals align during metamorphoses and cause the foliated weakness in the rock (Shea and Kronenberg, 1993). This is likely to be the case here. The foliation is sub horizontal, resulting in few open cracks along the foliation.

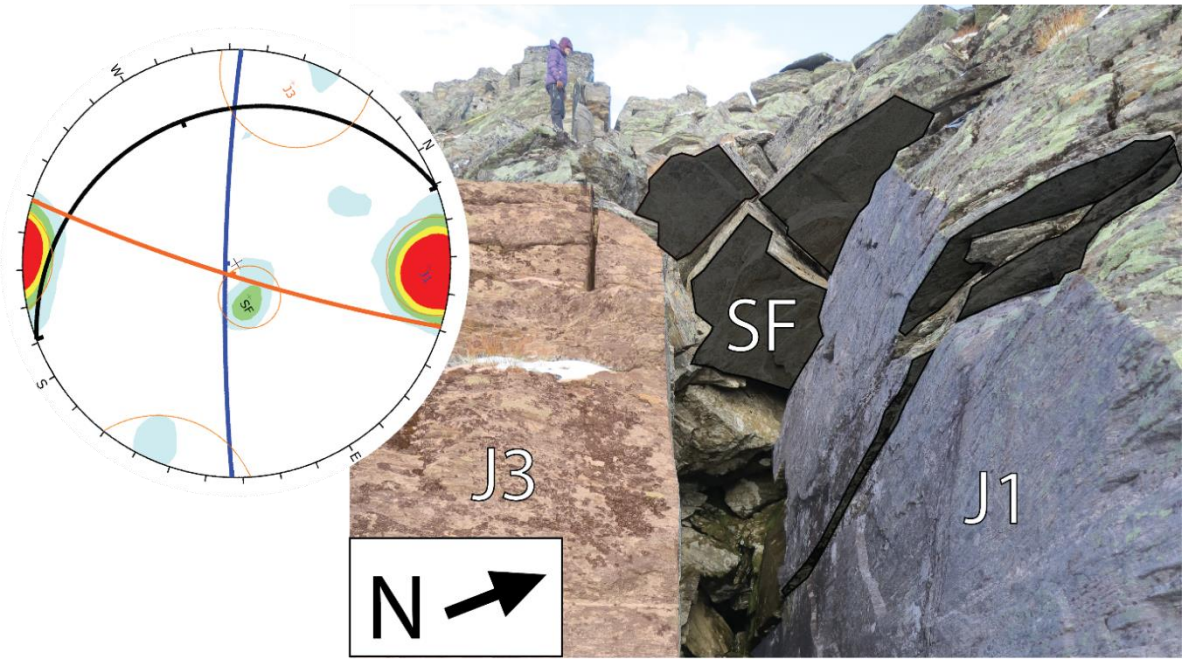

Figure 4.3 Picture taken towards NW-W in the western domain. Showing the foliation (SF), joint set 1 (J1) and joint set 3 (J3), looking at the foliation from below. The stereographic plot is oriented relative to the photo. Person in the background for scale

4.1.3 Joint sets

There have been defined two joint sets in the west domain (J1 and J3 shown in Figure 4.3) and three joint sets in the east domain (J1, J2 and J3). Joint sets in the two domains have similar orientation, in fact all mean poles of the plane sets lie within the variability cone of the corresponding plane set in the other domain (Table 4.2). As mentioned in section 3.3.1, the domains were divided based on the orientation of the back scarp, not the structural measurements.

Table 4.2 The mean joint sets of the two domains. J3 and J2 (bold) in the western domain was defined even though the density concentration of the contours were below 4%. Poles with density concentrations below 4% is considered not significant according to Rocscience (2016b).

Domain	Joint set 1	Joint set 2	Joint set 3
West, green	213/84 ± 14	093/65 ± 16	***139/83 ± 22***
East, pink	205/84 ± 20	099/58 ± 15	143/81 ± 19

Persistence and spacing of the joint sets varied throughout the field area, therefore the estimations are given as intervals, not single values (Table 4.3).

Table 4.3 Partly measured, partly estimated values of spacing, persistence and opening. Given for east and west domain. It is hard to estimate the values for joint set 2 from orthophotos, and values were not collected in the field.

Plane set	Spacing [m]		Persistence [m]		Opening [m]	
	West domain	East domain	West domain	East domain	West domain	East domain
Foliation	0.05 – 0,5	0.05 – 0,5	0.5 - 10	16	-	-
Joint set 1	0.3 - 2	0.3 - 2	0.1 - 130	0.1 - 60	0 – 6	0 – 0.1
Joint set 2	-	No data	-	No data	-	No data
Joint set 3	0.5 - 2	0.5 - 7	0.1 - 5	0.5 - 40	0.01-0.1	0-0.2

4.1.4 Joint set 1 (J1)

Joint set 1 is a steeply dipping (84°) plane that is very prominent throughout the field area. This joint set forms cracks, often with large openings. These cracks are the most persistent, and often form smooth surfaces (Figure 4.3). The back scarp in the main instability follow this joint set, it also forms cracks in the east domain. It is easily recognized and easy to measure, therefore this is the plane with most poles (205 for the west domain and 45 for the east domain). The spacing varies a bit, but in general the plane is closely spaced. Cracks following J1 step from one joint to another. Joint set 1 is found both in the west and the east domain. As mentioned, the main scarp in the west domain follow J1 (Figure 4.4), while in the east domain J1 only form cracks with minor openings (up to 10 cm).

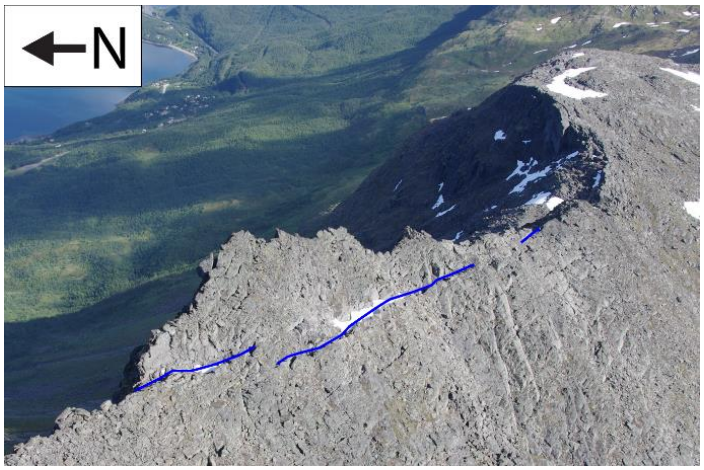

Figure 4.4 The back scarp of the scenario 1.B in the western domain follow J1 (blue line), the crack is partly filled with snow in this photo. Photo by Martina Böhme, 2015.

4.1.5 Joint set 2 (J2)

Joint set 2 (J2) could only be defined from data collected in the east domain with the density concentrations recommended by Rocscience (2016b). However, some poles can be seen in the west domain, but with lower density concentrations. The plane can be found in the field and on photos in the west domain as well, however, it is not as protruding as in the eastern domain (Figure 4.5).

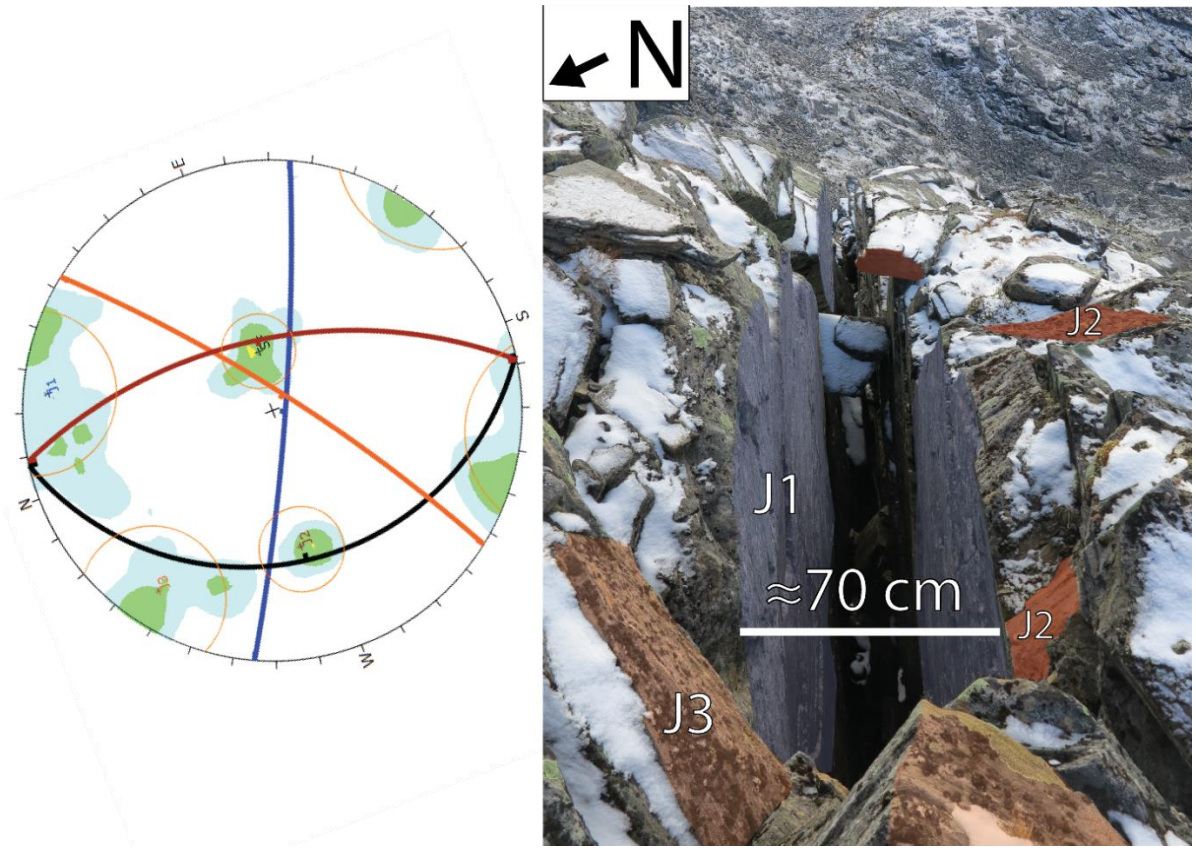

Figure 4.5 Stereographic plot from east domain oriented relative to the photo. Photo is edited to display planes better, the colors for planes in the photo is the same as in the plot.

4.1.6 Joint set 3 (J3)

This joint set is found both in the east and west domain, with the mean plane steeply dipping towards NW (143/81 ± 19, for the east domain). In the western domain the mean contour of this plane only has 2-3% density concentration which is below the recommendations (Rocscience, 2016b). However, it was found both in field and on photos (Figure 4.3) so its presence is well documented. It is possible that joint set 3 forms lateral release surfaces for scenario 1, and most likely this joint set formed lateral release surfaces for the 1996 rock fall.

4.2 Results of the kinematic analysis

This chapter is dedicated to present the results of the kinematic analysis from the two structural domains defined in chapter 2.2.1.

4.2.1 West domain (green)

Kinematic analysis of the west domain, with the mean slope angle (Figure 4.6, left), show that direct toppling along an intersection between SF and J3 is partly possible. Planar failure along J1 is also possible within the variability cone, in this case SF would provide a lateral release surface. However, only if lateral release surfaces are not considered. Wedge failure is partly possible on the intersection between J2 and SF. With max slope angle (Figure 4.6, right), direct toppling is possible along the intersection between J1 and J3. And partly possible along the intersection between SF and J3. In these cases, SF would be a release surface. Planar failure is partly possible along J1 (within the variability cone) with SF as one lateral release surface. Wedge failure is possible on the intersection between J3 and J2, and partly possible on the intersection between J2 and SF.

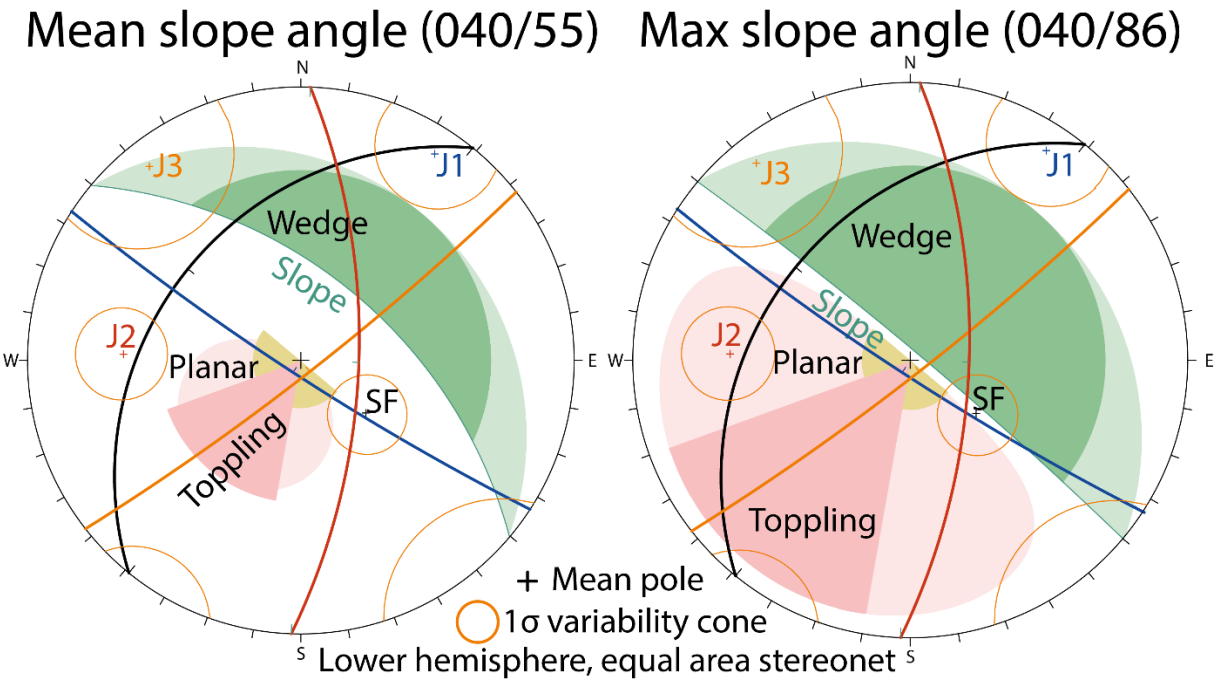

Figure 4.6 Result of the kinematic feasibility test in the west domain. Friction angle set to 20° and lateral tolerance 30°.

4.2.2 East domain (pink)

In the eastern domain, the kinematic feasibility test highlighted that direct toppling is possible along the intersection between J1 and J3. J2 would in this case represent the surface on which the blocks topple. This is the case, both for mean and max slope angle and are highlighted in by Figure 4.7.

Figure 4.7 The most striking instability (4.D) in the eastern domain, clearly look as a possible toppling failure.

Wedge sliding is possible on the intersection between SF and J1 with mean slope angle. Additionally, it is possible at max slope angle sliding along the J2/J3. Planar sliding is a possibility within the variability cone of SF, however, it isn't possible within the lateral limits of 30° (Figure 4.8).

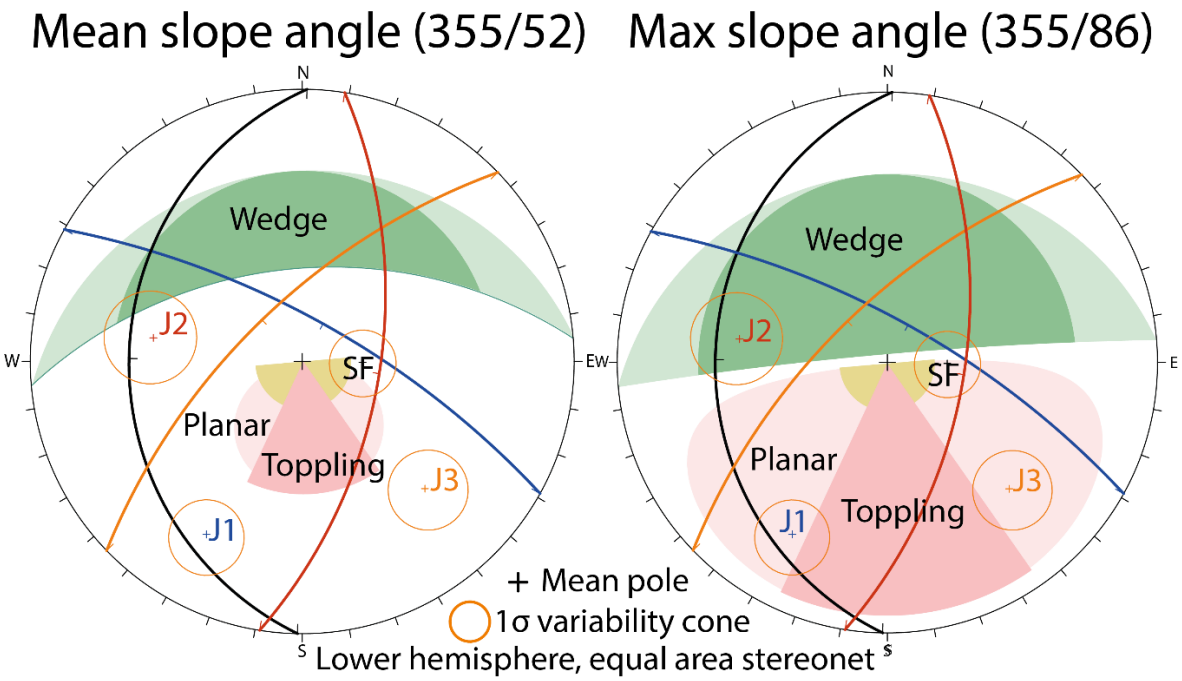

Figure 4.8 Result of the kinematic feasibility test in the east domain. Friction angle set to 20° and lateral tolerance 30°.

4.3 Failure scenarios and their run-out analysis

Based on field observations and remote sensing, and following recommendations in Hermanns et al. (2012b), eight scenarios have been defined. In volume, the medium SLBL calculations of the scenarios range from 10 000 m^3 to 4 650 000 m^3 (Table 4.4). Thus, between rock slide and rock avalanches. Spatially, the backscarp of the scenarios lie within one kilometer from each other. A numbering system from 1 to 4 is used for the scenarios, with a suffix of letters according to the size of the scenario. #.A represents the scenario with the largest volume, while following letters are used for smaller scenarios (Figure 4.9).

The results for the run-out modelling in Flow-R are given in this chapter. However, some scenarios have similar run-outs, so to increase the legibility, a few run-out maps can also be found in appendix G.

Table 4.4 Results of the volumes estimated through the SLBL method.

Scenario	Area [m^2]	Estimated volume [10^6 m^3]		
		Min. SLBL	Med. SLBL	Max. SLBL
1.A	40625	1.37	3.34	3.9
1.B	6500	0.10	0.21	0.22
2.A	4050	0.02	0.12	0.13
3.A	100550	1.32	4.65	6.33
4.A	90775	1.09	3.17	5.04
4.B	17275	0.20	0.40	0.60
4.C	1950	0.02	0.03	0.04
4.D	575	0.01	0.01	0.01

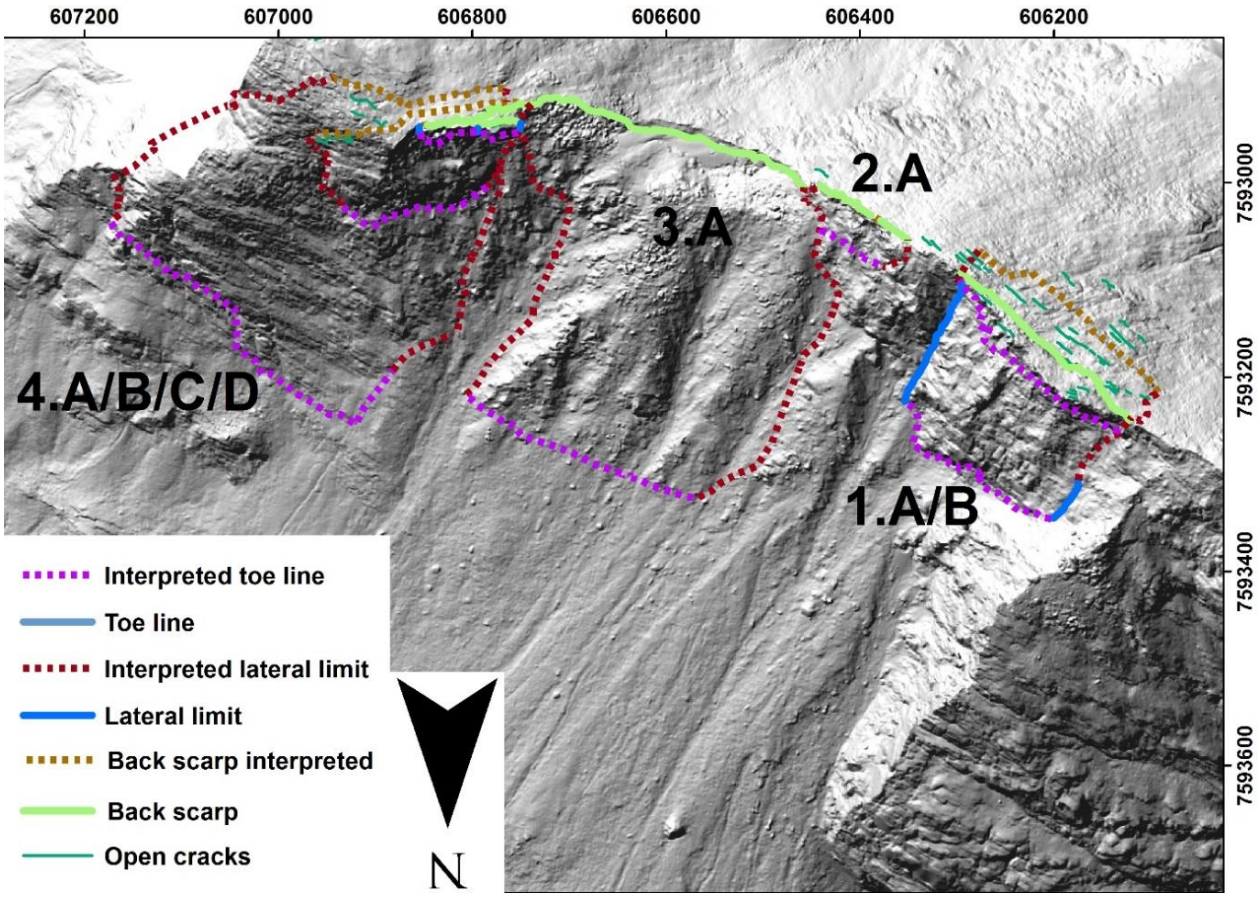

Figure 4.9 Overview of the different scenarios identified at Rombakstøtta. The largest scenarios are assigned with an A, and smaller scenarios with subsequent letters.

4.3.1 Scenario 1.A and 1.B

Scenario 1 is the westernmost scenario, and the scenario connected to the area with the prominent crack. 1.B is the smallest of the two, where the prominent crack is interpreted as the backscarp while the toe line is set along a break in slope. Which also have areas of crushed bedrock. At the top and in front, it does not seem like this block have been subject to much internal deformation.

Profiles perpendicular to the back scarp were taken from the DEM. And compared to each other and to possible basal rupture surfaces. This process resulted in the decision to place the backscarp for 1.A (the largest of the two) along cracks and depressions further into the plateau. The lateral limits were set along cracks and depressions in an almost perpendicular line to the back scarps. Along these lines, evidence of springs was detected. The toe line was set at the break of slope, in the transition from bedrock to scree deposits. By studying reports from the rock fall of 1996 and photos from the field, the rock fall scar from 1996 (Figure 4.10) was found within scenario 1.A (Larsen and Domaas, 1997). Measurements in ArcMap suggest a missing volume of ~300 m^3 (15 m×5 m×4 m) in the scar, while Larsen and Domaas (1997) suggest 50-100 m^3.

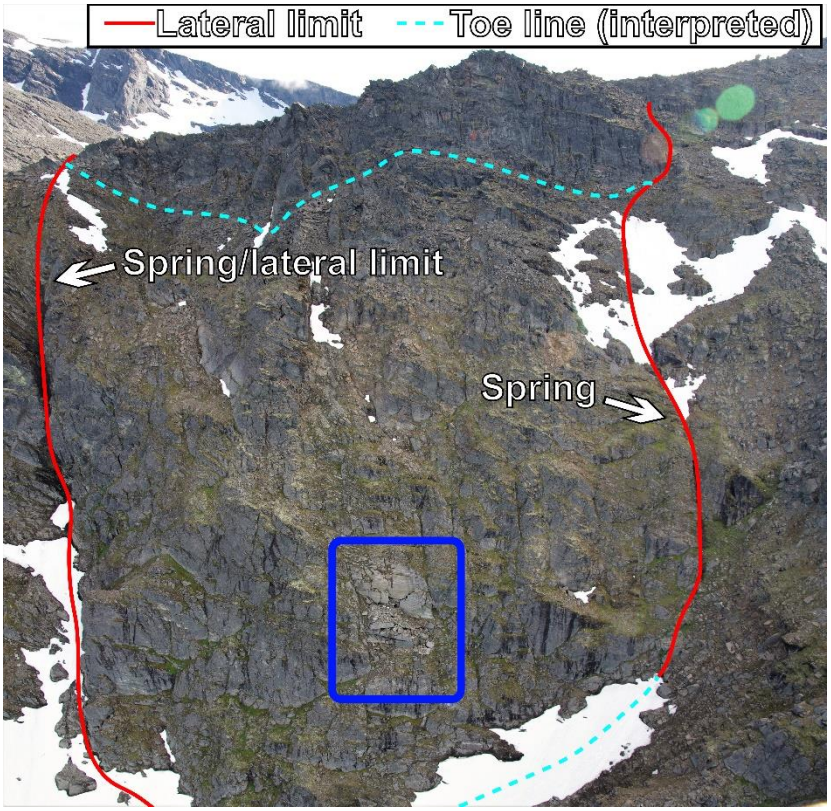

Figure 4.10 Scenario 1.A and 1.B. Interpreted lateral limits and toe lines are drawn. Note that there is at least one spring, possibly two at the interpreted lateral limits of the instability. The open back scarp/open cracks endpoints are where the lateral limits start. The red rectangle envelops the rock fall scar from 1996. Note that the lateral release surface on this scar follows a sub-vertical joint set, most likely J3.

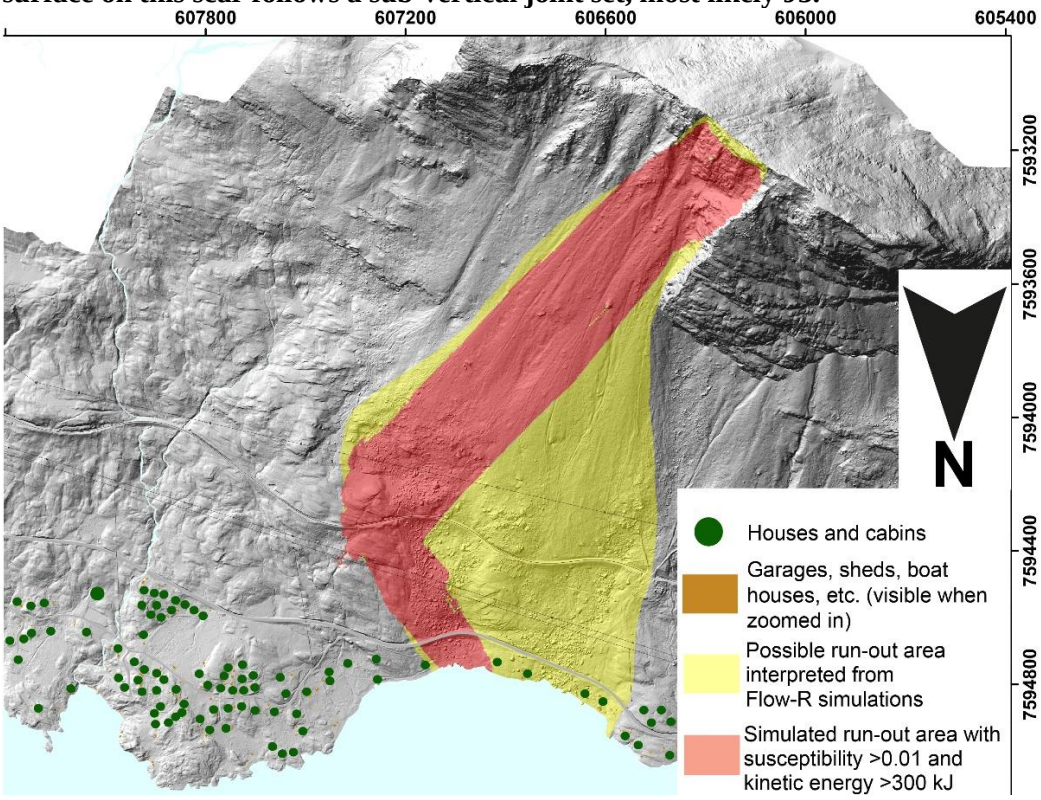

Figure 4.11Run-out analyses of scenario 1.B using Flow-R.

In accordance with the empirical run-out, the modelled run-out from Flow-R, will strike the fjord. Scenario 1.B (Figure 4.11) and scenario 1.A (Appendix G) both have similar run-out distances. Power lines, Ofotbanen, the E6 highway, and a few cabins are situated within the modeled run-out area.

4.3.2 Scenario 2.A

Scenario 2.A is located along the main backscarp ca. 120 m south-east of scenario 1. It is a rather small scenario, which seems to be an old scar. There is less vegetation within and below scenario 2.A than the surroundings, which may indicate recent rock fall activity in this area. The western delineation of the scenario is marked by the end of an open and prominent crack, which also makes up the back scarp of this scenario. Within the scenario there are also observed numerous loose blocks that can come down independently from any rock slope failure. The minimum SLBL volume is estimated to ~100 000 m^3, thus just passing the criteria for the definition of a rock avalanche. Neither the lateral limits nor the toe line are clearly delineated. Thus, the lateral limits and the toe line are interpreted from DEM and photo panoramas. The run-out for scenario 2.A can be found in Appendix G.

4.3.3 Scenario 3.A

Scenario 3.A represents the largest of the scenarios, both in area and volume. The back scarp follows a clear drop in the terrain, where the top "plateau" makes a 3-8-meter step along a scarp dipping about 60° towards a northerly direction. The easternmost 120 m of the back scarp is interpreted to be along a set of cracks, which delimitates an area of chaotically tilted large blocks. The characteristic drop suggests that the entire area has moved downslope. However, from evidence at the back scarp this seem like a slow process. It is difficult to exactly delimitate the lateral limits and the toe line. Therefore, a conservative approach was taken, and the toe line was set at the foot of the exposed bedrock. The lateral limits follow depressions and gullies in the terrain. Emphasis is put on the uncertainty of the extent of this scenario.

Figure 4.12 shows that the modelled run-out for scenario 3.A reaches the fjord in several places, it also passes over power lines, Ofotbanen, and the E6 highway in several places. A few houses and cabins could be reached as well.

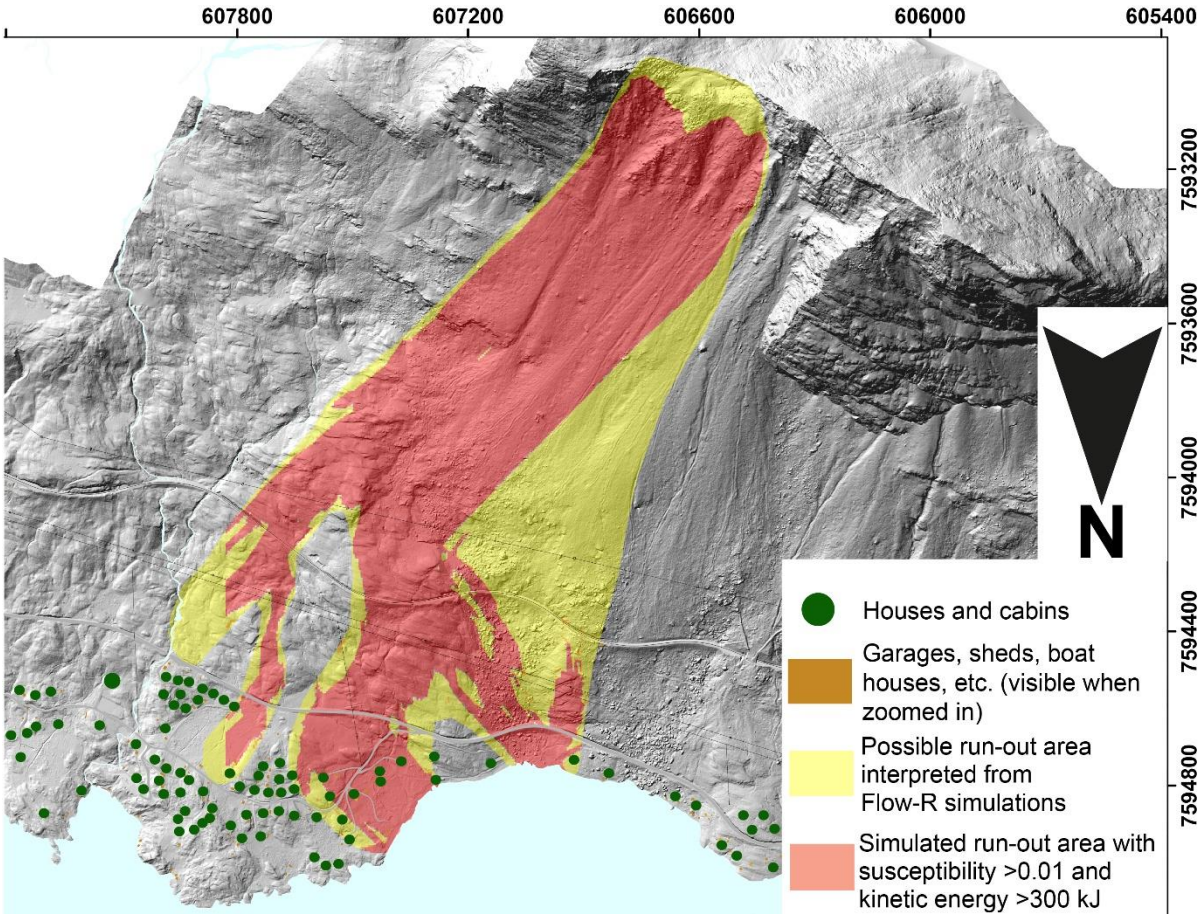

Figure 4.12 Run-out analyses of scenario 3.A using Flow-R.

4.3.4 Scenario 4.A

This is the second largest scenario in extent and the third largest in volume, with an intermediate SLBL volume of 3.17×10^6 m^3. Smaller scenarios are incorporated within the boundaries of the larger scenario, and assigned with a subsequent letter. Its back scarp is set partly along a depression and partly along a system of cracks in on the plateau. The cracks are only open with a few centimeters and there is not observed a lot of deformation within the delimitated area. However, it is worth noticing the depression in the area between the back scarp of scenario 4.A and 4.B as it appears a few decimeters lower than its surroundings. On the photo panoramas of the area, a set of cracks was observed that is defined to be a part of this scenario´s eastern lateral limit. The DEM is incomplete in the area where the eastern lateral limit is thought to be, this increased the uncertainty of the interpretation which had to be based on aerial photos only. Limitation to the west is set along the edge of an incision carving into the scree deposits. The toe line follows the border between exposed bedrock and scree deposits. However, the placement of the toe line is also uncertain. It would have been favorable with more photos in this area to lower the level of uncertainty.

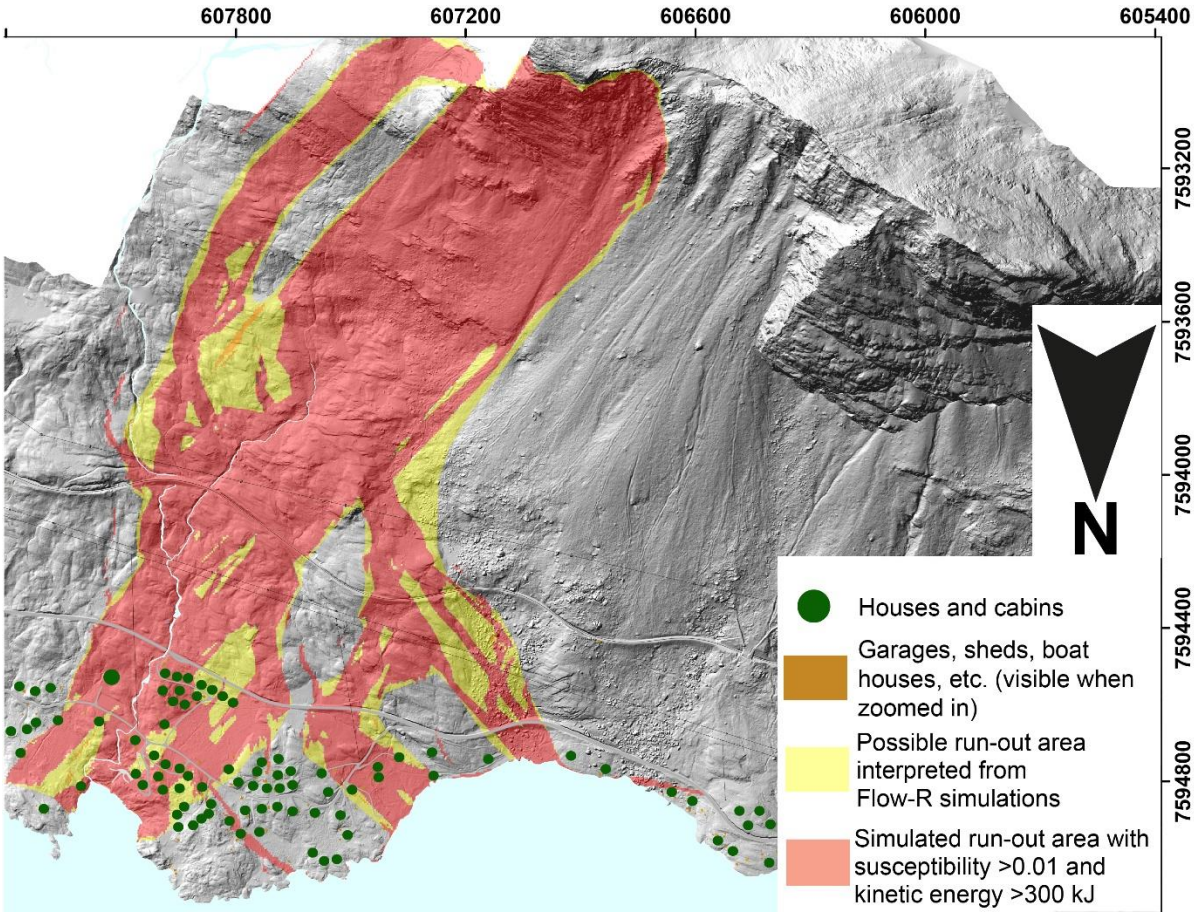

Figure 4.13 Run-out analyses of scenario 4.A using Flow-R.

Flow-R modelling of scenario 4.A (Figure 4.13) are affected by the hole in the DEM, which creates artifacts in the run-out distance. The easternmost lobe is the most prominent result of this. The main direction for the rock avalanche is toward the community of Straumsnes, and run-out modeling of scenario 4.A indicates that this scenario reaches more buildings than any other scenario.

4.3.5 Scenario 4.B

Scenario 4.B (Figure 4.14) is considerably smaller than 4.A, and has a different back scarp. 4.B's backscarp is set along a gentle depression, with cracks partly opened to 5 cm. A low degree of deformation is observed close to the back scarp, but it increases when approaching the back scarps of 4.C and 4.D which is incorporated in this scenario. To the east, the lateral limit follow several cracks that were observed on the photo panoramas, while the western limitation is shared with the top part of scenario 4. A's lateral limit. The toe line was interpreted along the foot of a step in the exposed bedrock. Scenario 4.B show a run-out that reaches Ofotbanen and the power lines.

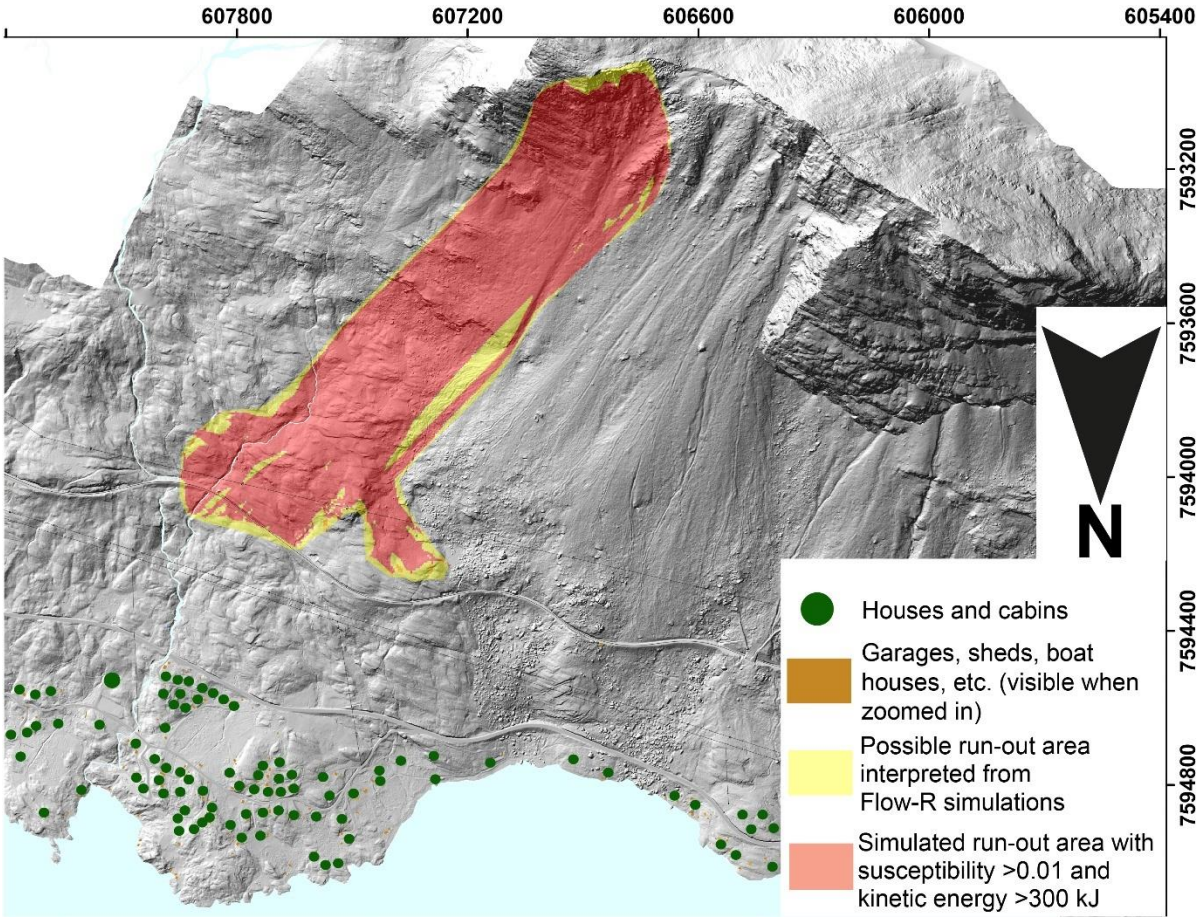

Figure 4.14 Run-out analyses of scenario 4.B using Flow-R.

4.3.6 Scenario 4.C and 4.D

Volume-vise, scenario 4.C and 4.D are below the Norwegian definition of a rock avalanche. They have a prominent backscarp; a crack ranging from centimeters to meters in opening. Scenario 4.C includes a very deformed rock mass in the east that consists of several large blocks. The lateral limits are almost non-existing, as the instabilities are very narrow. The toe line is placed at the foot of the first vertical drop from the plateau. Some crushing of the bedrock is observed along the toe line on the panorama photos. Scenario 4.D is a large detached block in the front of scenario 4.C, and the failure mode is thought to be toppling. Volume estimations from the SLBL method resulted in ~1000 m^3. By measuring in ArcMap and calculating it as a rectangular block, a volume of ~2000 m^3 was estimated.

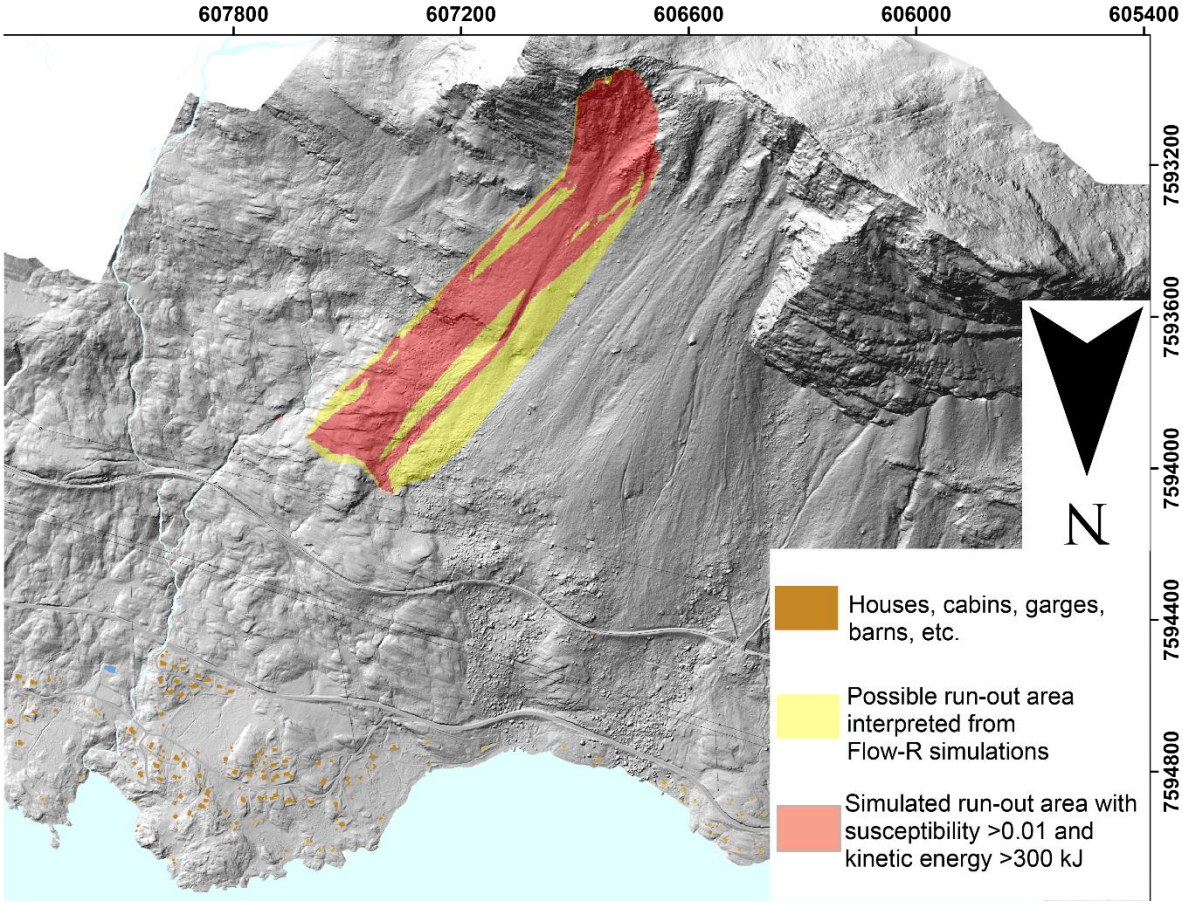

Figure 4.15 Run-out analyses of scenario 4.C using Flow-R.

The run-out for scenario 4.C (Figure 4.15) does not reach vital infrastructure, and the volume is below the volume defining a rock avalanche. It should rather be categorized as a rock fall, with twice to four times the volume of the 1996 event.

4.4 Results from the hazard assessment

The hazard assessment was done following the recommendations described in Hermanns et al. (2012b) and with personal guidance from Reginald Hermanns and Martina Böhme. A complete report for each scenario and with comments to each criterion can be found in appendix B. Resulting hazard scores are summarized in Table 4.5, and in the risk matrixes (appendix H).

Table 4.5 Summarized results of the hazard assessment for all the scenarios. Detailed information on every criterion can be found in Appendix B

Scenario	Intermediate SLBL volume [m^3]	Max hazard score	Mean hazard score	Hazard class
1.A	3.34	8.8	5.6	Medium
1.B	0.21	9.5	3.75	Medium
2.A	0.12	9.0	5.79	Medium
3.A	4.65	8.25	5.17	Medium /Low
4.A	3.17	9.0	5.42	Medium
4.B	0.40	9.25	6.03	Medium
4.C	0.03	9.25	6.42	Medium
4.D	0.01	10.00	7.47	High

Two scenarios stand out, scenario 3.A has a slightly lower hazard class and higher volume, compared to the other scenarios. While 4.D has a higher hazard class and lower volume. For scenario 1.B the difference between the max and mean hazard score is very big.

4.5 Rockyfor3D – rock fall analysis

Rock fall blocks in four different volume classes were simulated; 0.4-0.6 m^3 (A), 3.4-5 m^3 (B), 7.8-11.3 m^3 (C) and 10.4-15 m^3 (D). The range from 0.4-15 m^3 is chosen because it is similar to the mean block volume in the stations that are considered to be affected by rockfall (pkt400, pkt397, pkt405, pkt391 and pkt413 in Table 4.6). The source areas were chosen based on field observations and steepness of the slope. The size of the bins is set a bit smaller than the mean diameters, in order to take the breakage of the blocks into account. For A and B, 5 262 000 blocks were simulated, while for C and D, 2 631 000 blocks were simulated, however, both results have been normalized over 10 000 years. This was achieved with data on rock fall activity in the area in NVE´s online database (skredhendelser) (Norwegian Water Resources and Energy Directorate, 2017). In total six rock fall events reaching the railway near Rombakstøtta are registered. These entries account for about 100 years as the registering started in 1920. Assumingly, not all events have been registered in the database, however, assuming all six events happened inside the study area, this is compensated for. Judging from the size of the scree slope below the instability, the 2.1 km of railway inside the study area is also the most active rock fall area.

If each event consists of one block, and by extrapolating six events in 100 years to 10 000 years (as an approximation for the years since deglaciation) it makes up 600 events/blocks. By applying equation 4 and 5, it can be shown that the 2 631 000 blocks in the simulation would account for 43 850 000 years, and the 5 626 000 blocks would be 87 700 000 years. Thus, each raster cell represents the number of blocks passed in this amount of years. By using the raster calculator in ArcMap to divide each cell in A and B with 8770, and C and D by 4385, the number of blocks passing through each cell in 10 000 years is obtained (Figure 4.16).

$$\frac{600\ blocks}{10\ 000\ years} = 0.06\ \frac{blocks}{year} \tag{4}$$

$$Nr.of\ simulated\ blocks \Big/ 0.06\frac{blocks}{year} = Nr.of\ years\ simulated \tag{5}$$

These calculations are based on a series of assumptions and simplifications:

- 10000 years since deglaciation.
- One event in the database equals one block deposited.
- Six events over 2.1 km, when these events are spread over a larger area.
- Too little dataset to extrapolate into 10000 years.
- Same rate of rockfall in the last 10000 years as the last 100 years.
- Same tree cover during 10000 years, as the Rockyfor3D simulations was done with trees.

The validity of these assumptions is discussed in the discussion (section 5.4).

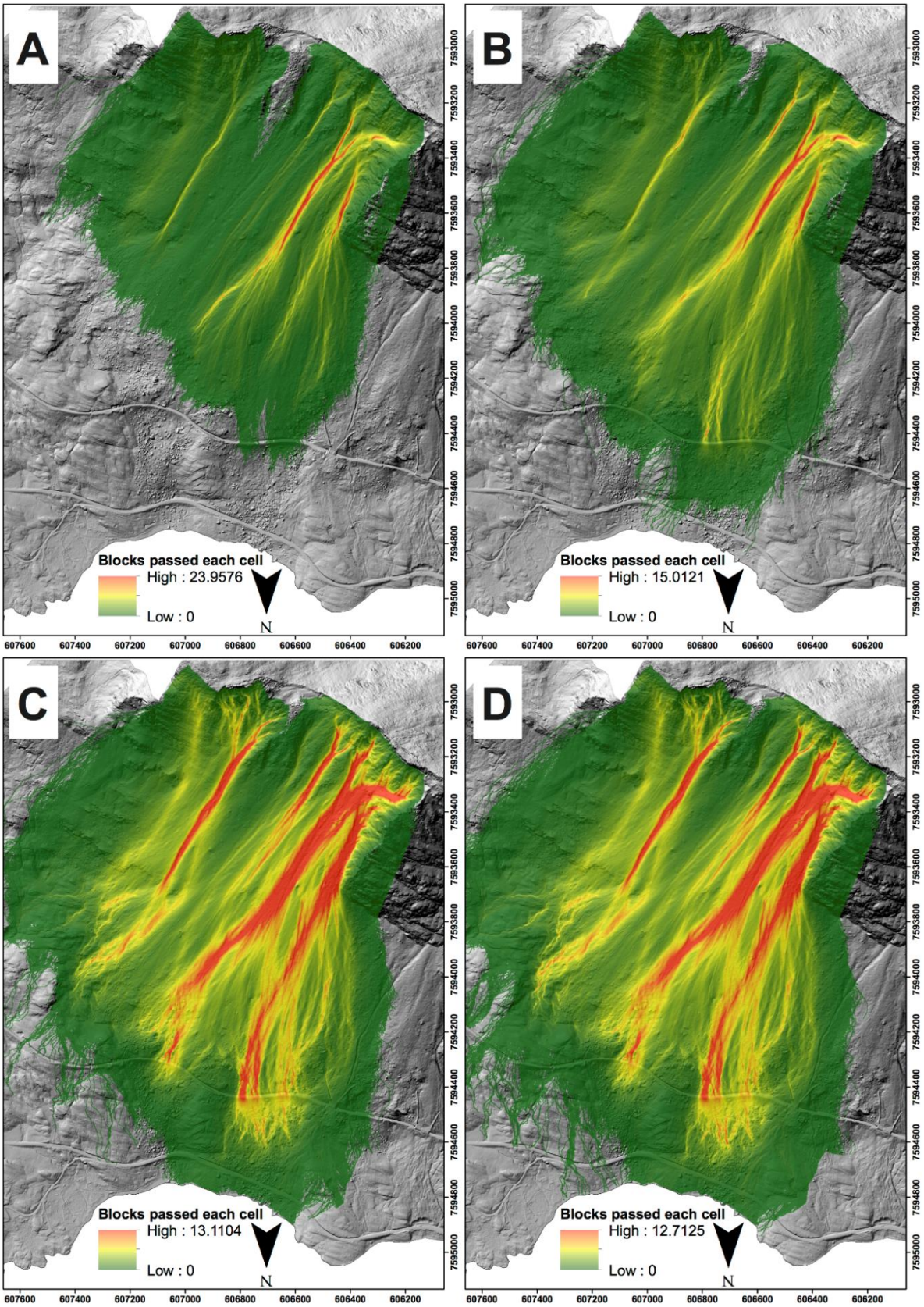

Figure 4.16 Maps showing the number of blocks assumed to have passed through each cell since deglaciation. Block volumes in each simulation is as follows: A) 0.4-0.6 m^3, B) 3.4-5 m^3, C) 7.8-11.3 m^3 and D) 10.4-15 m^3. The green shade could be considered a conservative maximum reach for each volume class.

4.5.1 A) 0.4-0.6 m^3

This is the smallest volume fraction, with the least kinetic energy and the shortest run-out. These small blocks are more affected by trees, than large blocks (Dorren, 2003). The simulated run-out near the easternmost yellow line is too short, compared to field observations. Measurement of blocks at pkt400 showed that almost 95% of the blocks here are in this volume fraction (Figure 4.17). This specific run-out length was hard to obtain by changing the input parameters to Rockyfor3D, as doing so overestimated the run-out lengths for larger block fractions. The blocks at pkt400 could originate from a source area further down than simulated, or the scree slope could have changed a lot since they were deposited.

4.5.2 B) 3.4-5 m^3

This volume fractions show slightly longer run-out, than in A). The possibility of reaching the railway increases. However, the blocks are effectively stopped by the rugged terrain and the large blocks close to the railway. The blocks are so small that they probably are retarded by tree impacts as well.

4.5.3 C) 7.8-11.3 m^3 and D) 10.4-15 m^3

These two volume fractions are a bit overlapping, and their run-out length are quite similar as well. However, the larger volume fraction has a slightly longer run-out and more blocks have reached further. There are also a possibility of these blocks reaching the fjord, but it is very low. By increasing the volume more, the maximum reach would get longer, as the blocks have more kinetic energy. However, based on the persistence of discontinuities in the source area, it is considered unlikely that blocks larger than this stay intact during a rock fall.

The upper part of the lobes can be considered a transition zone, where most blocks pass by while some are deposited. In the lower part of the lobes, the number of blocks passed reflect the number of deposited blocks. Up to ~13 blocks have passed the most passed cells (1x1 m) since deglaciation, according to this model. The coarse deposits between the railway and road could have been reached by 5-13 blocks per cell.

4.6 Block sizes and fragmentation cycle analysis

To get a better overview of the spatial variations in the block size histograms they were plotted in a map, with their position indicated on a hillshade of the deposits.

Figure 4.17 show a gentle coarsening trend for deposits further away from the source area, the trend is easiest to recognize when comparing the red and purple stations (pkt400 and pkt384). However, the mean block size at pkt391 are the same as pkt384, even though pkt384 is further

away from the source. Both the red and the yellow station lack observations from the >100 m^3 fraction, unlike the stations further away from the source area. It is also interesting to note that the 22 blocks from the scanline in the source area have a considerably higher number of blocks in the larger fractions than the deposits. Note that the mean and median is considerably larger in the source area, than in any of the stations in the deposits (Table 4.6).

Table 4.6 Statistics for the block sizes. Note that the "source"-station only has 22 entries, while the other stations have 100 entries. Columns are ordered with increasing distance from source.

	Source	Pkt400	Pkt397	Pkt405	Pkt391	Pkt413	Pkt384
Mean	41.2	2.3	5.9	8.7	18.9	12.2	21.2
Median	21.6	0.1	1.1	1.3	1.6	1.6	3.6
Mode	0.7	0.1	0.8	0.5	0.9	0.1	2.6
Range	215.2	164.6	84.7	310.3	485.3	563.8	394.5

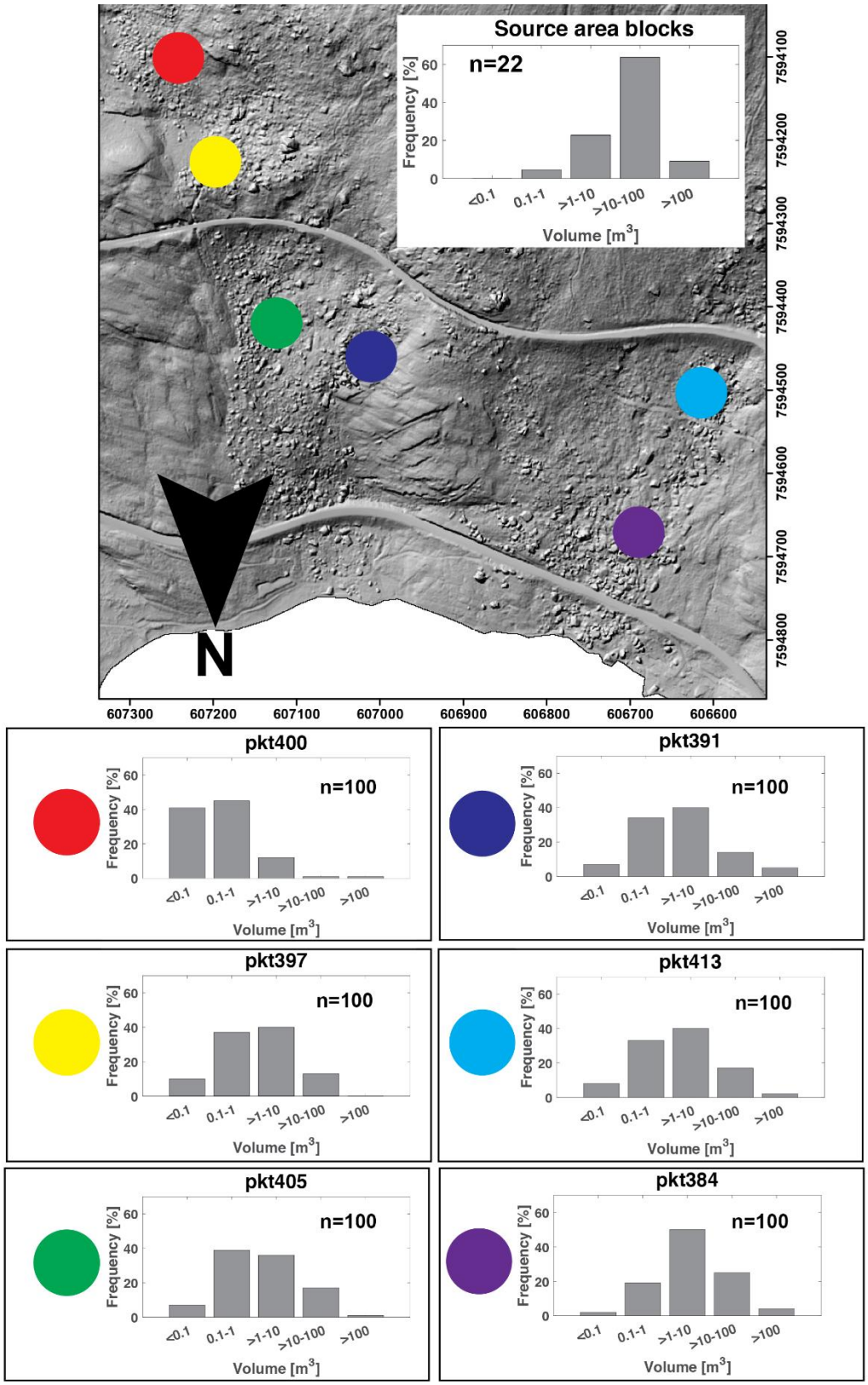

Figure 4.17 Histograms for the relative frequency (%) of rock volumes in the deposits, and one of the source areas at the top. Note that the histograms contain 100 observations, while the one in the map only contains 22 observations. The source area is to the south (upwards) outside of the map, while the fjord is the white to the north (downwards) in the map.

An estimation of the fracture cycles during the transport from the source area to the depositional zone was done with the MATLAB code crush_code.m as mentioned in the methods section 3.7.

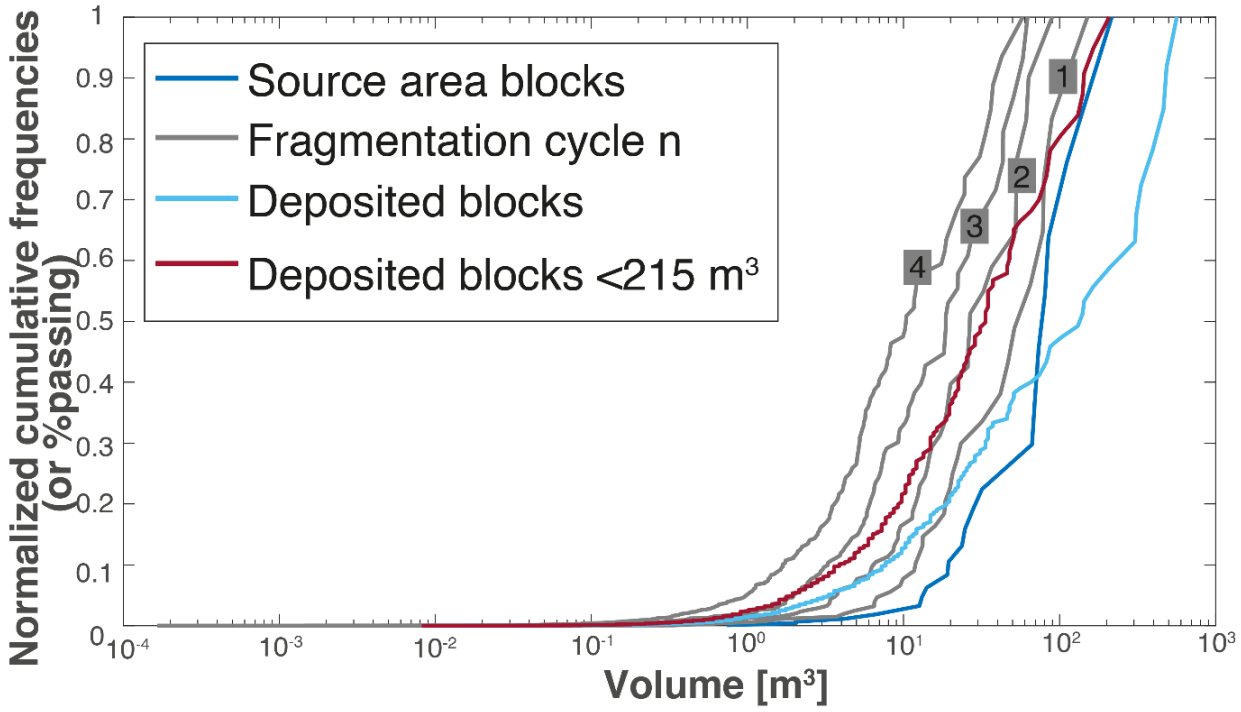

Figure 4.18 A semi logarithmic grain size distribution plot of the modelled and actual deposits at Rombakstøtta. Each line represents either the source area blocks, calculated fragmented blocks or the deposited blocks. Each plot does not represent the same sampling range.

Some of the blocks measured in the deposits were larger than the ones found in the source area. To make the data from the deposits fit better with the data from the source area, deposited blocks larger than the largest block in the source area (215 m^3) were removed. The resulting grain size distribution was plotted separately in Figure 4.18. The number of interpreted fragmentation cycles are summarized in Table 4.7.

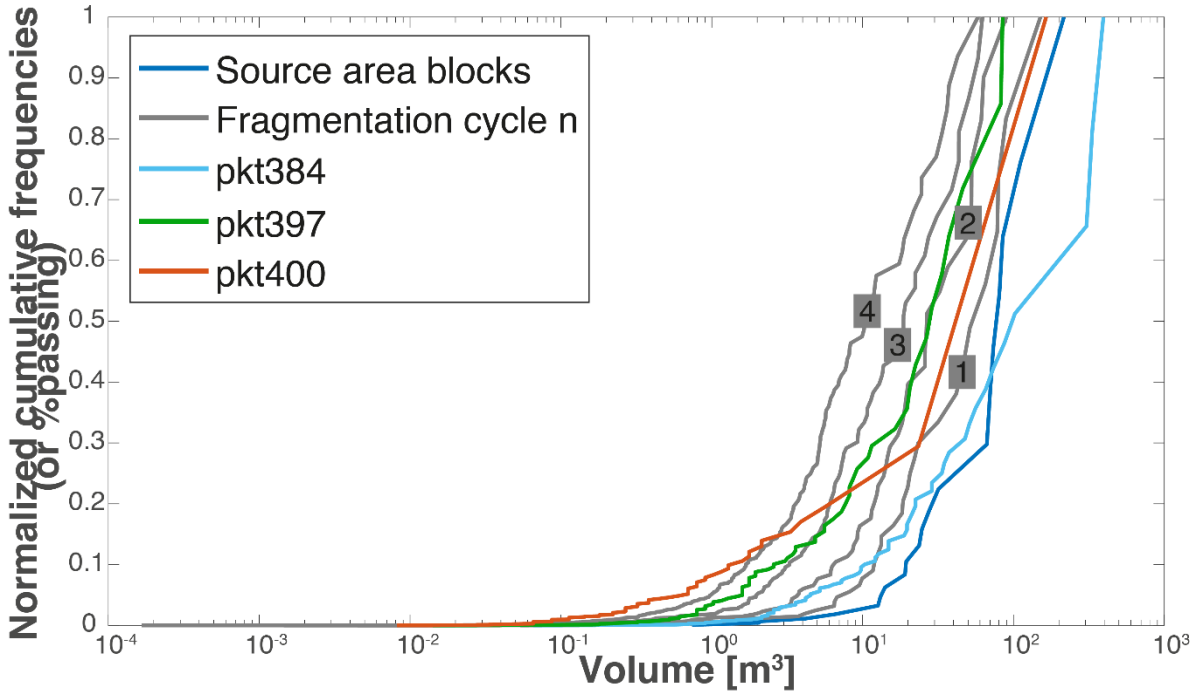

Figure 4.19 Grain size distribution for stations pkt384, pkt397 and pkt400.

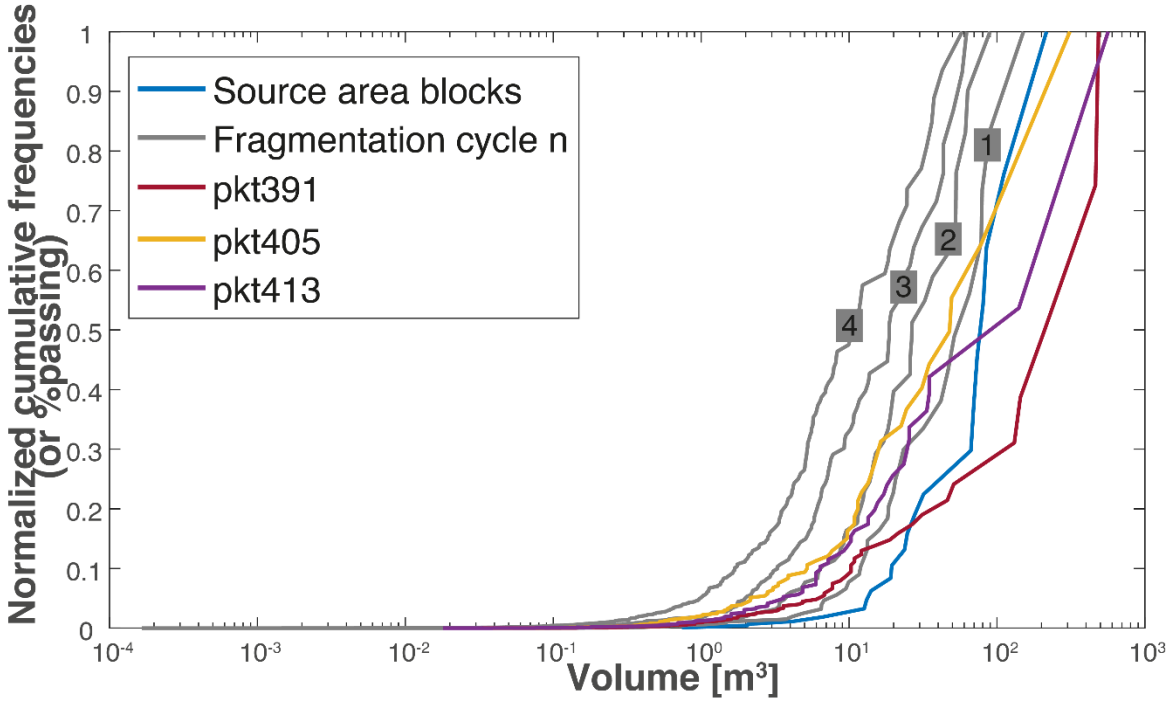

Figure 4.20 Grain size distribution for stations pkt391, pkt405 and pkt413.

Each station has a couple of blocks that is larger than the largest block in the source area, with pkt397 being the exception. Pkt400 were thought to be rock fall deposits in the field, in Figure 4.19 it is apparent that the station has four blocks which is larger than the plot of four fragmentation cycles. Pkt405 (Figure 4.20) match the theory of 0-3 fragmentations cycles well.

Table 4.7 Resulting fragmentation cycles at each station. Zero fragmentation cycles are assigned to stations that have blocks larger than the grain size distribution for one fragmentation cycle.

Station	Pkt384	Pkt397	Pkt400	Pkt391	Pkt405	Pkt413
Fragmentation cycles	0-2	1-4	0-5	0-3	0-3	0-2

4.7 Result of the ^{14}C dating

Dating of the sample at The National Laboratory of Age Determination in Trondheim, resulted in a conventional ^{14}C age of 1645 ± 25. Which is equivalent to a calibrated date of 336 AD – 433 AD with a 2σ probability of 86.7% (Figure 4.21).

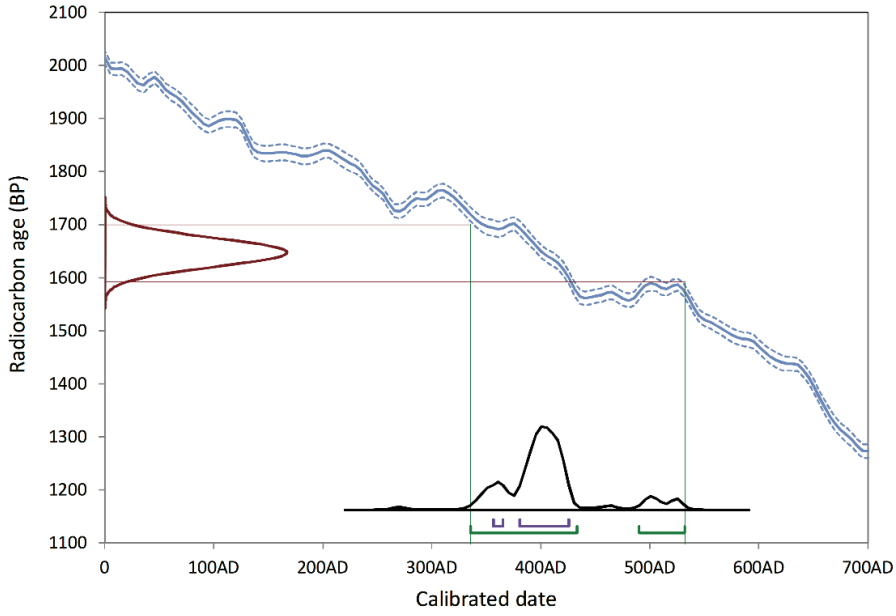

Figure 4.21 Graph describing the uncertainty and the coherence between the radiocarbon age and the calibrated date.

4.8 Schmidt hammer measurements of deposits

One of the reasons why Schmidt hammer measurements were done was that a PhD in process could correlate them with cosmogenic nuclide dating ages. They could also be correlated with the ^{14}C age from this thesis, but the Schmidt-readings are from deposits with slightly different morphology and another area than the deposits in which the ^{14}C-sample was found. Thus, direct correlation is not carried out and relative age cannot be backed up by numerical dating methods, yet. The two lobes from which the Schmidt readings were recorded are assumed to be those with the largest temporal separation. This assumption was based on the general impression of the deposits, and considering the general size, lichen and moss cover, lithology, and rounding.

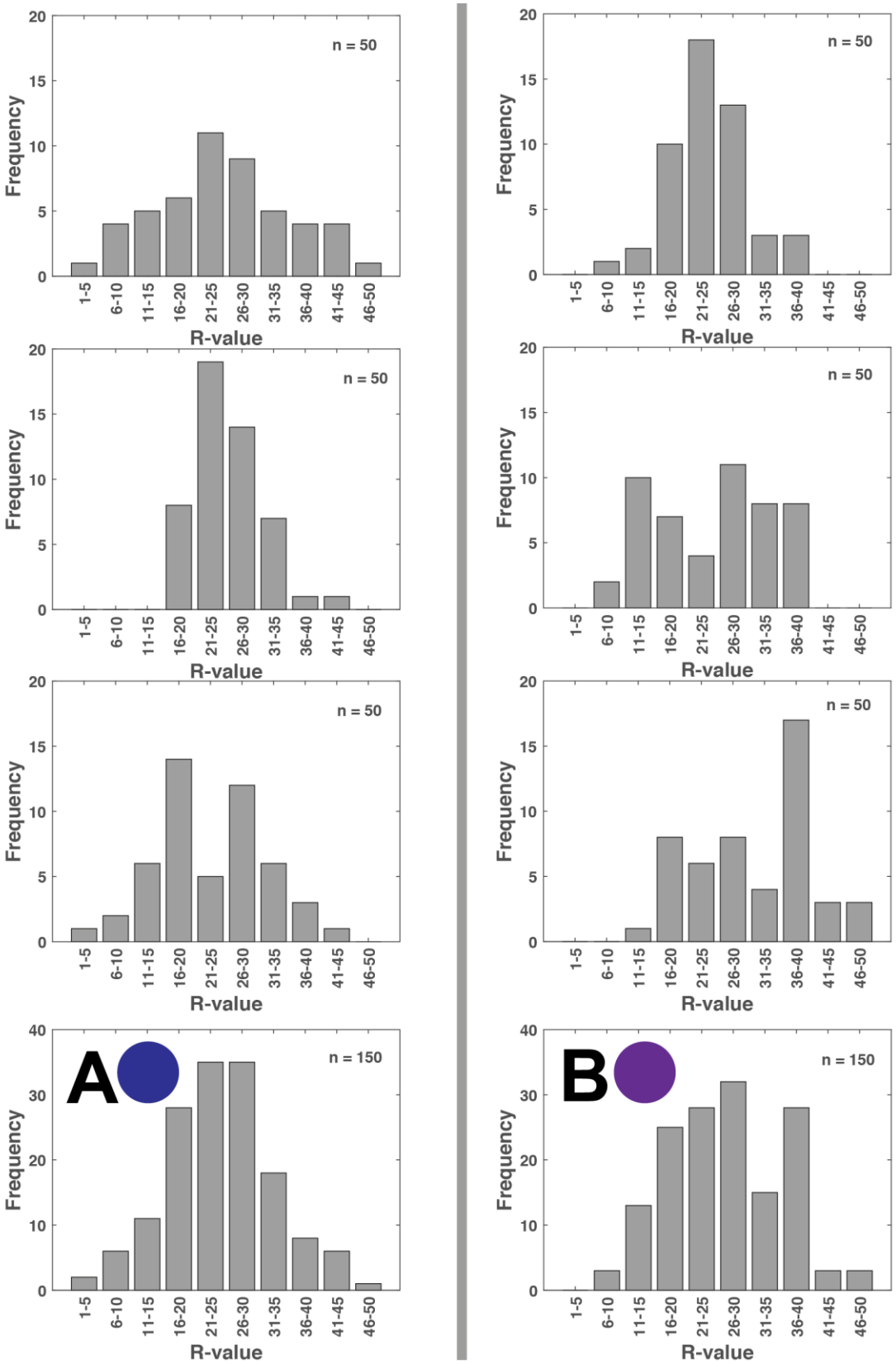

Figure 4.22 Histograms of the Schmidt-measurements on two of the deposited lobes. The right column is deposits closer to the road (purple dot in Figure 4.17) while the blocks measured in the left column is located above the railway (dark blue dot in Figure 4.17). There are 50 readings in each of the top six histograms, each histogram from a separate block. A) and B) are all readings from each column assembled.

Histograms from the two different deposits are similar at first glance, but a few differences can be pointed out with help from Table 4.8. Both the mean and median of the left column is slightly lower than the right column. However, the mode and range are higher for the left column. Pkt474 has a very low mode. Moss and lichens (Figure 4.23) can be the cause of "misfires" which result in low values.

Table 4.8 Mean, median, mode and range of values given for each measured block, in accordance with Aydin (2008).

	Pkt470	**Pkt471**	**Pkt472**	**Left**	**Pkt473**	**Pkt474**	**Pkt475**	**Right**
Mean	25.0	26.2	22.6	24.6	24.3	25.1	31.2	26.9
Median	24.5	25	21.5	25	24	26	34	26
Mode	24	25	26	26	22	12	36	22
Range	43	24	38	43	28	30	38	40
Lithology	Biotite Quartz Garnet → Gneiss	Biotite Quartz Garnet Feldspar	Biotite Quartz Garnet Feldspar		Garnet Biotite Quartz Feldspar →Gneiss	Garnets Micas Quartz	Less garnet More mica than Pkt474	
Notes	Overhang Dry surface	Wet	Wet		Wet	Wet	Overhang Relatively dry	

Most of the blocks have a weak foliation with low spacing (~5-10 cm), for pkt471 the Schmidt-readings were taken orthogonal to the foliation. However, the foliation is so weak that it is thought to affect the readings to little degree.

Figure 4.23 Typical deposit for Schmidt-hammer measurements. Photo from the lower deposit (purple dot in Figure 4.17). Lots of moss, lichens, and wet conditions during sampling.

5 Discussion

5.1 Delimiting the scenarios

The interpreted limits of the scenarios at Rombakstøtta are given in the results section 4.3. On the map (Figure 4.9), it is indicated whether lineaments are interpreted or placed with less uncertainty.

5.1.1 Toe lines

Uncertainty is connected to the placement of toe lines, especially on the larger scenarios. In general, they are placed on a break of slope or at the lowermost point of exposed bedrock in the scenario. For scenario 1.B, 4.C, 4.D and partly 1.A the uncertainty is lower as the toe lines could be observed in photo panoramas. In the photos of scenario 1.A the anticipated toe line is covered with snow.

5.1.2 Lateral limits

For scenarios 1.B, 4.C and 4.D the lateral limits are placed with low uncertainty, as it is a short distance between back scarp and toe line. The end of the open back scarp is interpreted as the lateral delimitation. For scenario 1.A, the western lateral limit is hard to trace near the top of the slope. For scenario 2.A, the lateral limits were mostly based on observations of several cracks made on the photo panoramas, because there were few morphological expressions visible elsewhere on the DEM. The two largest scenarios 3.A and 4.A had few clear indicators of the lateral limits which result in greater uncertainty.

5.1.3 Back-scarp

Development of the back-scarp is one of the nine criteria in the hazard assessment, information regarding this can therefore be found in the detailed information on the hazard assessment of each scenario; appendix B. Scenario 1.B, 3.A, 4.C and 4.D have the most pronounced back scarps, and therefore these are assigned with higher certainty than the back scarps for the other scenarios.

5.2 Hazard assessment

To reduce the uncertainty of the results from the hazard assessment, it would have been beneficial with more trustworthy displacement data over the entire instability. Measurement of the bolts that were mounted in 1996 have been conducted approximately every second year. Except for a 5-year period from 1999 to 2004. In this 5-year period one bolt couplet have moved 88 mm relative to each other; far more than the inaccuracy of the method (measuring tape).

Thus, the local displacement rate here was 1.7 cm/year in this 5-year period. However, the displacement rate has ceased after this. These bolts cover only scenario 1.A and 1.B, the other scenarios are not covered by any displacement measurements.

Absolute dating of earlier events would also lower the uncertainty, such dates might become available through a PhD in process within the CryoWALL project. Once they become available a reevaluation of the hazard assessment should be done. Because of this, both the probability of events older than 5000 years and younger than 5000 years are set to 50%.

5.2.1 Failure kinematics of the scenarios

5.2.1.1 Scenario 1.A and 1.B

Planar failure is partly possible along the foliation of scenarios 1.A and 1.B. Wedge failure and toppling failure is possible, but less likely to cause failure of the entire scenarios. However, parts of scenario 1.B are prone to toppling failure causing rock fall. High mica content is known to have a destabilizing effect on planar failure along the foliation (Shea and Kronenberg, 1993). Rock mechanical tests should be carried out to quantify this.

5.2.1.2 Scenario 2.A

Scenario 2.A lie within the same structural domain as 1.A and 1.B (appendix D), thus the same failure modes are possible. However, scenario 2.A is more prone to toppling or wedge failure because of its location and volume.

5.2.1.3 Scenario 3.A

Planar failure is not possible, and the other failure modes is not feasible due to the nature of the scenario. The back scarp of scenario 3.A, resembles a double ridge. This scenario is too large and complex to be explained by the kinematic analysis. The sag and the deformation could be caused by other mechanisms, e.g. biplanar failure (Sollie, 2014). However, further field investigations are needed to conclude.

Based on the observations of the morphology, and the deposits of previous rock avalanches in the area, failure of this scenario is thought to be unlikely.

5.2.1.4 Scenario 4.A and 4.B

Planar failure is partly possible along the foliation. However, due to the scenarios extent and the variability of the foliation, other failure mechanisms are needed for catastrophic failure to occur. For instance, biplanar failure (Sollie, 2014).

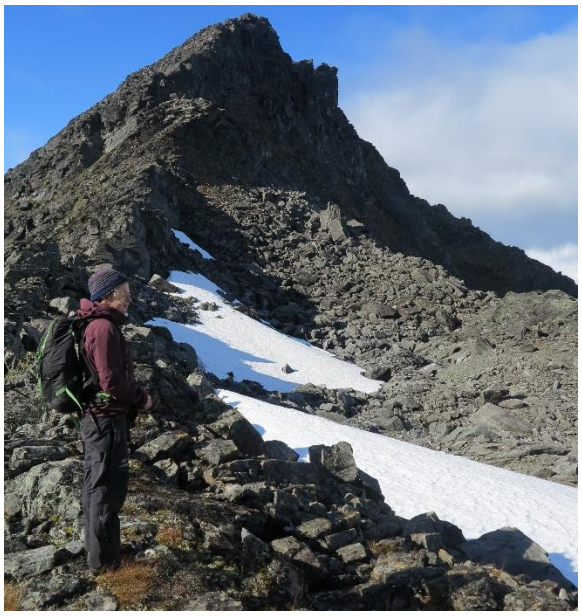

Figure 5.1 View towards west along the back scarp of scenario 3.A. Note the drop along the back scarp, and that the material that has dropped down is sloping towards the back scarp.

5.2.1.5 Scenario 4.C and 4.D

Planar failure is possible, and the foliation is a potential basal release surface for toppling with J1 as back scarp. Toppling is unlikely for the full volume of scenario 4.C, but likely for scenario 4.D.

5.3 Run-out modelling from Flow-R

In general, the scenarios with volumes above >210 000 m^3 reach the railroad. The smallest scenarios have volumes below the Norwegian definition for rock avalanches, therefore the run-out lengths modelled in Flow-R might not be valid for these scenarios. This is the case for scenario 4.B, 4.C and 4.D. If treated like rock fall (or steinskred by the Norwegian definition), the run-out length would lie between the run-out length for the easternmost lobe in Figure 4.16 and the run-out computed by the empirical relation from Corominas (1996). The latter, lies between Ofotbanen and the E6 highway. The actual run-out depends on how the blocks would fracture over the rock fall run-out track.

Scenario 4.B and 4.C are placed high in the medium hazard class, while 4.D has the overall highest hazard ranking and is placed in the high hazard class.

5.3.1 Scenario 1.B and 1.A

Scenario 1.B has the highest hazard class of the scenarios with run-out reaching the fjord, placed high in the medium hazard class. It also has a pronounced back scarp (section 4.3.1). Another factor that raise the hazard score is that failure is kinematically possible on penetrative

structures with high certainty. Because this scenario has a vertical front section the penetrative structures daylight at the foot or in the slope, causing unfavorable conditions for stability.

Scenario 1.A have a similar setting as 1.B, but the back scarp is less pronounced and the flanks of 1.A are less developed. The front cliff or toe is also dipping more gently, thus lower probability for penetrative structures to daylight in the slope. These three factors are the main reasons for 1.B lower hazard score. As seen in Figure 4.10 a couple of springs were found along the lateral limits of scenario 1.A, this can be a sign of internal deformation allowing water to penetrate through the rock mass. Which can cause increased weathering and frost weathering, along with lubrication of penetrative structures (Davies et al., 2001).

5.3.2 Scenario 4.A

Modelled run-out for scenario 4.A is subject to uncertainty due to the hole in the DEM which alter the run-out analysis. It would be beneficial to obtain better data in this area and rerun the analysis. Better aerial photos of this area would also benefit the analysis, as interesting details about the lateral limit might be revealed. Hazard analysis of this scenario resulted in placement in the lower part of the medium hazard class, with high uncertainty. More information on the lateral limit might lower the hazard class and certainly the uncertainty.

5.3.3 Reduction of uncertainty

The uncertainty of the scenarios can be reduced through periodic displacement rate measurements. For scenario 1.B, 4.C and 4.D mobile extensometer monitoring would be sufficient. Due to a less pronounced back scarp, and the size, of the other scenarios either dGNSS or InSAR measurements could be conducted to quantify displacement rates.

5.4 Rock fall analysis

To find the rock fall frequency, data gathered the last 100 years was extrapolated 10 000 years. This is a very long extrapolation, longer than the data is suited for. So, the uncertainty is very large. However, it is one of the best possible assumptions with the available data.

Data from the last 100 years are probably representable for a relative stable situation, due to low displacement rates and no large collapses in historic time. Publications from around the world report that rock fall activity increases temporarily close to a landslide or rock avalanche event (i.e. Sartori et al., 2003; Abellán et al., 2009; Hermanns et al., 2012b; Hermanns and Longva, 2012; Loew et al., 2017). Therefore, it is likely that there have been times before these registrations started, with more intense rock fall activity.

Another assumption with large uncertainty is that one entry/event in the database, equals one block deposited. This could be correct for some events, but the 1996-event is an example of one event with several blocks deposited.

An ever-existing problem with back calculation of slope processes is that the DEM on which the run-out calculations are done, represent the present-day conditions. Decades or millennia's ago, the slope and therefore the run-out could be different.

The resulting maps show that the coarse deposits between the railway and the road could have been reached by 5-13 blocks per cell since deglaciation. This could have a major impact on cosmogenic nuclide dating of these deposits.

5.5 Implications of the fragmentation cycle analysis

Results from the fragmentation cycle model (Figure 4.18) show that the blocks from the source area underwent 0-3 fragmentation cycles. In comparison, findings from a similar study by Charrière et al. (2016) of the Frank Slide in Canada imply 2-5 cycles of fragmentation. The fall height for the Frank Slide is 800 meters for the center of mass, and the travel length is greater than 3 km. For Rombakstøtta, the fall height is ~1100 meter and the travel length is up to 1.6 km for the measured deposits. A higher number of fragmentation cycles in the Frank Slide, could be due to the longer run-out, different lithology or a difference in the method. Charrière et al. (2016) based their fragmentation modelling on a set starting volume of 215 m^3, while this thesis´s modelling is based on 22 blocks with different volumes (215 m^3 being the largest volume) as the starting fraction.

Pkt400 were thought to be rock fall deposits in the field, in figure 4.19 it is showed that the station has 4 blocks which is larger than the plot of 4 fragmentation cycles. Thus, 4 fragmentation cycles could be interpreted as the boundary between rock avalanche deposits and rock fall deposits at Rombakstøtta.

5.5.1 Assumptions and weaknesses for the fragmentation cycle modelling

When creating the fragmentation cycle modelling, several assumptions and simplifications were made. Their impact on the resulting model is discussed in the following.

5.5.1.1 Block volumes for fragmentation cycle model

All volumes should be treated as rough estimations, more precise calculations would require thorough measurements of dimensions and angles which would result in much longer field campaigns. The blocks in the source area are assumed to be quadratic with the shortest axis as

the thickness of the block. This assumption is hard to argue both for and against, as the thickness of the blocks vary greatly in the source area (**Error! Reference source not found.**). At least, the assumption is consistent through all the blocks in the source area. The volumes of the blocks in the source area are compared with the volumes of the blocks in the deposits, which also are calculated with estimated dimensions for one axis. Thus, the level of uncertainty is high.

A weakness of the model is that the source area lack blocks larger than the largest deposited block. This could be due to:

- Error in assumption of source block thickness.
- Error in assumption of deposited blocks volume.
- Different source area for the deposited blocks, or larger spacing of unconformities in the in the rock mass that formed the deposits.

This could probably have been avoided by sampling more blocks in the source area.

Figure 5.2 Photo showing the thickness vs. shortest axis ratio of the blocks along the main scanline in the source area. Unfortunately, the photo does not have any scale, but the open crack is measured to be 4.5 m wide.

5.5.1.2 Rand-function in MATLAB

The randomness of the fragmentation of blocks are based on the rand-function in MATLAB, which creates random uniformly distributed numbers in the interval (0,1). Keep in mind that the rand-function is not unpredictable, but are generated by a deterministic algorithm. However, it seems random and can pass various statistical tests of randomness (The MathWorks Inc., 2017).

5.5.1.3 Other assumptions

For each fragmentation cycle of a block, the block is broken into two and the initial total volume is kept. It may not be a liable assumption, that blocks are only broken into two. When a rock fall block hits the ground, it is more likely that it will break into many blocks, including small splinters that barely have any volume. In the interior of a rock avalanche, however, the details of rock fragmentation are little known (Davies and McSaveney, 2002). Charrière et al. (2016) proposed that the primarily control for the fragmentation is the initial fracturing of the source area. So, the preexisting discontinuities in the rock mass controls the degree of fragmentation of the deposits.

Keep in mind that the blocks measured in the deposits were mostly measured on top of the deposits, and that there is usually a grain size reduction vertically in a rock avalanche deposit (Dunning, 2006; Charrière et al., 2016). This could alter the grain size distribution to have an even flatter curve.

5.6 Implications and assumptions regarding the ^{14}C dating

The assumption of the age determination was that a block had landed on top of a tree, killed it and squeezed the wood. Dating revealed a calibrated date of 336 AD – 433 AD with a 2σ probability of 86.7%. Whether this block came down as a rockfall, or as part of a rock avalanche cannot be stated with certainty. But, the morphology of the block and the surroundings points towards a rock avalanche. The block is angular and surrounded by similar blocks (**Error! Reference source not found.**).

Figure 5.3 A) The wooden sample was found beneath the block under which the field assistant is sitting. There is a larger block partly hidden behind the small trees in the foreground (A), or to the left of the field assistant (B). B) In the right picture the field assistant is standing on the block which squeezed the tree.

However, the tree might have been killed by detachment and toppling from an earlier deposited block. Both the large block and the smaller block have a pronounced foliation, that could match each other if they were attached. Thus, the small block could have toppled from the larger, landed on the tree and preserved it.

Any conclusion regarding dates on a rock avalanche should not be based on only one date, but the date can serve as a supplement to other dates. Anyhow, the date tells when this block moved the last time.

5.7 Relative dating with Schmidt hammer measurements

By interpreting and comparing the A and B histogram in Figure 4.22 it can be pointed out that the readings for the most proximal deposits (A) look like a normal distribution around R=21-30. This could indicate that the blocks in this area were deposited at the same time, they have weathered at the same rate for the same amount of time. The distal deposits (B) have more unevenly distributed Schmidt-readings, which could indicate that the different blocks were deposited at separate times. Either as separate rock avalanches, or that some of the blocks are rock fall blocks. The block at pkt475 have high R-values, with mean 31.2, and could possibly be a younger rock fall block (Table 4.8). However, the mean, median, mode and range for the two lobes are quite similar. Thus, the relative dating is ambiguous.

The Schmidt readings do not differ much from each other, the differences between the lobes are not clear. In retrospective, it would have been beneficial with readings from more than two separate lobes, readings from the area where the ^{14}C sample was found would have been advantageous.

5.7.1 Errors

Differences in the R-values could come from other sources than differences in rock strength or weathering. It could be from changes from dry to wet conditions during sampling, sampling at rock surfaces with moss or lichens, sampling at rough surfaces with protruding grains. All the readings in this thesis were taken with the same hammer, so it’s viable to compare the results. A lot of samples are taken at each block to statistically reduce the errors. When comparing separate blocks and lobes, there is also a possibility that the signal could come from differences in lithology. Even though the lithology were noted in the field, minor differences could alter the R-values.

6 Conclusions and further investigations

6.1 Structural analysis and hazard assessment

The main findings of the structural analysis and hazard assessment can be summarized as follows:

- Based on the study of a DEM, aerial photos, photo panoramas and field observations eight scenarios were defined at Rombakstøtta. By applying a method for volume calculation developed at NGU, volumes from 10 000 m^3 to 4 650 000 m^3 were estimated for the different scenarios.
- Based on the orientation of the back scarp the unstable slope was divided into two structural domains. The structural analysis led to a characterization of three joint sets based on 658 structural measurements collected in field, and 947 measurements collected with the software Coltop3D. The joint sets had slightly different mean orientations within each domain: (dip direction/dip)
    - **West domain:** J1 (213/84±14), J2 (093/65 ± 16), J3 (139/83±22), foliation (281/19±16)
    - **East domain:** J1 (205/84±20), J2 (099/58±15), J3 (143/81±19), foliation (278/27±16)
- A kinematic analysis was preformed and revealed that failure was kinematically possible in both structural domains. However, for the largest scenarios simple kinematic failure is not possible. The possibility for biplanar failure is suggested, but not fully studied. There is a need for further investigations to illuminate whether this is possible. For scenarios 1.A, 1.B, 2.A, 4.C, and 4.D, failure is kinematically possible. The analysis also shows that the back scarp in the western domain follow J1. The steeper foliation in the east domain makes planar failure more feasible here.
- Application of the hazard assessment resulted in assigning scenario 4.D into the high hazard class, scenarios 1.A, 1.B, 2.A, 4.A, 4.B, and 4.C into the medium hazard class, and scenario 3.A into the medium/low hazard class. Due to the existence of displacement measurements for scenario 1.B, this scenario has the lowest uncertainty. Displacement measurements would reduce the uncertainty for the other scenarios as well. For scenario 1.B, 4.C, and 4.D, mobile extensometer monitoring would be sufficient. For the other scenarios either dGNSS or InSAR, should be used for monitoring, due to larger size and less pronounced back scarp.

- Run-out modelling in Flow-R showed that scenarios 1.A, 1.B, 3.A, and 4.A reach houses, Ofotbanen, the E6 highway, and the fjord below Rombakstøtta. Scenarios 2.A and 4.B reach Ofotbanen.
- To complete the hazard and consequence assessment of Rombakstøtta, run-out modelling in DAN3D with subsequent displacement wave analysis should be performed. This would determine the potential loss of life, and thus the risk connected to failure.

6.2 Rock fall analysis

Rock fall run-out length, and frequency, since deglaciation were assessed in Rockyfor3D. Results show that rock fall blocks >7.8 m^3 can reach into the rock avalanche deposits, and that the frequency since deglaciation can be 5-13 blocks per cell. This could have a major impact on cosmogenic nuclide dating of these deposits.

6.3 Fragmentation cycle analysis

A fragmentation cycle analysis developed by the author of this thesis, after inspiration by Charrière et al. (2016), have been tested. The results suggest the following:

- By comparing the deposited blocks <215 m^3 to the fragmentation cycle plots (Figure 4.18), it can be deduced that the deposits below Rombakstøtta underwent 0-3 fragmentation cycles during failure and transport.
- From Figure 4.19 and Figure 4.20 it is evident that there are blocks in most of the stations that are larger than the largest block in the source area. This indicates that the source area dataset does not match the deposits. The reason could be wrong assumptions when calculating the block volumes, or that the source for the deposits had larger spacing between the discontinuities.
- From the limited dataset, it could be interpreted that four fragmentation cycles are the boundary between rock avalanche deposits and rock fall deposits at Rombakstøtta. Due to the assumption that most of the deposits at pkt400 are rock fall deposits.
- The fragmentation cycle analysis should be tested out on a larger dataset, with more measured blocks in the source area.

6.4 Relative dating with Schmidt-hammer

The mean, median, mode, and range for the two lobes are quite similar. Thus, the relative dating is ambiguous. It would have been beneficial with readings from more than two separate lobes.

Readings from the area where the ^{14}C sample was found would also have been advantageous. If the participants in the CryoWALL-project want to carry out relative dating or correlation with numerical dating methods, the dataset should be expanded in the coming field season.

7 References

Aa, A. R., Sjåstad, J., Sønstegaard, E. and Blikra, L. H. (2007) Chronology of Holocene rock-avalanche deposits based on Schmidt-hammer relative dating and dust stratigraphy in nearby bog deposits, Vora, inner Nordfjord, Norway, *The Holocene*, 17(7), pp. 955-964.

Abellán, A., Jaboyedoff, M., Oppikofer, T. and Vilaplana, J. (2009) Detection of millimetric deformation using a terrestrial laser scanner: experiment and application to a rockfall event, *Natural Hazards and Earth System Sciences*, 9(2), pp. 365-372.

Andersen, B. G., Boen, F., Nydal, R., Rasmussen, A. and Vallevik, P. N. (1981) Radiocarbon dates of marginal moraines in Nordland, North Norway, *Geografiska Annaler. Series A, Physical Geography*, 63(3), pp. 155-159.

Atkinson, R., Bamford, W., Broch, E., Deere, D., Franklin, J., Nieble, C., Rummel, F., Tarkoy, R. and Van Duyse, H. (1978) Suggested methods for determining hardness and abrasiveness of rocks, *International Journal of Rock Mechanics and Mining Sciences*, 15(3), pp. 89-97.

Augland, L. E., Andresen, A., Gasser, D. and Steltenpohl, M. G. (2014) Early Ordovician to Silurian evolution of exotic terranes in the Scandinavian Caledonides of the Ofoten–Troms area–terrane characterization and correlation based on new U–Pb zircon ages and Lu–Hf isotopic data, *Geological Society, London, Special Publications*, 390(1), pp. 655-678.

Aydin, A. and Basu, A. (2005) The Schmidt hammer in rock material characterization, *Engineering Geology*, 81(1), pp. 1-14. doi: http://dx.doi.org/10.1016/j.enggeo.2005.06.006.

Aydin, A. (2008) ISRM suggested method for determination of the Schmidt hammer rebound hardness: revised version *The ISRM Suggested Methods for Rock Characterization, Testing and Monitoring: 2007-2014*. Springer, pp. 25-33.

Bargel, T. H., Boyd, R. and Dahl, R. (1995) *En vandring i tid og rom: geologien i Narvik*. Norges Geologiske Undersøkelse.

Bargel, T. H. (2003) *Quaternary geological mapping of Central Fennoscandia and Nordland: deglaciation, deposition, stratigraphy and applications*. Doctoral dissertation, The Norwegian University of Science and technology.

Blikra, L., Braathen, A. and Skurtveit, E. (2001) *Hazard evaluation of rock avalanches; the Baraldsnes–Oterøya area*. (NGU-rapport). Trondheim: Geological Survey of Norway (NGU).

Blikra, L., Longva, O., Braathen, A., Anda, E., Dehls, J. and Stalsberg, K. (2006) Rock slope failures in Norwegian fjord areas: examples, spatial distribution and temporal pattern *Landslides from massive rock slope failure*. Springer, pp. 475-496.

Blikra, L., Majala, G., Anda, E., Berg, H., Eikenæs, O., Helgås, G., Oppikofer, T., Hermanns, R. and Böhme, M. (2016) Fare-og risikoklassifisering av ustabile fjellparti. Faresoner, arealhandtering og tiltak *NVE Report 77/2016, Norwegian Water Ressources and Energy Directorate, Oslo.*

Blikra, L. H. and Christiansen, H. H. (2014) A field-based model of permafrost-controlled rockslide deformation in northern Norway, *Geomorphology*, 208, pp. 34-49. doi: http://dx.doi.org/10.1016/j.geomorph.2013.11.014.

Breien, H. and Høydal, Ø. (2013) *Forslag til kriterier for vernskog mot skred*. (NGI-rapport). Oslo: Norwegian Geotechnical Institute (NGI).

Böhme, M. (2016) Personal communication, 26.10.2016.

Böhme, M., Bunkholt, H., Dehls, J., Oppikofer, T., Hermanns, R. L., Dalsegg, E., Kristensen, L., Lauknes, T. R. and Eriksen, H. Ø. (2016) *Geologisk modell og fare- og risikoklassifisering av det ustabile fjellpartiet Gamanjunni 3 i Manndalen, Troms* Trondheim: NGU.

Charrière, M., Humair, F., Froese, C., Jaboyedoff, M., Pedrazzini, A. and Longchamp, C. (2016) From the source area to the deposit: Collapse, fragmentation, and propagation of the Frank Slide, *Geological Society of America Bulletin*, 128(1-2), pp. 332-351.

Christiansen, H. H., Etzelmüller, B., Isaksen, K., Juliussen, H., Farbrot, H., Humlum, O., Johansson, M., Ingeman-Nielsen, T., Kristensen, L., Hjort, J., Holmlund, P., Sannel, A. B. K., Sigsgaard, C., Åkerman, H. J., Foged, N., Blikra, L. H., Pernosky, M. A. and Ødegård, R. S. (2010) The thermal state of permafrost in the nordic area during the international polar year 2007–2009, *Permafrost and Periglacial Processes*, 21(2), pp. 156-181. doi: 10.1002/ppp.687.

Cook-Talbot, J. D. (1991) Sorted circles, relative-age dating and palaeoenvironmental reconstruction in an alpine periglacial environment, eastern Jotunheimen, Norway: lichenometric and weathering-based approaches, *The Holocene*, 1(2), pp. 128-141.
Corominas, J. (1996) The angle of reach as a mobility index for small and large landslides, *Canadian Geotechnical Journal*, 33(2), pp. 260-271.
Crosta, G. B. and Agliardi, F. (2003) Failure forecast for large rock slides by surface displacement measurements, *Canadian Geotechnical Journal*, 40(1), pp. 176-191. doi: 10.1139/t02-085.
Cruden, D. M. and Varnes, D. J. (1996) Landslides: investigation and mitigation. Chapter 3-Landslide types and processes, *Transportation research board special report*, (247).
d'Angelo, P. (2016) Hugin - Panorama Photo Stitcher (vol. 2016.2.0). Germany. Available at: http://hugin.sourceforge.net/.
Davies, M. C., Hamza, O. and Harris, C. (2001) The effect of rise in mean annual temperature on the stability of rock slopes containing ice-filled discontinuities, *Permafrost and Periglacial Processes*, 12(1), pp. 137-144.
Davies, T. and McSaveney, M. (2002) Dynamic simulation of the motion of fragmenting rock avalanches, *Canadian Geotechnical Journal*, 39(4), pp. 789-798.
Devoli, G., Eikenæs, O., Taurisano, A., Hermanns, R., Fischer, L., Oppikofer, T. and Bunkholt, H. (2011) Plan for skredfarekartlegging–Delrapport steinsprang, steinskred og fjellskred, *NVE rapport*, 15, pp. 2011.
Dorren, L. K. (2003) A review of rockfall mechanics and modelling approaches, *Progress in Physical Geography*, 27(1), pp. 69-87.
Dorren, L. K. A. and Seijmonsbergen, A. C. (2003) Comparison of three GIS-based models for predicting rockfall runout zones at a regional scale, *Geomorphology*, 56(1–2), pp. 49-64. doi: http://dx.doi.org/10.1016/S0169-555X(03)00045-X.
Dorren, L. K. A. (2014) FINT - Find individual trees. User manual (Version 13 edn.). Geneva, Switzerland: ecorisQ - International association for natural hazard risk management. Available at: https://www.ecorisq.org/ecorisq-tools.
Dorren, L. K. A. (2015) Rockyfor3D (v5.2) revealed - Transparent description of the complete 3D rockfall modell., *ecorisQ paper*, pp. 32. Available at: http://www.ecorisq.org/.
Dunning, S. (2006) The grain size distribution of rock-avalanche deposits in valley-confined settings, *Ital J Eng Geol Environ*, 1, pp. 117-121.
ESRI (2016) ArcMap 10.4. Redlands, California: ESRI.
Etzelmüller, B. (2015) *CryoWALL - Steep permafrost slopes in Norway* Available at: http://www.mn.uio.no/geo/english/research/projects/cryowall/ (Accessed: 14.05 2017).
Gisnås, K., Etzelmüller, B., Lussana, C., Hjort, J., Sannel, A. B. K., Isaksen, K., Westermann, S., Kuhry, P., Christiansen, H. H., Frampton, A. and Åkerman, J. (2016) Permafrost Map for Norway, Sweden and Finland, *Permafrost and Periglacial Processes*, pp. n/a-n/a. doi: 10.1002/ppp.1922.
Harbitz, C., Glimsdal, S., Løvholt, F., Kveldsvik, V., Pedersen, G. and Jensen, A. (2014) Rockslide tsunamis in complex fjords: from an unstable rock slope at Åkerneset to tsunami risk in western Norway, *Coastal engineering*, 88, pp. 101-122.
Heim, A. (1932) *Bergsturz und menschenleben*. Fretz & Wasmuth.
Hermanns, R., Hansen, L., Sletten, K., Böhme, M., Bunkholt, H., Dehls, J., Eilertsen, R., Fischer, L., LHeureux, J. and Høgaas, F. (2012a) Systematic geological mapping for landslide understanding in the Norwegian context, *Landslide and engineered slopes: protecting society through improved understanding. Taylor & Francis Group, London*, pp. 265-271.
Hermanns, R., Oppikofer, T., Anda, E., Blikra, L. H., Böhme, M., Bunkholt, H., Crosta, G. B., Dahle, H., Devoli, G., Fischer, L., Jaboyedoff, M., Loew, S., Sætre, S. and Yugsi Molina, F. (2012b) *Recommended hazard and risk classification system for large unstable rock slopes in Norway*. (NGU-report 2012.029). Available at: http://www.ngu.no/upload/Publikasjoner/Rapporter/2012/2012_029.pdf.
Hermanns, R. (2015) Landslide displacement measurements, monitoring and early warning 1 lecture notes, TGB4290 Landslide processes Norwegian University of Science and Technology, delivered delivered 17.09.2015

Hermanns, R. L. and Longva, O. (2012) Rapid rock-slope failures, *Landslides (types, mechanisms and modeling). Cambridge University Press, Cambridge*, pp. 59-70.
Hermanns, R. L., Oppikofer, T., Anda, E., Blikra, L. H., Böhme, M., Bunkholt, H., Crosta, G. B., Dahle, H., Devoli, G. and Fischer, L. (2013) Hazard and risk classification for large unstable rock slopes in Norway, *Ital J Eng Geol Environ. doi*, 10, pp. 2013-2006.
Hermanns, R. L., Oppikofer, T., Molina, F. X. Y., Dehls, J. F. and Böhme, M. (2014) Approach for Systematic Rockslide Mapping of Unstable Rock Slopes in Norway, in Sassa, K., *et al.* (ed.) *Landslide Science for a Safer Geoenvironment: Volume 3: Targeted Landslides.* Cham: Springer International Publishing, pp. 129-134.
Hermanns, R. L. (2016) Landslide *Encyclopedia of Engineering Geology.* Springer, pp. 1-3.
Highland, L. and Bobrowsky, P. T. (2008) *The landslide handbook: a guide to understanding landslides*. US Geological Survey Reston.
Hoek, E. and Bray, J. D. (1981) *Rock slope engineering*. CRC Press.
Holmgren, P. (1994) Multiple flow direction algorithms for runoff modelling in grid based elevation models: an empirical evaluation, *Hydrological processes*, 8(4), pp. 327-334.
Horton, P., Jaboyedoff, M., Rudaz, B. and Zimmermann, M. (2013) Flow-R, a model for susceptibility mapping of debris flows and other gravitational hazards at a regional scale, *Natural Hazards and Earth System Sciences*, 13(4), pp. 869.
Hsü, K. J. (1975) Catastrophic debris streams (sturzstroms) generated by rockfalls, *Geological Society of America Bulletin*, 86(1), pp. 129-140.
Huggel, C., Salzmann, N., Allen, S., Caplan-Auerbach, J., Fischer, L., Haeberli, W., Larsen, C., Schneider, D. and Wessels, R. (2010) Recent and future warm extreme events and high-mountain slope stability, *Philosophical Transactions of the Royal Society A: Mathematical, Physical and Engineering Sciences*, 368(1919), pp. 2435-2459. doi: 10.1098/rsta.2010.0078.
Hughes, A. L. C., Gyllencreutz, R., Lohne, Ø. S., Mangerud, J. and Svendsen, J. I. (2015) DATED-1: compilation of dates and time-slice reconstruction of the build-up and retreat of the last Eurasian (British-Irish, Scandinavian, Svalbard-Barents-Kara Seas) Ice Sheets 40-10 ka: PANGAEA. doi: 10.1594/PANGAEA.848117.
Hungr, O., Leroueil, S. and Picarelli, L. (2014) The Varnes classification of landslide types, an update, *Landslides*, 11(2), pp. 167-194.
Høeg, K., Lied, K., Karlsrud, K., Gregory, T. and Norges geotekniske, i. (2014) *Skred : skredfare og sikringstiltak : praktiske erfaringer og teoretiske prinsipper*. Oslo: NGI Universitetsforl.
Jaboyedoff, M. and Labiouse, V. (2003) CONEFALL: a program for the quick preliminary estimation of the rock-fall potential of propagation zones, *Computer & Geosciences*.
Jaboyedoff, M., Baillifard, F., Couture, R., Locat, J. and Locat, P. (2004) Toward preliminary hazard assessment using DEM topographic analysis and simple mechanical modeling by means of sloping local base level, *Landslides: Evaluation and Stabilization, Taylor & Francis Group*, pp. 199-205.
Jaboyedoff, M., Metzger, R., Oppikofer, T., Couture, R., Derron, M., Locat, J. and Turmel, D. (2007) New insight techniques to analyze rock-slope relief using DEM and 3D-imaging cloud points: COLTOP-3D software, *Rock mechanics: Meeting Society's Challenges and demands*. pp. 61-68.
Jaboyedoff, M., Couture, R. and Locat, P. (2009) Structural analysis of Turtle Mountain (Alberta) using digital elevation model: toward a progressive failure, *Geomorphology*, 103(1), pp. 5-16.
Jaboyedoff, M., Oppikofer, T., Abellán, A., Derron, M.-H., Loye, A., Metzger, R. and Pedrazzini, A. (2012) Use of LIDAR in landslide investigations: a review, *Natural Hazards*, 61(1), pp. 5-28. doi: 10.1007/s11069-010-9634-2.
Jaboyedoff, M., Derron, M., Rudaz, B., Oppikofer, T., Penna, I. and Daicz, S. (2015) A review of geometrical methods for determination of landslide volume and failure surface geometry, *Proceedings of the 68th Canadian Geotechnical Conference GEOQuébec 2015-Challenges from North to South*.
Jernbaneverket (2016) *Ofotbanen*. Available at: http://www.jernbaneverket.no/Jernbanen/Banene/Ofotbanen/ (Accessed: 21.10 2016).
Karlsen, T. A. (1991) Narvik. Berggrunnskart; Narvik; 14314; 1:50 000; sort/hvitt; : Norges geologiske undersøkelse.

Krogh, K. (2017) *The Unstable Rock Slope Kassen-A Hazard, Consequence and Stability Assessment of the Rock Slope*. Master´s thesis, NTNU.
Larsen, J. O. and Domaas, U. (1997) *Rombakstøtta, Narvik: Vurdering av fare for fjellskred*. (NGI-rapporter 964097-2). Oslo: NGI.
Larsen, J. O. (1999) *Rombakstøtta, Narvik: Vurdering av skredfare og bevegelse på tensjons-sprekker*. (97.15). Trondheim: NTNU.
Loew, S., Gschwind, S., Gischig, V., Keller-Signer, A. and Valenti, G. (2017) Monitoring and early warning of the 2012 Preonzo catastrophic rockslope failure, *Landslides*, 14(1), pp. 141-154. doi: 10.1007/s10346-016-0701-y.
Matthews, J. A. and Shakesby, R. A. (1984) The status of the 'Little Ice Age'in southern Norway: relative-age dating of Neoglacial moraines with Schmidt hammer and lichenometry, *Boreas*, 13(3), pp. 333-346.
McCaffrey, K., Jones, R., Holdsworth, R., Wilson, R., Clegg, P., Imber, J., Holliman, N. and Trinks, I. (2005) Unlocking the spatial dimension: digital technologies and the future of geoscience fieldwork, *Journal of the Geological Society*, 162(6), pp. 927-938.
McCarroll, D. (1989) Potential and limitations of the Schmidt hammer for relative-age dating: field tests on Neoglacial moraines, Jotunheimen, southern Norway, *Arctic and Alpine Research*, pp. 268-275.
Metzger, R., Jaboyedoff, M., Oppikofer, T., Viero, A. and Galgaro, A. (2009) Coltop3D: a new software for structural analysis with high resolution 3D point clouds and DEM, *AAPG Search and Discovery Article*, 90171, pp. 4-8.
Microsoft (2015) Image Composite Editor 2.0 (ICE). Redmond, Washington, USA. Available at: http://research.microsoft.com/en-us/um/redmond/projects/ice/.
Nesje, A., Blikra, L. H. and Anda, E. (1994) Dating rockfall-avalanche deposits from degree of rock-surface weathering by Schmidt-hammer tests: a study from Norangsdalen, Sunnmøre, Norway, *Norsk Geologisk Tidsskrift*, 74, pp. 108-113.
Nicolet, P. (2014) PimpMyRockyfor (vol. v1.1). Lausanne, Switzerland. Available at: https://wp.unil.ch/risk/software/pimpmyrockyfor/.
Norwegian Meteorological Institute (2016) *Monthly normal values*. Available at: http://sharki.oslo.dnmi.no/pls/portal/BATCH_ORDER.PORTLET_UTIL.Download_BLob?p_BatchId=854912&p_IntervalId=1646587 (Accessed: 12.12 2016).
Norwegian Water Resources and Energy Directorate (2017) Skredhendelser. Available at: http://gis3.nve.no/link/?link=SkredHendelser (Accessed: 16.03.2017).
Oppikofer, T., Nordahl, B., Bunkholt, H., Nicolaisen, M., Jarna, A., Iversen, S., Hermanns, R. L., Böhme, M. and Molina, F. X. Y. (2015) Database and online map service on unstable rock slopes in Norway—From data perpetuation to public information, *Geomorphology*, 249, pp. 69-81.
Oppikofer, T., Böhme, M., Nicolet, P., Penna, I. and Hermanns, R. (2016) *Metodikk for konsekvensanalyse av fjellskred*. (NGU-report). Trondheim: NGU.
Priest, S. and Hudson, J. (1981) Estimation of discontinuity spacing and trace length using scanline surveys, *International Journal of Rock Mechanics and Mining Sciences & Geomechanics*. Elsevier, pp. 183-197.
Priest, S. D. (2012) *Discontinuity analysis for rock engineering*. Springer Science & Business Media.
Reimer, P. J., Baillie, M. G., Bard, E., Bayliss, A., Beck, J. W., Blackwell, P. G., Ramsey, C. B., Buck, C. E., Burr, G. S. and Edwards, R. L. (2009) IntCal09 and Marine09 radiocarbon age calibration curves, 0–50,000 years cal BP, *Radiocarbon*, 51(04), pp. 1111-1150.
Rem, Ø. B., Hermanns, R. and Böhme, M. (2016) *The Rock Slope Instability at Tytefjell in Vindafjord, Rogaland - Hazard Assessment for Different Failure Scenarios*. Master´s thesis, NTNU.
Rocscience (2016a) *Dips*. Available at: https://rocscience.com/rocscience/products/dips (Accessed: 25.10 2016).
Rocscience (2016b) *Tutorial 4 - Toppling, Planar Sliding, Wedge Sliding*. Available at: https://www.rocscience.com/help/dips/webhelp7/pdf_files/tutorials/Tutorial_04_Toppling_Planar_and_Wedge_Sliding.pdf (Accessed: 25.10 2016).

Sartori, M., Baillifard, F., Jaboyedoff, M. and Rouiller, J. D. (2003) Kinematics of the 1991 Randa rockslides (Valais, Switzerland), *Nat. Hazards Earth Syst. Sci.*, 3(5), pp. 423-433. doi: 10.5194/nhess-3-423-2003.

Scheidegger, A. E. (1973) On the prediction of the reach and velocity of catastrophic landslides, *Rock Mechanics and Rock Engineering*, 5(4), pp. 231-236.

Shan, J. and Toth, C. K. (2008) *Topographic laser ranging and scanning: principles and processing*. CRC press.

Shea, W. T. and Kronenberg, A. K. (1993) Strength and anisotropy of foliated rocks with varied mica contents, *Journal of Structural Geology*, 15(9), pp. 1097-1121. doi: http://dx.doi.org/10.1016/0191-8141(93)90158-7.

Sollie, I. L. (2014) *The Håkåneset rockslide, Tinnsjø-Stability analysis of a potentially rock slope instability*. Master´s thesis, NTNU.

Sosio, R., Crosta, G. B. and Hungr, O. (2008) Complete dynamic modeling calibration for the Thurwieser rock avalanche (Italian Central Alps), *Engineering Geology*, 100(1-2), pp. 11-26. doi: 10.1016/j.enggeo.2008.02.012.

Taylor, R. E. (1997) Radiocarbon dating *Chronometric dating in archaeology*. Springer, pp. 65-96.

The MathWorks Inc. (2016) MATLAB R2016a (Version 9.1). Natick, MA, USA.

The MathWorks Inc. (2017) *Controlling random number generation*. Available at: https://se.mathworks.com/help/matlab/examples/controlling-random-number-generation.html#responsive_offcanvas (Accessed: 01.05.2017 2017).

Travelletti, J., Demand, J., Jaboyedoff, M. and Marillier, F. (2010) Mass movement characterization using a reflexion and refraction seismic survey with the sloping local base level concept, *Geomorphology*, 116(1), pp. 1-10.

Varnes, D. J. (1978) Slope movement types and processes, *Special report*, 176, pp. 11-33.

Viles, H., Goudie, A., Grab, S. and Lalley, J. (2011) The use of the Schmidt Hammer and Equotip for rock hardness assessment in geomorphology and heritage science: a comparative analysis, *Earth Surface Processes and Landforms*, 36(3), pp. 320-333.

Walker, M. (2005) *Quaternary dating methods*. John Wiley and Sons.

Wyllie, D. C. and Mah, C. (2004) *Rock slope engineering*. CRC Press.

8 Appendix

8.1 Appendix A: Bedrock map

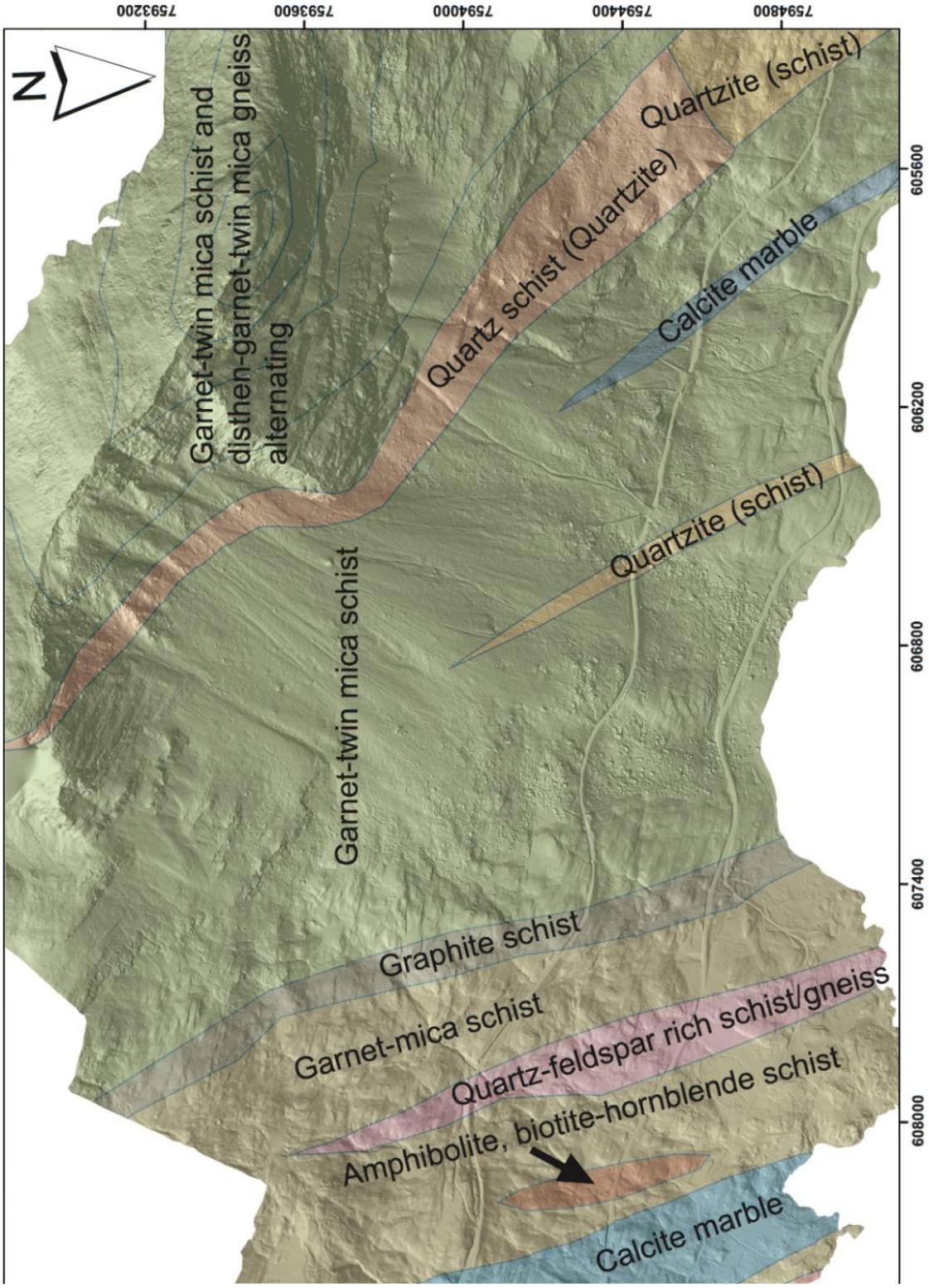

Figure 8.1 Bedrock map of Rombakstøtta from NGU displayed on the LiDAR/DEM of the field area. Keep in mind that the bedrock map is made in 1:50 000 scale, while in this figure it is displayed on a much smaller scale, therefore it may be inaccurate. Contains data under Norwegian License for Public Data (NLOD), communicated to the public by NGU

8.2 Appendix B: Hazard assessments

8.2.1 Scenario 1.A

Hazard assessment of large unstable rock slopes in Norway

Site name: Rombakstøtta **Scenario:** 1.A **Made by:** Odd Andre Morker **Date:** 04.05.2017

Hazard classes	Probability	Cumulative prob.
Very low	0.0 %	0.0 %
Low	31.7 %	31.7 %
Medium	54.9 %	86.6 %
High	13.4 %	100.0 %
Very high	0.0 %	100.0 %

Hazard score	
Minimum	3.0
Maximum	8.8
Mode	5.0
Mean	5.6
5% percentile	3.8
95% percentile	7.6

Fitted normal distrubution	
Mean μ	5.4
St. dev. σ	1.3
μ - 2σ	2.9
μ + 2σ	7.9
Corr. Coeff..	0.9993
K-S-test	5.3 %

1. Backscarp	**Score**	**Norm. prob.**
Not developed	0	60.0 %
Partly open over width of slide body (few cm to m)	0.5	40.0 %
Fully open over width of slide body (few cm to m)	1	0.0 %
Comment: The most southerly depression as back scarp, not open at all		

2.Potential sliding structures	**Score**	**Norm. prob.**
No penetrative structures dip out of the slope	0	15.0 %
Penetrative structures dip on average < 20 degree or steeper than the slope	0.5	70.0 %
Penetrative structures dip on average > 20 degree and daylight with the slope	1	15.0 %
Comment: Possibly J5, or biplanar failure along J1 and the SF. Using mean slope on this scenario.		

3. Lateral release surfaces	**Score**	**Norm.prob.**
Not developed	0	0.0 %
Partly developed on 1 side	0.25	0.0 %
Fully developed or free slope on 1 side or partly developed on 2 sides	0.5	50.0 %
Fully developed or free slope on 1 side and partly developed on 1 side	0.75	50.0 %
Fully developed or free slope on 2 sides	1	0.0 %
Comment: Fully developed to the east. Partly developed to the west.		

4. Kinematic feasibility test	**Score**	**Norm. prob.**
Kinematic feasibility test does not allow for planar sliding, wedge sliding or toppling	0	0.0 %
Failure is partly kinematically possible (movement direction is more than ±30° to slope orientation)	0.5	0.0 %
Failure is kinematically possible (movement direction is less than ±30° to slope orientation)	0.75	0.0 %
Failure is partly kinematically possible on persistent discontinuities (movement direction is more than ±30° to slope orientation)	0.75	0.0 %
Failure is kinematically possible on persistent discontinuities (movement direction is less than ±30° to slope orientation)	1	100.0 %
Comment: Planar failure partly possible (>30 deg) within the variability cone of SF. Wedge failure possible on intersection between J5 and J3 for max slope, but not for mean slope. Toppling failure possible on intersection between SF and J3 for max slope, but not for mean slope.		

5. Morphologic expression of the rupture surface	**Score**	**Norm. prob.**
No indication on slope morphology	0	30.0 %
Slope morphology suggests formation of a rupture surface (bulging, concavity -convexity, springs)	0.5	70.0 %
Continuous rupture surface is suggested by slope morphology and can be mapped out	1	0.0 %
Comment: Springs on the lateral expressions of rupture surfaces, no other expression along the toe line except change in morphology		

6. Displacement rates	**Score**	**Norm. prob.**
No significant movement	0	33.3 %
>0 - 0.5 cm/year	1	33.3 %
0.5 - 1 cm/year	2	33.3 %
1 - 4 cm/year	3	0.0 %
4 - 10 cm/year	4	0.0 %
> 10 cm/year	5	0.0 %
Comment: Measurements by BaneNOR. Low deformation rate		

7. Acceleration (if velocity is >0.5 cm/yr and <10 cm/yr)	**Score**	**Norm. prob.**
No acceleration or change in displacement rates	0	50.0 %
Increase in displacement rates	1	50.0 %
Comment: Not known, but it does not seem like there is any accelration		

8. Increase of rock fall activity	**Score**	**Norm. prob.**
No increase of rock fall activity	0	0.0 %
Increase of rock fall activity	1	100.0 %
Comment: Yes, compared to sorrounding areas		

9. Past events	**Score**	**Norm. prob.**
No post-glacial events of similar size	0	0.0 %
One or several events older than 5000 years of similar size	0.5	50.0 %
One or several events younger than 5000 years of similar size	1	50.0 %
Comment: Several earlier events, but not dated yet.		

8.2.2 Scenario 1.B

Hazard assessment of large unstable rock slopes in Norway

Site name: Rombakstøtta **Scenario:** 1.B **Made by:** Odd Andre Morker **Date:** 31.01.2017

Hazard classes	Probability	Cumulative prob.
Very low	0.0 %	0.0 %
Low	0.4 %	0.4 %
Medium	61.0 %	61.4 %
High	38.6 %	100.0 %
Very high	0.0 %	100.0 %

Hazard score	
Minimum	3.8
Maximum	9.5
Mode	6.0
Mean	6.9
5% percentile	5.3
95% percentile	8.5

Fitted normal distrubution	
Mean μ	6.8
St. dev. σ	1.0
μ - 2σ	4.7
μ + 2σ	8.9
Corr. Coeff..	0.9992
K-S-test	5.1 %

1. Backscarp	**Score**	**Norm. prob.**
Not developed	0	0.0 %
Partly open over width of slide body (few cm to m)	0.5	5.0 %
Fully open over width of slide body (few cm to m)	1	95.0 %
Comment: ca 10 m isnt open this is ca 5% of the total length of 238 m		

2.Potential sliding structures	**Score**	**Norm. prob.**
No penetrative structures dip out of the slope	0	0.0 %
Penetrative structures dip on average < 20 degree or steeper than the slope	0.5	30.0 %
Penetrative structures dip on average > 20 degree and daylight with the slope	1	70.0 %
Comment: Could be a biplanar failure along J1 and the foliation, but the foliations dip is very shallow. Need a lot of deformation to happen.		
Possibly J5, with max slope dip		

3. Lateral release surfaces	**Score**	**Norm.prob.**
Not developed	0	0.0 %
Partly developed on 1 side	0.25	0.0 %
Fully developed or free slope on 1 side or partly developed on 2 sides	0.5	0.0 %
Fully developed or free slope on 1 side and partly developed on 1 side	0.75	10.0 %
Fully developed or free slope on 2 sides	1	90.0 %
Comment: Both flanks look free.		

4. Kinematic feasibility test	**Score**	**Norm. prob.**
Kinematic feasibility test does not allow for planar sliding, wedge sliding or toppling	0	0.0 %
Failure is partly kinematically possible (movement direction is more than ±30° to slope orientation)	0.5	4.8 %
Failure is kinematically possible (movement direction is less than ±30° to slope orientation)	0.75	0.0 %
Failure is partly kinematically possible on persistent discontinuities (movement direction is more than ±30° to slope orientation)	0.75	0.0 %
Failure is kinematically possible on persistent discontinuities (movement direction is less than ±30° to slope orientation)	1	95.2 %
Comment: Using max slope: Planar partly possible (>30 deg from slope dip direction). Wedge possible on intersection between J5 and J3,		
partly possible on SF and J5 intersection		

5. Morphologic expression of the rupture surface	**Score**	**Norm. prob.**
No indication on slope morphology	0	30.0 %
Slope morphology suggests formation of a rupture surface (bulging, concavity -convexity, springs)	0.5	70.0 %
Continuous rupture surface is suggested by slope morphology and can be mapped out	1	0.0 %
Comment: Some crushing/deformation of rockmass at the foot of the steepest slope, but not along the entirety of the slope.		

6. Displacement rates	**Score**	**Norm. prob.**
No significant movement	0	33.3 %
>0 - 0.5 cm/year	1	33.3 %
0.5 - 1 cm/year	2	33.3 %
1 - 4 cm/year	3	0.0 %
4 - 10 cm/year	4	0.0 %
> 10 cm/year	5	0.0 %
Comment: Measurements by BaneNOR. Low deformation rate		

7. Acceleration (if velocity is >0.5 cm/yr and <10 cm/yr)	**Score**	**Norm. prob.**
No acceleration or change in displacement rates	0	90.0 %
Increase in displacement rates	1	10.0 %
Comment: Not known, but it does not seem like there is any accelration		

8. Increase of rock fall activity	**Score**	**Norm. prob.**
No increase of rock fall activity	0	0.0 %
Increase of rock fall activity	1	100.0 %
Comment: Yes, compared to sorrounding areas		

9. Past events	**Score**	**Norm. prob.**
No post-glacial events of similar size	0	0.0 %
One or several events older than 5000 years of similar size	0.5	50.0 %
One or several events younger than 5000 years of similar size	1	50.0 %
Comment: Several earlier events, but not dated yet.		

8.2.3 Scenario 2.A

Hazard assessment of large unstable rock slopes in Norway

Site name: Rombakstøtta **Scenario:** 2.A **Made by:** Odd Andre Morken **Date:** 31.01.2017

Hazard classes	Probability	Cumulative prob.
Very low	0.0 %	0.0 %
Low	23.6 %	23.6 %
Medium	60.6 %	84.1 %
High	15.9 %	100.0 %
Very high	0.0 %	100.0 %

Hazard score	
Minimum	3.0
Maximum	9.0
Mode	5.0
Mean	5.8
5% percentile	4.0
95% percentile	7.8

Fitted normal distrubution	
Mean μ	5.6
St. dev. σ	1.2
μ - 2σ	3.1
μ + 2σ	8.1
Corr. Coeff..	0.9991
K-S-test	5.4 %

1. Backscarp	**Score**	**Norm. prob.**
Not developed	0	0.0 %
Partly open over width of slide body (few cm to m)	0.5	10.0 %
Fully open over width of slide body (few cm to m)	1	90.0 %
Comment: 11 m not fully open, of 110 m back scarp.		

2.Potential sliding structures	**Score**	**Norm. prob.**
No penetrative structures dip out of the slope	0	15.0 %
Penetrative structures dip on average < 20 degree or steeper than the slope	0.5	70.0 %
Penetrative structures dip on average > 20 degree and daylight with the slope	1	15.0 %
Comment: Possibly J5, or biplanar failure along J1 and the SF. Using mean slope on this scenario.		

3. Lateral release surfaces	**Score**	**Norm.prob.**
Not developed	0	20.0 %
Partly developed on 1 side	0.25	30.0 %
Fully developed or free slope on 1 side or partly developed on 2 sides	0.5	50.0 %
Fully developed or free slope on 1 side and partly developed on 1 side	0.75	0.0 %
Fully developed or free slope on 2 sides	1	0.0 %
Comment: Hard to say, but the sides is partly free/free. However, the lateral limits is not well defined morphologically.		

4. Kinematic feasibility test	**Score**	**Norm. prob.**
Kinematic feasibility test does not allow for planar sliding, wedge sliding or toppling	0	0.0 %
Failure is partly kinematically possible (movement direction is more than ±30° to slope orientation)	0.5	0.0 %
Failure is kinematically possible (movement direction is less than ±30° to slope orientation)	0.75	0.0 %
Failure is partly kinematically possible on persistent discontinuities (movement direction is more than ±30° to slope orientation)	0.75	0.0 %
Failure is kinematically possible on persistent discontinuities (movement direction is less than ±30° to slope orientation)	1	100.0 %
Comment: Planar failure partly possible (>30 deg) within the variability cone of SF. Wedge failure possible on intersection between J5 and J3 for max slope. Toppling failure possible on intersection between SF and J3 for max slope.		
5. Morphologic expression of the rupture surface	**Score**	**Norm. prob.**
No indication on slope morphology	0	80.0 %
Slope morphology suggests formation of a rupture surface (bulging, concavity -convexity, springs)	0.5	20.0 %
Continuous rupture surface is suggested by slope morphology and can be mapped out	1	0.0 %
Comment: Rupture surface is assumed by indication of morphology from photos.		

6. Displacement rates	**Score**	**Norm. prob.**
No significant movement	0	33.3 %
>0 - 0.5 cm/year	1	33.3 %
0.5 - 1 cm/year	2	33.3 %
1 - 4 cm/year	3	0.0 %
4 - 10 cm/year	4	0.0 %
> 10 cm/year	5	0.0 %
Comment: No measurements. Low deformation rate.		

7. Acceleration (if velocity is >0.5 cm/yr and <10 cm/yr)	**Score**	**Norm. prob.**
No acceleration or change in displacement rates	0	50.0 %
Increase in displacement rates	1	50.0 %
Comment: Not known, but it does not seem like there is any accelration		

8. Increase of rock fall activity	**Score**	**Norm. prob.**
No increase of rock fall activity	0	0.0 %
Increase of rock fall activity	1	100.0 %
Comment: Yes, compared to sorrounding areas		

9. Past events	**Score**	**Norm. prob.**
No post-glacial events of similar size	0	0.0 %
One or several events older than 5000 years of similar size	0.5	50.0 %
One or several events younger than 5000 years of similar size	1	50.0 %
Comment: Several earlier events, but not dated yet.		

8.2.4 Scenario 3.A

Hazard assessment of large unstable rock slopes in Norway

Site name: Rombakstøtta **Scenario:** 3.A **Made by:** Odd Andre Morker **Date:** 31.01.2017

Hazard classes	Probability	Cumulative prob.
Very low	0.0 %	0.0 %
Low	43.3 %	43.3 %
Medium	51.3 %	94.6 %
High	5.4 %	100.0 %
Very high	0.0 %	100.0 %

Hazard score	
Minimum	3.0
Maximum	8.3
Mode	4.5
Mean	5.2
5% percentile	3.4
95% percentile	7.1

Fitted normal distrubution	
Mean μ	5.0
St. dev. σ	1.2
μ - 2σ	2.5
μ + 2σ	7.4
Corr. Coeff..	0.9988
K-S-test	7.6 %

1. Backscarp	**Score**	**Norm. prob.**
Not developed	0	0.0 %
Partly open over width of slide body (few cm to m)	0.5	10.0 %
Fully open over width of slide body (few cm to m)	1	90.0 %
Comment: Back scarp fully developed over the entire slope.		

2.Potential sliding structures	**Score**	**Norm. prob.**
No penetrative structures dip out of the slope	0	60.0 %
Penetrative structures dip on average < 20 degree or steeper than the slope	0.5	30.0 %
Penetrative structures dip on average > 20 degree and daylight with the slope	1	10.0 %
Comment: Possibly J5, or biplanar failure along J1 and the SF. Using mean slope on this scenario.		

3. Lateral release surfaces	**Score**	**Norm.prob.**
Not developed	0	80.0 %
Partly developed on 1 side	0.25	20.0 %
Fully developed or free slope on 1 side or partly developed on 2 sides	0.5	0.0 %
Fully developed or free slope on 1 side and partly developed on 1 side	0.75	0.0 %
Fully developed or free slope on 2 sides	1	0.0 %
Comment: Not developed at all, picked the limits based on weak morphologic expressions.		

4. Kinematic feasibility test	**Score**	**Norm. prob.**
Kinematic feasibility test does not allow for planar sliding, wedge sliding or toppling	0	0.0 %
Failure is partly kinematically possible (movement direction is more than ±30° to slope orientation)	0.5	0.0 %
Failure is kinematically possible (movement direction is less than ±30° to slope orientation)	0.75	0.0 %
Failure is partly kinematically possible on persistent discontinuities (movement direction is more than ±30° to slope orientation)	0.75	0.0 %
Failure is kinematically possible on persistent discontinuities (movement direction is less than ±30° to slope orientation)	1	100.0 %
Comment: Planar failure not possible. Wedge failure possible on intersection between J5 and J3 for max slope, but not for mean slope.		

5. Morphologic expression of the rupture surface	**Score**	**Norm. prob.**
No indication on slope morphology	0	100.0 %
Slope morphology suggests formation of a rupture surface (bulging, concavity -convexity, springs)	0.5	0.0 %
Continuous rupture surface is suggested by slope morphology and can be mapped out	1	0.0 %
Comment: Not any particular morphlogic expression, toe line picked based on the lowest visible bedrock in the scree.		

6. Displacement rates	**Score**	**Norm. prob.**
No significant movement	0	33.3 %
>0 - 0.5 cm/year	1	33.3 %
0.5 - 1 cm/year	2	33.3 %
1 - 4 cm/year	3	0.0 %
4 - 10 cm/year	4	0.0 %
> 10 cm/year	5	0.0 %
Comment: No measurements. Low deformation rate		

7. Acceleration (if velocity is >0.5 cm/yr and <10 cm/yr)	**Score**	**Norm. prob.**
No acceleration or change in displacement rates	0	50.0 %
Increase in displacement rates	1	50.0 %
Comment: Not known, but it does not seem like there is any accelration		

8. Increase of rock fall activity	**Score**	**Norm. prob.**
No increase of rock fall activity	0	0.0 %
Increase of rock fall activity	1	100.0 %
Comment: Yes, compared to sorrounding areas		

9. Past events	**Score**	**Norm. prob.**
No post-glacial events of similar size	0	0.0 %
One or several events older than 5000 years of similar size	0.5	50.0 %
One or several events younger than 5000 years of similar size	1	50.0 %
Comment: Several earlier events, but not dated yet.		

8.2.5 Scenario 4.A

Hazard assessment of large unstable rock slopes in Norway

Site name: Rombakstøtta **Scenario:** 4.A **Made by:** Odd Andre Morken **Date:** 31.01.2017

Hazard classes	Probability	Cumulative prob.
Very low	0.0 %	0.0 %
Low	37.5 %	37.5 %
Medium	51.9 %	89.4 %
High	10.6 %	100.0 %
Very high	0.0 %	100.0 %

Hazard score	
Minimum	2.5
Maximum	9.0
Mode	4.8
Mean	5.4
5% percentile	3.6
95% percentile	7.4

Fitted normal distrubution	
Mean μ	5.2
St. dev. σ	1.3
μ - 2σ	2.7
μ + 2σ	7.7
Corr. Coeff..	0.9993
K-S-test	5.3 %

1. Backscarp	**Score**	**Norm. prob.**
Not developed	0	20.0 %
Partly open over width of slide body (few cm to m)	0.5	75.0 %
Fully open over width of slide body (few cm to m)	1	5.0 %
Comment: 24 m fully open of 316 m		

2.Potential sliding structures	**Score**	**Norm. prob.**
No penetrative structures dip out of the slope	0	10.0 %
Penetrative structures dip on average < 20 degree or steeper than the slope	0.5	80.0 %
Penetrative structures dip on average > 20 degree and daylight with the slope	1	10.0 %
Comment: Looks like a bilateral failure on the surface.		

3. Lateral release surfaces	**Score**	**Norm.prob.**
Not developed	0	10.0 %
Partly developed on 1 side	0.25	50.0 %
Fully developed or free slope on 1 side or partly developed on 2 sides	0.5	40.0 %
Fully developed or free slope on 1 side and partly developed on 1 side	0.75	0.0 %
Fully developed or free slope on 2 sides	1	0.0 %
Comment: Part of the west flank is fully developed, the east flank is almost free		

4. Kinematic feasibility test	**Score**	**Norm. prob.**
Kinematic feasibility test does not allow for planar sliding, wedge sliding or toppling	0	0.0 %
Failure is partly kinematically possible (movement direction is more than ±30° to slope orientation)	0.5	0.0 %
Failure is kinematically possible (movement direction is less than ±30° to slope orientation)	0.75	0.0 %
Failure is partly kinematically possible on persistent discontinuities (movement direction is more than ±30° to slope orientation)	0.75	0.0 %
Failure is kinematically possible on persistent discontinuities (movement direction is less than ±30° to slope orientation)	1	100.0 %
Comment: Mean slope: Planar failure partly possible along SF within variability cone. SF can be a base plane for toppling. In the steeper parts planar failure along J1 and J3, partly possible. Possible within variability cones. Wedge failure possible on intersection between J1 and J3.		
5. Morphologic expression of the rupture surface	**Score**	**Norm. prob.**
No indication on slope morphology	0	50.0 %
Slope morphology suggests formation of a rupture surface (bulging, concavity -convexity, springs)	0.5	50.0 %
Continuous rupture surface is suggested by slope morphology and can be mapped out	1	0.0 %
Comment: Spring on one lateral flank, but mostly indicated by a break in slope (slope morphology)		

6. Displacement rates	**Score**	**Norm. prob.**
No significant movement	0	33.3 %
>0 - 0.5 cm/year	1	33.3 %
0.5 - 1 cm/year	2	33.3 %
1 - 4 cm/year	3	0.0 %
4 - 10 cm/year	4	0.0 %
> 10 cm/year	5	0.0 %
Comment: No measurements. Low deformation rate		

7. Acceleration (if velocity is >0.5 cm/yr and <10 cm/yr)	**Score**	**Norm. prob.**
No acceleration or change in displacement rates	0	50.0 %
Increase in displacement rates	1	50.0 %
Comment: Not known, but it does not seem like there is any accelration		

8. Increase of rock fall activity	**Score**	**Norm. prob.**
No increase of rock fall activity	0	0.0 %
Increase of rock fall activity	1	100.0 %
Comment: Yes, compared to sorrounding areas		

9. Past events	**Score**	**Norm. prob.**
No post-glacial events of similar size	0	0.0 %
One or several events older than 5000 years of similar size	0.5	50.0 %
One or several events younger than 5000 years of similar size	1	50.0 %
Comment: Several earlier events, but not dated yet.		

8.2.6 Scenario 4.B

Hazard assessment of large unstable rock slopes in Norway

Site name: Rombakstøtta **Scenario:** 4.B **Made by:** Odd Andre Morken **Date:** 31.01.2017

Hazard classes	Probability	Cumulative prob.
Very low	0.0 %	0.0 %
Low	18.7 %	18.7 %
Medium	60.0 %	78.7 %
High	21.3 %	100.0 %
Very high	0.0 %	100.0 %

Hazard score	
Minimum	3.3
Maximum	9.3
Mode	5.3
Mean	6.0
5% percentile	4.1
95% percentile	8.1

Fitted normal distrubution	
Mean μ	5.8
St. dev. σ	1.3
μ - 2σ	3.3
μ + 2σ	8.4
Corr. Coeff..	0.9994
K-S-test	4.4 %

1. Backscarp	**Score**	**Norm. prob.**
Not developed	0	11.1 %
Partly open over width of slide body (few cm to m)	0.5	44.4 %
Fully open over width of slide body (few cm to m)	1	44.4 %
Comment: 130 m partially open, 130 m fully open, some places not developed at all.		

2.Potential sliding structures	**Score**	**Norm. prob.**
No penetrative structures dip out of the slope	0	0.0 %
Penetrative structures dip on average < 20 degree or steeper than the slope	0.5	70.0 %
Penetrative structures dip on average > 20 degree and daylight with the slope	1	30.0 %
Comment: Toppling of the entire slope is not possible, biplanar failure is possible.		

3. Lateral release surfaces	**Score**	**Norm.prob.**
Not developed	0	0.0 %
Partly developed on 1 side	0.25	20.0 %
Fully developed or free slope on 1 side or partly developed on 2 sides	0.5	40.0 %
Fully developed or free slope on 1 side and partly developed on 1 side	0.75	40.0 %
Fully developed or free slope on 2 sides	1	0.0 %
Comment: Fully developed on the west side, partly developed and not so protruding on the east side.		

4. Kinematic feasibility test	**Score**	**Norm. prob.**
Kinematic feasibility test does not allow for planar sliding, wedge sliding or toppling	0	0.0 %
Failure is partly kinematically possible (movement direction is more than ±30° to slope orientation)	0.5	0.0 %
Failure is kinematically possible (movement direction is less than ±30° to slope orientation)	0.75	0.0 %
Failure is partly kinematically possible on persistent discontinuities (movement direction is more than ±30° to slope orientation)	0.75	0.0 %
Failure is kinematically possible on persistent discontinuities (movement direction is less than ±30° to slope orientation)	1	100.0 %
Comment: Mean slope: Planar failure partly possible along SF within variability cone. SF can be a base plane for toppling. In the steeper parts planar failure along J1 and J3 as well, partly possible. Possible within variability cones. Wedge failure possible on intersection between J1 and J3 in steeper		

5. Morphologic expression of the rupture surface	**Score**	**Norm. prob.**
No indication on slope morphology	0	50.0 %
Slope morphology suggests formation of a rupture surface (bulging, concavity -convexity, springs)	0.5	50.0 %
Continuous rupture surface is suggested by slope morphology and can be mapped out	1	0.0 %
Comment: Toe line at a break of slope, a spring at the east flank		

6. Displacement rates	**Score**	**Norm. prob.**
No significant movement	0	33.3 %
>0 - 0.5 cm/year	1	33.3 %
0.5 - 1 cm/year	2	33.3 %
1 - 4 cm/year	3	0.0 %
4 - 10 cm/year	4	0.0 %
> 10 cm/year	5	0.0 %
Comment: No measurements. Low deformation rate		

7. Acceleration (if velocity is >0.5 cm/yr and <10 cm/yr)	**Score**	**Norm. prob.**
No acceleration or change in displacement rates	0	50.0 %
Increase in displacement rates	1	50.0 %
Comment: Not known, but it does not seem like there is any accelration		

8. Increase of rock fall activity	**Score**	**Norm. prob.**
No increase of rock fall activity	0	0.0 %
Increase of rock fall activity	1	100.0 %
Comment: Yes, compared to sorrounding areas		

9. Past events	**Score**	**Norm. prob.**
No post-glacial events of similar size	0	0.0 %
One or several events older than 5000 years of similar size	0.5	50.0 %
One or several events younger than 5000 years of similar size	1	50.0 %
Comment: Several earlier events, but not dated yet.		

8.2.7 Scenario 4.C

Hazard assessment of large unstable rock slopes in Norway

Site name: Rombakstøtta **Scenario:** 4.C **Made by:** Odd Andre Morker **Date:** 31.01.2017

Hazard classes	Probability	Cumulative prob.
Very low	0.0 %	0.0 %
Low	7.5 %	7.5 %
Medium	64.3 %	71.8 %
High	28.2 %	100.0 %
Very high	0.0 %	100.0 %

Hazard score	
Minimum	3.8
Maximum	9.3
Mode	5.8
Mean	6.4
5% percentile	4.6
95% percentile	8.4

Fitted normal distrubution	
Mean μ	6.2
St. dev. σ	1.2
μ - 2σ	3.7
μ + 2σ	8.7
Corr. Coeff..	0.9992
K-S-test	4.9 %

1. Backscarp	**Score**	**Norm. prob.**
Not developed	0	0.0 %
Partly open over width of slide body (few cm to m)	0.5	20.0 %
Fully open over width of slide body (few cm to m)	1	80.0 %
Comment: ca 20 m of 110 m back scarp is fully open		

2.Potential sliding structures	**Score**	**Norm. prob.**
No penetrative structures dip out of the slope	0	0.0 %
Penetrative structures dip on average < 20 degree or steeper than the slope	0.5	70.0 %
Penetrative structures dip on average > 20 degree and daylight with the slope	1	30.0 %
Comment: Same as in scenario 4.D, however scenario 4.C is larger and toppling of the entire block seems unlikely.		

3. Lateral release surfaces	**Score**	**Norm.prob.**
Not developed	0	0.0 %
Partly developed on 1 side	0.25	10.0 %
Fully developed or free slope on 1 side or partly developed on 2 sides	0.5	40.0 %
Fully developed or free slope on 1 side and partly developed on 1 side	0.75	50.0 %
Fully developed or free slope on 2 sides	1	0.0 %
Comment: Free on east slope, but not for the entire depth. Partly developed on west side.		

4. Kinematic feasibility test	**Score**	**Norm. prob.**
Kinematic feasibility test does not allow for planar sliding, wedge sliding or toppling	0	0.0 %
Failure is partly kinematically possible (movement direction is more than ±30° to slope orientation)	0.5	0.0 %
Failure is kinematically possible (movement direction is less than ±30° to slope orientation)	0.75	0.0 %
Failure is partly kinematically possible on persistent discontinuities (movement direction is more than ±30° to slope orientation)	0.75	0.0 %
Failure is kinematically possible on persistent discontinuities (movement direction is less than ±30° to slope orientation)	1	100.0 %
Comment: Max slope is used: Wedge possible along J1/J3 intersection. Planar failure possible within variability cone for J1, J3 and SF.		
SF potential release surface for toppling.		
5. Morphologic expression of the rupture surface	**Score**	**Norm. prob.**
No indication on slope morphology	0	30.0 %
Slope morphology suggests formation of a rupture surface (bulging, concavity -convexity, springs)	0.5	70.0 %
Continuous rupture surface is suggested by slope morphology and can be mapped out	1	0.0 %
Comment: Some crushing visible along toe, but mostly mapped out based on the break of slope.		

6. Displacement rates	**Score**	**Norm. prob.**
No significant movement	0	33.3 %
>0 - 0.5 cm/year	1	33.3 %
0.5 - 1 cm/year	2	33.3 %
1 - 4 cm/year	3	0.0 %
4 - 10 cm/year	4	0.0 %
> 10 cm/year	5	0.0 %
Comment: No measurements. Little deformation.		

7. Acceleration (if velocity is >0.5 cm/yr and <10 cm/yr)	**Score**	**Norm. prob.**
No acceleration or change in displacement rates	0	50.0 %
Increase in displacement rates	1	50.0 %
Comment: Not known, but it does not seem like there is any accelration		

8. Increase of rock fall activity	**Score**	**Norm. prob.**
No increase of rock fall activity	0	0.0 %
Increase of rock fall activity	1	100.0 %
Comment: Yes, compared to sorrounding areas		

9. Past events	**Score**	**Norm. prob.**
No post-glacial events of similar size	0	0.0 %
One or several events older than 5000 years of similar size	0.5	50.0 %
One or several events younger than 5000 years of similar size	1	50.0 %
Comment: Several earlier events, but not dated yet.		

8.2.8 Scenario 4.D

Hazard assessment of large unstable rock slopes in Norway

Site name: Rombakstøtta **Scenario:** 4.D **Made by:** Odd Andre Morken **Date:** 31.01.2017

Hazard classes	Probability	Cumulative prob.
Very low	0.0 %	0.0 %
Low	0.0 %	0.0 %
Medium	45.8 %	45.8 %
High	51.3 %	97.2 %
Very high	2.9 %	100.0 %

Hazard score	
Minimum	4.8
Maximum	10.0
Mode	6.5
Mean	7.5
5% percentile	5.8
95% percentile	9.5

Fitted normal distrubution	
Mean μ	7.3
St. dev. σ	1.2
μ - 2σ	4.8
μ + 2σ	9.7
Corr. Coeff..	0.9988
K-S-test	5.7 %

1. Backscarp	**Score**	**Norm. prob.**
Not developed	0	0.0 %
Partly open over width of slide body (few cm to m)	0.5	5.0 %
Fully open over width of slide body (few cm to m)	1	95.0 %
Comment: Ca 30 m of 110 m partly open, the rest is fully open.		

2.Potential sliding structures	**Score**	**Norm. prob.**
No penetrative structures dip out of the slope	0	0.0 %
Penetrative structures dip on average < 20 degree or steeper than the slope	0.5	60.0 %
Penetrative structures dip on average > 20 degree and daylight with the slope	1	40.0 %
Comment: The foliation, however a bit too gentle dipping (mean foliation: 27 deg, but look much more flatlying in photos). Could be biplanar on SF and J1.		

3. Lateral release surfaces	**Score**	**Norm.prob.**
Not developed	0	0.0 %
Partly developed on 1 side	0.25	0.0 %
Fully developed or free slope on 1 side or partly developed on 2 sides	0.5	0.0 %
Fully developed or free slope on 1 side and partly developed on 1 side	0.75	30.0 %
Fully developed or free slope on 2 sides	1	70.0 %
Comment: Free flanks on both sides, but on west side it is only partly free. Only half of the hight of the block is free.		

4. Kinematic feasibility test	**Score**	**Norm. prob.**
Kinematic feasibility test does not allow for planar sliding, wedge sliding or toppling	0	0.0 %
Failure is partly kinematically possible (movement direction is more than ±30° to slope orientation)	0.5	0.0 %
Failure is kinematically possible (movement direction is less than ±30° to slope orientation)	0.75	0.0 %
Failure is partly kinematically possible on persistent discontinuities (movement direction is more than ±30° to slope orientation)	0.75	0.0 %
Failure is kinematically possible on persistent discontinuities (movement direction is less than ±30° to slope orientation)	1	100.0 %
Comment: Max slope used: Wedge possible along J1/J3 intersection. Planar failure possible within variability cone for J1, J3 and SF.		
SF potential release surface for toppling.		
5. Morphologic expression of the rupture surface	**Score**	**Norm. prob.**
No indication on slope morphology	0	0.0 %
Slope morphology suggests formation of a rupture surface (bulging, concavity -convexity, springs)	0.5	10.0 %
Continuous rupture surface is suggested by slope morphology and can be mapped out	1	90.0 %
Comment: Taking the mechanics of the scenario into account, it is most likely that the rupture surface is along the foot of the steep slope.		
If a toppling of the entire block occur, it is likely that it detaches here.		
6. Displacement rates	**Score**	**Norm. prob.**
No significant movement	0	33.3 %
>0 - 0.5 cm/year	1	33.3 %
0.5 - 1 cm/year	2	33.3 %
1 - 4 cm/year	3	0.0 %
4 - 10 cm/year	4	0.0 %
> 10 cm/year	5	0.0 %
Comment: This scenario has more deformation than scenario 4.B, it has moved the same amount as 4.B + an additional 2 m. But no measurements.		

7. Acceleration (if velocity is >0.5 cm/yr and <10 cm/yr)	**Score**	**Norm. prob.**
No acceleration or change in displacement rates	0	50.0 %
Increase in displacement rates	1	50.0 %
Comment: Not known, but it does not seem like there is any acceleration.		

8. Increase of rock fall activity	**Score**	**Norm. prob.**
No increase of rock fall activity	0	0.0 %
Increase of rock fall activity	1	100.0 %
Comment: Yes, compared to sorrounding areas		

9. Past events	**Score**	**Norm. prob.**
No post-glacial events of similar size	0	0.0 %
One or several events older than 5000 years of similar size	0.5	50.0 %
One or several events younger than 5000 years of similar size	1	50.0 %
Comment: Several earlier events, but not dated yet.		

8.3 Appendix C: Structural measurement stations

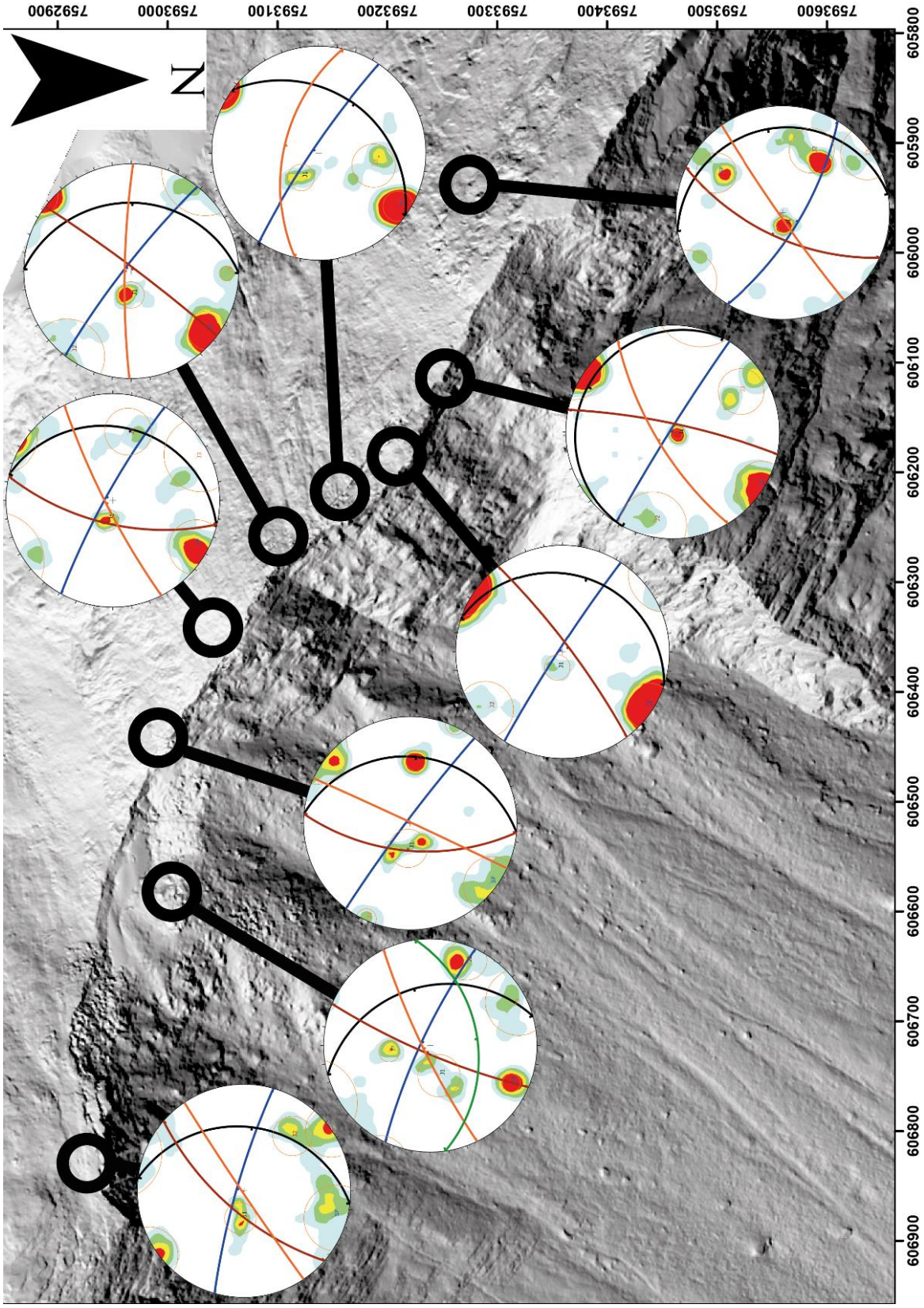

Figure 8.2 All the structural measurements divided into stations based on their spatial relationship and plotted in Dips 7.0. Foliations and joint sets defined based on field observations and contour density concentrations. Displayed on the LiDAR/DEM.

8.4 Appendix D: Structural domains

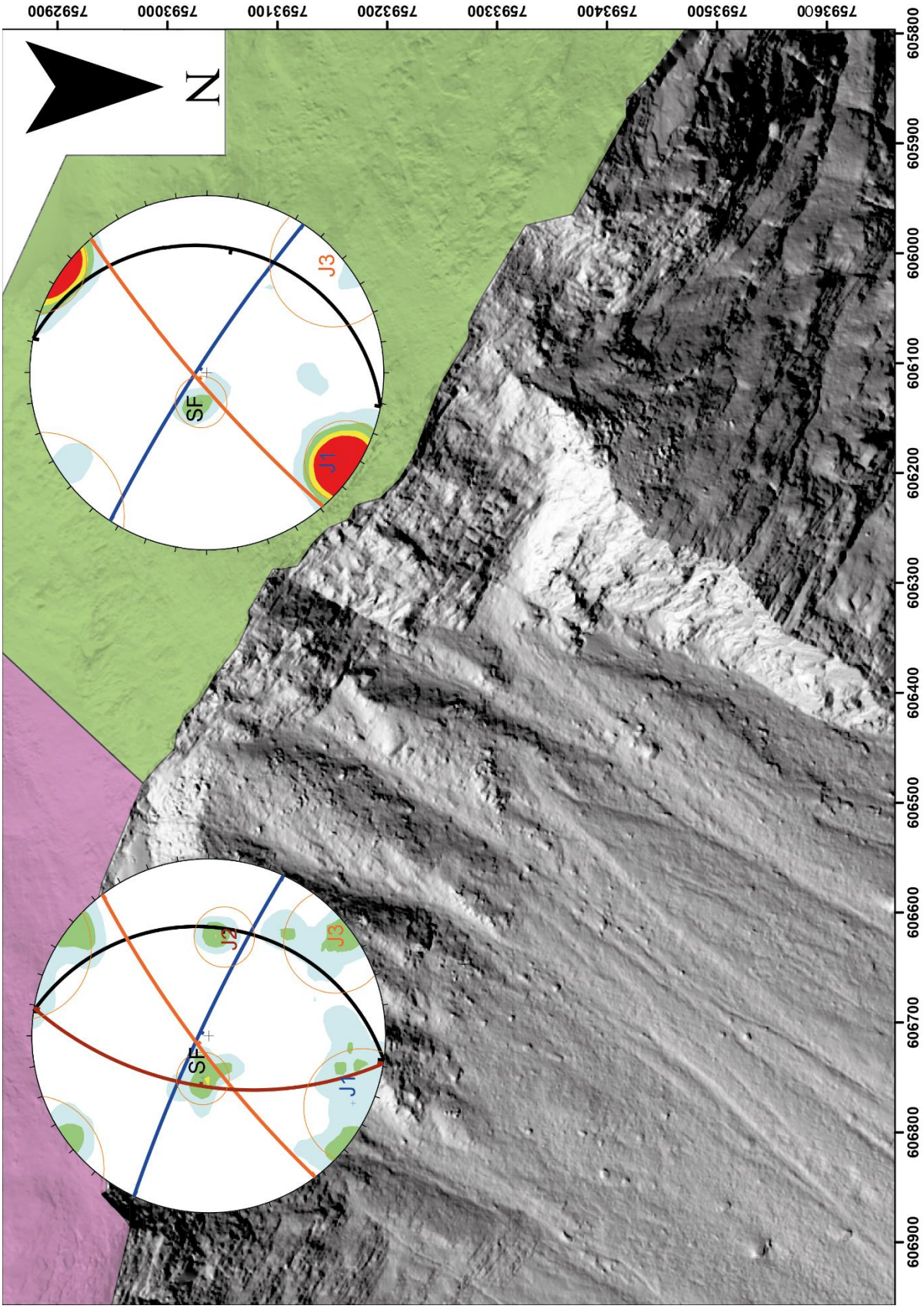

Figure 8.3 Map of structural domains. The east domain (pink) and the west domain (green). Poles from the field work only. The stereographic plots are oriented to the north arrow.

8.5 Appendix E: MATLAB-script for the fragmentation modelling

The crush_code.m script written in MATLAB, to model fragmentation of blocks.

```
% Number of fragmentation cycles
n = 5;

%Number of blocks after n cycles(V0 = source area blocks)
X = length(V0)*(2^(n-1));

%Length of the start vector (number of source area blocks)
LV0 = length(V0);

%Make sure MATLAB use the same "random" numbers each time script is
run
rng default



%Create a matrix with 0`s with size according to fragmentation
cycles
crush_mat = zeros(n,X);

%First row in matrix = source area blocks
crush_mat(1,1:LV0)=V0;

for i = 1:(n-1)
      %Find the length of the matrix row
            AntNon0 = length(V0)*(2^(i-1));

      %Make a vector of random numbers between 0 and 1
            random = rand(1,AntNon0);

      %Multiply the random vector with the blocks calculated in the
      last step, and put them in the start of the next matrix row.
            crush_mat(i+1,1:AntNon0)=random.*crush_mat(i,1:AntNon0);

      %Subtract the last block sizes from the new(those multiplied
      with random numbers) and place them in the end of the new
      matrix row. This way the new row of block sizes has the same
      volume as the source blocks.
            crush_mat(i+1,(AntNon0+1):(AntNon0*2)) = ...
                  crush_mat(i,1:AntNon0)-crush_mat((i+1),1:AntNon0);
end
```

8.6 Appendix F: MATLAB-script for plotting fragmentation results

The plot_crush.m script written in MATLAB, to plot the model for fragmentation of blocks in a semi logarithmic grain size distribution plot.

```
%for inputs from from crush_code

%sort according to volumes
crush_mat_sorted = sort(crush_mat,2);

cum_mat = zeros(5,352);

%get sorted cumulative sum matrix
for i = 1:5
    cum_mat(i,:) = cumsum(crush_mat_sorted(i,:));
    cum_mat(i,:) = cum_mat(i,:)/norm(cum_mat(i,:),Inf);
end

%for inputs from the actual deposits
all_sorted = sort(all);
cum_all_sorted = cumsum(all_sorted);

%get a normalized cumulative sum of the all vector
cum_norm=cum_all_sorted/norm(cum_all_sorted,Inf);

%for deposits with blocks larger than source area blocks removed
cum_all_sorted_tweek = cumsum(all_sorted_tweek);

%get a normalized cumulative sum of the inputs without the large
blocks
cum_norm_tweek=cum_all_sorted_tweek/norm(cum_all_sorted_tweek,Inf);

%plot the figure itself
figure('DefaultLegendFontSize',12,'DefaultLegendFontSizeMode','manua
l');
semilogx(crush_mat_sorted(1,:), cum_mat(1,:)...
    , crush_mat_sorted(2,:), cum_mat(2,:)...
    , crush_mat_sorted(3,:), cum_mat(3,:)...
    , crush_mat_sorted(4,:), cum_mat(4,:)...
    , crush_mat_sorted(5,:), cum_mat(5,:)...
    , all_sorted, cum_norm...
    , all_sorted_tweek, cum_norm_tweek,'LineWidth',1.5)
xlabel('Volume [m^3]', 'FontWeight', 'bold', 'FontSize', 14);
str = ('Normalized cumulative frequencies', '(or %passing)');
ylabel(str, 'FontWeight', 'bold', 'FontSize', 14);
legend('Source area blocks','Fragmentation cycle 1', ...
     'Fragmentation cycle 2','Fragmentation cycle 3', ...
     'Fragmentation cycle 4','Deposited blocks',...
      'Deposited blocks <215 m^3', 'Location','northwest');
set(gca,'fontsize',12);
```

8.7 Appendix G: Run-out modelled in Flow-R

8.7.1 Scenario 1.A

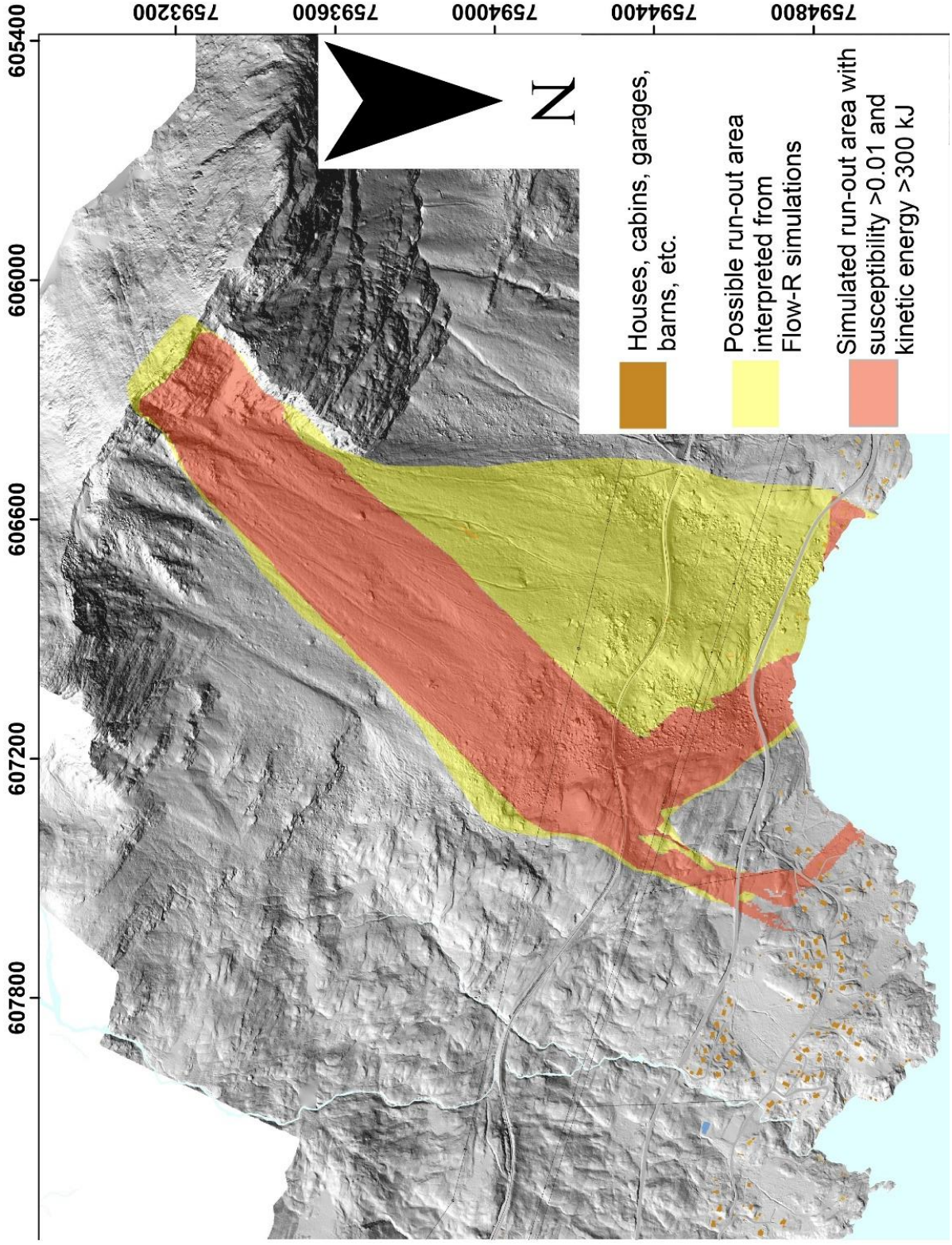

Figure 8.4 Run-out modelled in Flow-R for scenario 1.A

8.7.2 Scenario 2.A

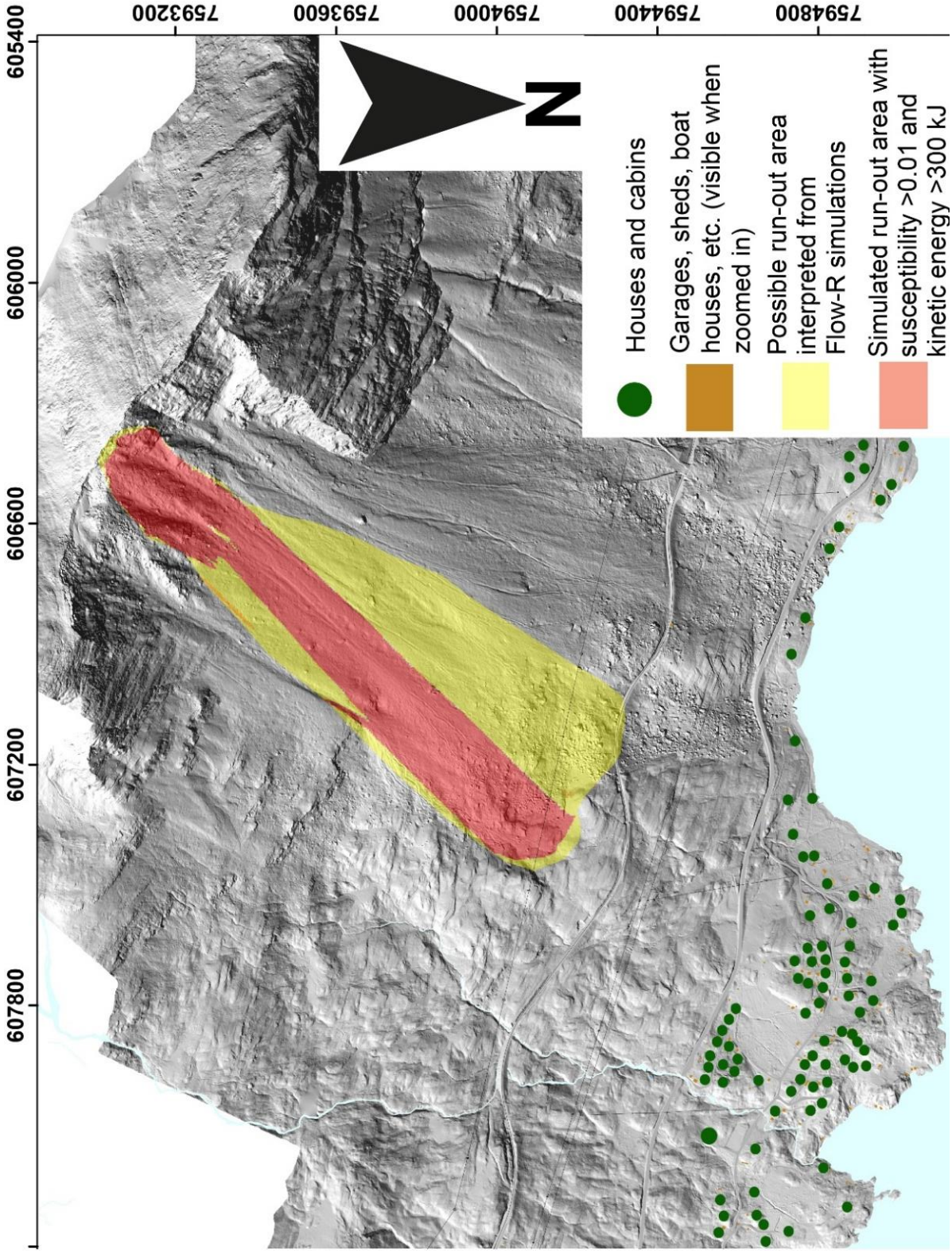

Figure 8.5 Flow-R simulated and interpreted run-out distances for scenario 2.A.

8.7.3 Scenario 4.D

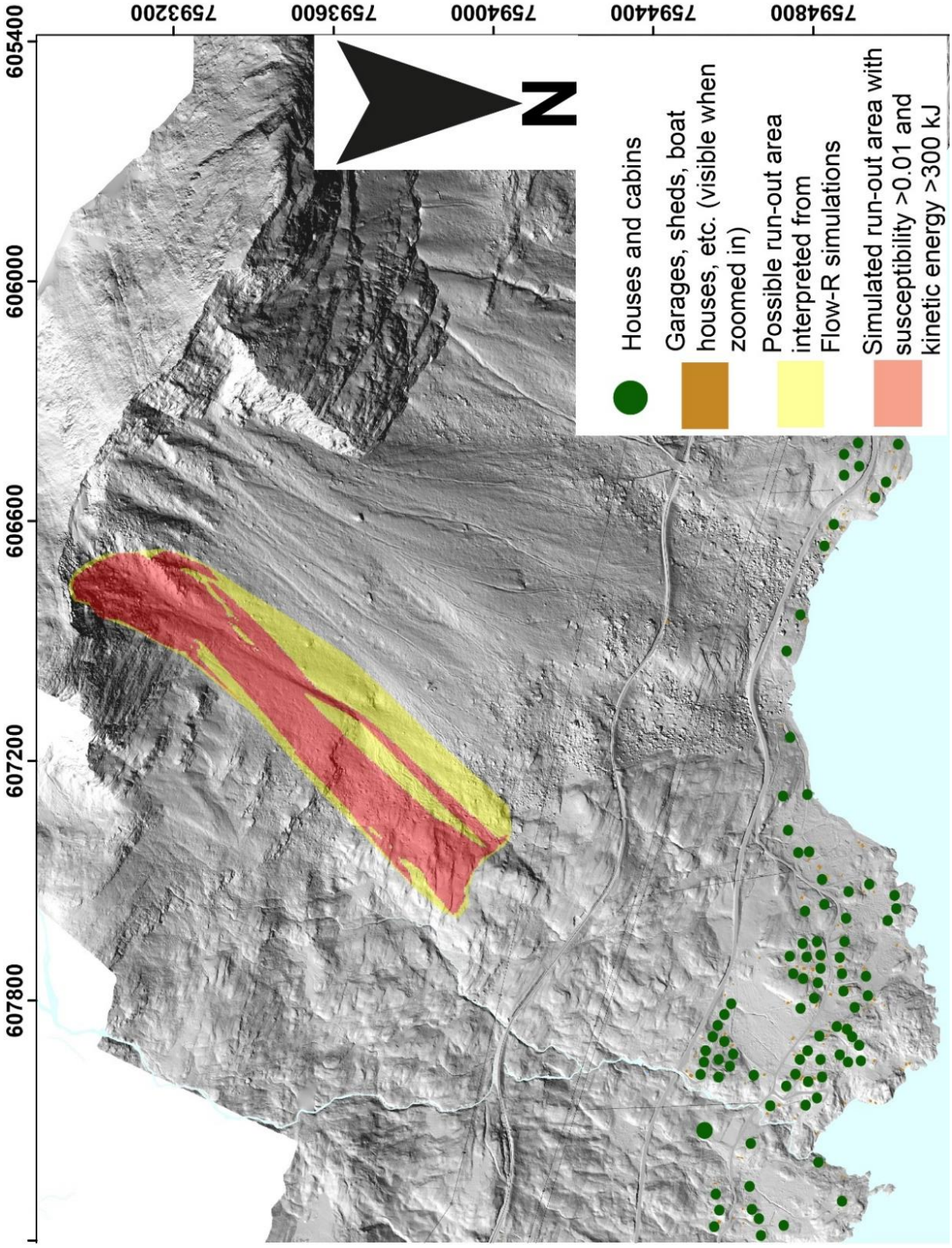

Figure 8.6 Flow-R simulated and interpreted run-out distances for scenario 4.D.

8.8 Appendix H: Risk matrices

Risk matrix Rombakstøtta scenario 1.A

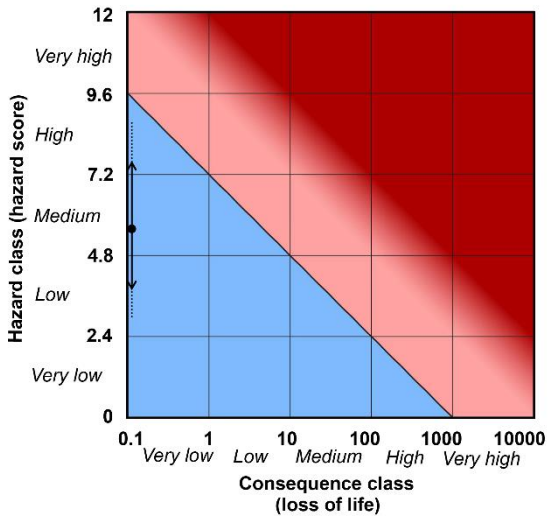

Risk matrix Rombakstøtta scenario 1.B

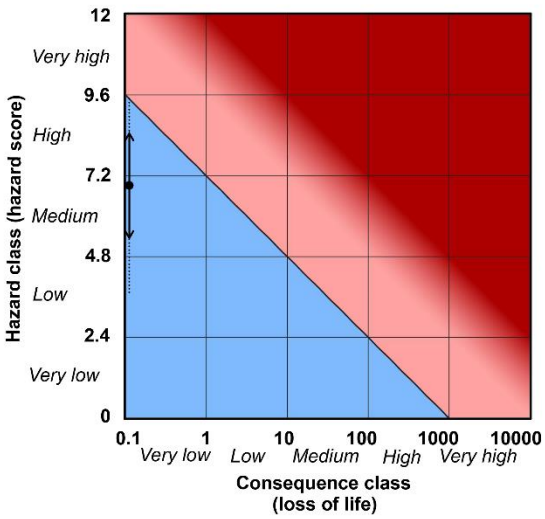

Risk matrix Rombakstøtta scenario 2.A

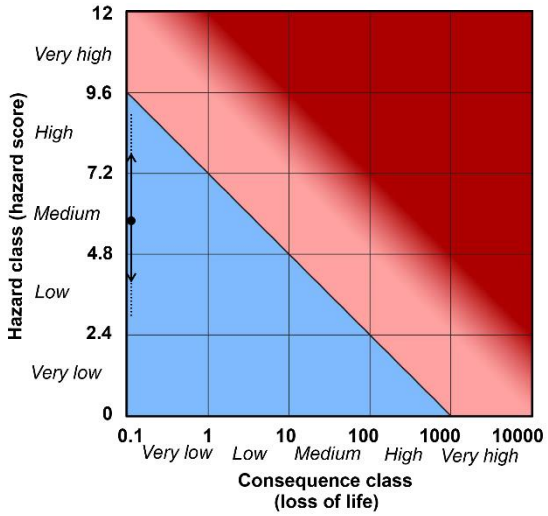

Risk matrix Rombakstøtta scenario 3.A

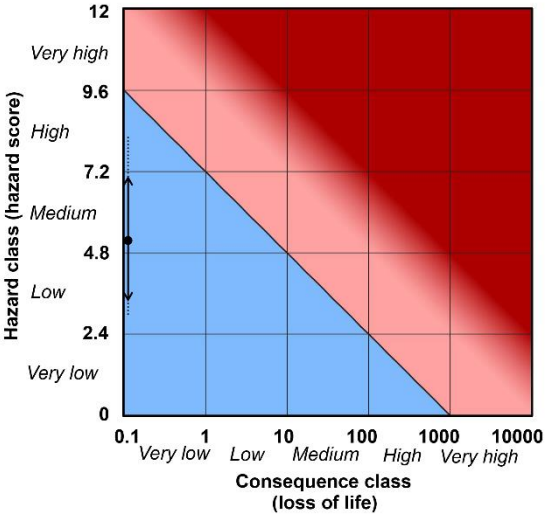

Risk matrix Rombakstøtta scenario 4.A

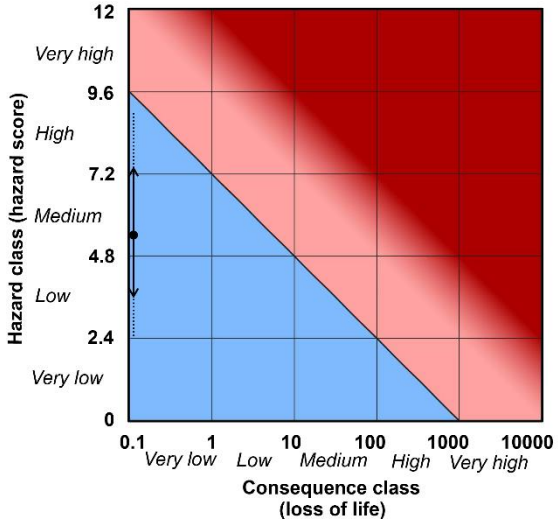

Risk matrix Rombakstøtta scenario 4.B

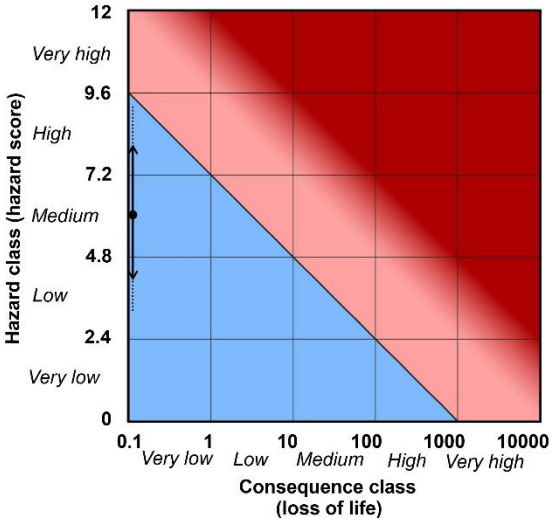

8.8.1 Risk matrices